Stability of a Rotating Cylindrical Shell Containing Axial Viscous Flow

by

Frédérick Gosselin

Department of Mechanical Engineering
McGill University
Montréal, Québec, Canada

Under the supervision of
Dr Michael P. Païdoussis

Submitted in September 2006

Thesis submitted to McGill University in partial fulfillment of the requirements of the degree of Master of Engineering

Your file Votre référence
ISBN: 978-0-494-32592-6
Our file Notre référence
ISBN: 978-0-494-32592-6

Table of contents

Abstract

The present thesis studies the stability of a rotating cylindrical shell containing a co-rotating axial viscous flow. The system can be thought of as a long thin-walled pipe carrying an internal axial flow while the whole is in a frame of reference rotating at a prescribed rate. The equations of the previously solved inviscid model are rederived and the problem is studied further. The results obtained for purely axial flow are reproduced, but as expected from literature, it is impossible to obtain satisfactory results for the system subjected to rotation due to the presence of singularities in the flow pressure solution. A hypothetical physical explanation for these singularities is put forward and has similarities with the phenomenon of atmospheric flow blocking.

Considering the unsuccessful results obtained with the inviscid theory, it is believed that the added realism brought in by the introduction of viscosity in the theory can lead to a successful model. Assuming a travelling-wave perturbation scheme, the linear Donnell-Mushtari thin shell equations are coupled with the fluid stresses obtained by solving numerically the incompressible Navier-Stokes equation for a laminar or turbulent flow. A novel triple-perturbation approach is established to consider the interaction between the fluid and the structure. This triple-perturbation approach is in essence a superposition of three fluid fields caused by the three components of the shell deformation for a given oscillation mode. It is found that the usual technique for linear aeroelasticity studies consisting of applying the fluid boundary conditions at the undeformed position of the wall instead of the instantaneous deformed position greatly alters the stability of the system. To remedy to this problem, three different corrections are applied and tested on the carefully derived model. The dynamics of the system subjected to purely axial flow with no rotation is successfully studied with the viscous model for both laminar and turbulent flow conditions. Because no experimental or previous theoretical data is available, it is impossible to validate the results obtained in the laminar regime. For the turbulent regime, as the Reynolds number is increased, the results tend more and more towards those obtained with the inviscid theory.

The results obtained for small rates of rotation show that both in the laminar and in the turbulent regime, the system tends to be stabilised when subjected to a small rate of

rotation. On the other hand, this tendency should be reversed for higher rates of rotation, but it is impossible to show this due to the limitations of the root-finding method employed.

Sommaire

Le présent mémoire a pour but d'étudier la stabilité d'une coque cylindrique en rotation contenant un écoulement axial visqueux lui aussi soumis à la même rotation. On peut imaginer le système comme étant un long tuyau à parois mince contenant un écoulement axial, alors que le tout est en rotation autour de l'axe du tuyau. Les équations du modèle non visqueux déjà résolu sont redérivées et la compréhension du problème est approfondie. Les résultats obtenus pour un écoulement purement axial sont reproduits mais tel que mentionné dans la littérature, il est impossible d'obtenir des résultats satisfaisants pour le system sujet à la rotation dû à la présence de singularités dans la solution de la pression de l'écoulement. Une hypothétique explication physique de ces singularités est avancée et a des similarités avec le phénomène de blocage atmosphérique.

Considérant les résultats infructueux obtenus avec la théorie non visqueuse, on est porté à croire que le réalisme que peut apporter l'introduction de viscosité dans la théorie peut mener à un modèle qui fonctionne. En cherchant une solution de la forme d'une onde progressive de perturbation, les équations linéaires de Donnell-Mushtari pour modéliser une coque mince sont couplées avec les contraintes du fluide obtenues en résolvant numériquement les équations de Navier-Stokes pour un écoulement incompressible laminaire ou turbulent. Une nouvelle approche de triple perturbation est établie pour prendre en considération l'interaction entre le fluide et la structure. Cette approche de triple perturbation est en fait une superposition de trois écoulements de perturbation causés par les trois composantes de la déformation de la coque pour un mode d'oscillation donné. Il est démontré que la technique conventionnelle d'aéroélasticité linéaire consistant à appliquer les conditions frontières du fluide à la position non déformée du mur au lieu de la position déformée instantanée influence grandement la stabilité du système. Pour remédier à ce problème, des trois types de corrections sont appliqués et testés sur le modèle visqueux. La dynamique du système sujet à un écoulement purement axial sans rotation est étudiée avec succès avec le modèle visqueux pour des écoulements laminaires et des écoulements turbulents. Parce qu'il n'y a pas de résultats expérimentaux ou théoriques disponible pour comparer les résultats du régime laminaire, il est impossible de les valider. Cependant, pour le régime turbulent, à mesure que le nombre

de Reynolds est augmenté, les résultats obtenus tendent de plus en plus vers ceux obtenus avec la théorie non visqueuse.

Les résultats obtenus pour de petits taux de rotation montrent que dans le régime laminaire et dans le régime turbulent, le système tend à se stabiliser lorsque le taux de rotation augmente. D'un autre côté, cette tendance devrait s'inverser pour de plus hauts taux de rotation, cependant il n'est pas possible de le démontrer dû aux limitations de la méthode employée pour trouver les fréquences complexes admissibles du système.

Acknowledgements

The supervision Professor Païdoussis provided to me during this thesis has been tremendous. Being deeply involved in the research project, he made me benefit from his technical insight and knowledge throughout the entire duration of my Master's degree. I am grateful of him for sharing his wisdom and philosophy of academic life as well as helping me overcome considerable obstacles which arose during the project. I have a great respect for Professor Michael P. Païdoussis, and I would undertake a new enterprise with him any day.

Je dois beaucoup à mes parents Philippe Gosselin et Louise Cloutier de même qu'à ma sœur cadette Élisabeth Gosselin. Avec eux dans ma vie, je n'ai jamais été pris au dépourvu; je sais qu'ils ont toujours été là pour moi et qu'ils le seront toujours.

Je tiens à remercier Martine Dubé qui m'a permis, lors de plusieurs fins de semaines d'escapades fabuleuses, de décrocher de la vie parfois stressante d'étudiant de second cycle et d'avoir un avant-goût de la retraite!

Durant mes études à McGill, Matthew Wadham Gagnon fut mon coéquipier au flagball et au hockey, mon colocataire, mon partenaire d'étude et de laboratoire, ainsi qu'un ami très proche. Nos discussions, parfois techniques, parfois philosophiques sur nos projets de maîtrise furent des plus enrichissantes. Un jour peut-être partirons-nous ensemble en business!

As he puts it: "When Frédérick walked in the lab, he was no more than 5 foot tall. After I took him under my wing and nurtured him, he grew to become the tall and smart engineer that he is now!" Konstantinos Karagiozis was my teaching assistant for all my mechanics courses and if there was such a thing, he would have been my thesis teaching assistant as well. In fact, he was almost like a second supervisor to me!

I am grateful to NSERC and FQRNT for funding this research.

Chapter 1

Introduction

1.1 Preliminary remarks

Ever since the seventies, the dynamics of thin cylindrical shells coupled with subsonic flows has been of interest to engineers. Paidoussis and Denise (1972) made the fortuitous discovery that shells containing low-speed flow do flutter and paved the way to a new area of research in fluid-structure interactions (FSI). Since then, the research has evolved in different branches ranging from the stability of coaxial shells with flow [see Païdoussis et al. (1984)], the dynamics of pliable shells resembling physiological systems [see Shapiro (1977)], the study of the non-linear large amplitude behaviour of shells [see Karagiozis et al. (2005)] to name only a few. See Paidoussis (2003) for a full review of the research done on the dynamics of shells interacting with fluid.

The present thesis studies the stability of a rotating cylindrical shell containing a co-rotating axial viscous flow. The system can be thought of as a long thin-walled pipe carrying an internal axial flow while the whole is in a frame of reference rotating at a prescribed rate. Practical examples of such a system include swirling flow in dual spool aircraft jet-engines, rotating drums used in the process industry, some nuclear applications [Païdoussis (2003, section 7.6)], spin-stabilised rockets, piping in a rotating space-station. There are also many applications to slightly different systems such as fluid prerotation in the inlet region of a centrifugal pump, cyclone dust separators [Pareschi and Montanelli (1980)], or the intense neutron generator system [Païdoussis (2003, section 7.6.3)].

A literature review is presented in the following section, divided in four parts: (i) cylindrical shells subjected to swirling flows, (ii) pipe flow and rotating flow, (iii) shear-flow-structure interaction, and (iv) numerical solutions to pipe flow. This literature review is essential to understand the motivations and objectives of the present research work. These motivations and objectives along with the detailed overview of the thesis are

presented at the end of the present chapter (Section 1.2).

1.1. Literature review

1.1.1 Cylindrical shells subjected to swirling flow

Only a handful of studies have been conducted on the problem of shells subjected to a swirling (helical) flow. Paidoussis (2003, section 7.6) offers a review of the work performed in this field and on related problems. Srinivasan (1971) undertook the first study that added the complexity of rotation to the problem of a cylindrical shell subjected to axial flow. In this study, the stability of a thin infinitely long cylindrical shell exposed to an outer inviscid helical flow is investigated. Through numerical simulations, it is found that when the critical velocity is reached, the system loses stability by coupled mode flutter as the forward and the backward travelling waves coalesce. Past the critical flow velocity, the forward travelling waves become unstable while the backward travelling ones tend to remain stable.

In Lai and Chow (1973), the stability of a rotating thin shell containing inviscid fluid flow is investigated. Here, just as in the present study, both the fluid and the shell are rotating about the axis of the cylindrical shell at a constant given rate. * The linear Donnell shell theory is modified to account for the solid body rotation and is coupled to the fluid equations, similar in essence to those derived by Chow (1969). It is found that the critical flow rate in the shell decreases with increasing angular velocity. Using essentially the same method of solution as Lai and Chow, Chen and Bert (1977) study the dynamics of a stationary shell carrying a rotating flow. This study differs from Lai and Chow's only in the fact that the shell is not rotating. Once again, it is found that rotation severely decreases the stability of the fluid-shell system.

The validity of the results obtained by Lai and Chow and Chen and Bert was questioned by Cortelezzi, Pong and Païdoussis (2004), who found it impossible to reproduce the results of Lai and Chow. In particular regions of the parameter space, the flow solution is not bounded, which makes it impossible to obtain the critical velocity of

* It has come to the attention of the author of the present thesis that equation (2.4) in Lai and Chow (1973) has two typographic errors in it. In Lai (1972), the equivalent equation (4) is written correctly.

the system in many cases. It is emphasised that the problem lies within the flow solution and is possibly due to the absence of viscous effects.

Based on some work by Cortelezzi et al. (2004), Chaumond (2003) made a first attempt at incorporating viscosity in the problem of rotating shells with a co-rotating axial flow. In this work the equations of motion for a viscous rotating flow first derived by Cortelezzi (2002) are rederived from the Navier-Stokes equations by using a travelling wave linear perturbation scheme. The system of equations thus obtained was solved numerically by using a finite-difference algorithm. Difficulties were encountered while applying boundary conditions on the flow at the flow-wall interface, because the pressure exerted by the wall on the fluid is not known a priori. For this reason, the flow-field was solved for a prescribed external wall pressure. A full coupled FSI analysis was attempted without success.

1.1.2 Pipe flow and rotating flow

As mentioned above, it was found by Cortelezzi et al. (2004) that the region of no solution in the parameter space of the problem of rotating shells with a co-rotating axial flow has its origin in the fluid model. For this reason, a review of the literature on the fluid mechanics problem of swirling flow is desirable.

Rayleigh (1917) treats the stability of Couette flow, i.e. the steady circular flow of a fluid between two rotating coaxial cylinders. The equations of motion derived are for a 3-D inviscid theory and axisymmetric disturbances. The analysis led Rayleigh to define the general criterion, named after him, which states that: "... the equilibrium of fluid revolving one way round in cylindrical layers and included between coaxial cylindrical walls is stable only under the condition that the circulation ($k = vr = \Omega r^2$) always increases [in magnitude] with r." In other words the inviscid flow rotating between two coaxial cylinders is stable if $d\left(r^4\Omega^2\right)/dr > 0$ everywhere in the interval; and further, that it is unstable if $\left(r^2\Omega\right)^2$ should decrease anywhere inside the annulus.

Chandrasekhar (1961) applies the equations derived by Lord Rayleigh for revolving fluids to study the stability of a rotating fluid flowing axially between

concentric cylinders. The equation of motion of the flow is derived starting with Euler's equation and applying a linear perturbation scheme while considering only small axisymmetric disturbances. It is found that the addition of rotation to the axial flow changes qualitatively the problem. In the presence of rotation, the stability of the axially moving flow depends solely on Rayleigh's criterion. Through a method making use of the variational principle, it is shown that Rayleigh's criterion for the stability of a pure rotational flow continues to be valid in the presence of an arbitrary axial flow (for any profile in r). This is a very bold claim. It implies that the stability of the flow is independent of the axial flow velocity in the presence of an arbitrarily small rotation rate.

Howard and Gupta (1962) attempt to derive a general stability criterion for non-dissipative swirling flows in the same fashion as was done by Rayleigh (1917) with the Rayleigh number. The stability of a rotating flow with no axial component between two concentric cylinders is analogous to that of a density-stratified fluid at rest, under the action of gravity; so long as only axisymmetric perturbations are considered. If the analogy is pushed further, it suggests that, when an axial flow is also present, the effect of the swirl component may be analogous to the effect of density stratification (in the presence of gravity) on a parallel shear flow. It is known that, for flows in the presence of gravity, statically stable density stratification tends to have a stabilising influence on any shear instability. This effect is measured by the Richardson number which is given by

$$J(z)=\frac{-g(d\rho/dz)}{\rho(dU/dz)^2},$$

where g is the gravity acceleration, ρ is the density of the stratified fluid, U is the velocity of the flow, and z is the vertical coordinate. Pursuing the analogy further, an appropriate Richardson number for the swirling flow is introduced as a sufficient condition for stability to axisymmetric perturbations. For the specific case of solid rotation, the condition simplifies to

$$J(y)=4\Omega^2\left(\frac{\partial U}{\partial r}\right)^{-2},$$

where Ω is the rotation rate and r is the radial coordinate. As with the density stratification problem, the sufficient stability condition is $J(y)\geq\frac{1}{4}$ everywhere. Work is

also done in that paper on non-axisymmetric disturbances. Although a general stability criterion for non-axisymmetric disturbances is not found, a sufficient stability condition for particular wavelengths and wavenumbers is obtained. For the particular case of solid rotation, the stability condition which depends on the wavelength and the circumferential wavenumber simplifies to

$$4k^2\Omega^2 - 2kn\Omega\frac{dU}{dr} - \frac{1}{4}k^2\left(\frac{dU}{dr}\right)^2 \geq 0, \tag{1.1}$$

everywhere. This condition ensures stability; but failing to satisfy it does not automatically imply instability. Although the authors do not discuss this, their results imply that rotation has a strong stabilising effect on the flow. By their results and also with concrete examples, Howard and Gupta also refute the result by Chandrasekhar (1961) affirming that the stability of inviscid flows with both axial and swirl components is determined by Rayleigh's criterion alone, without reference to the axial component. Also, the effect of (electromagnetic) force fields on the fluid flow is studied but is of no interest in the present study.

In Chow (1969), the swirling inviscid and incompressible fluid flow in cylindrical tubes with axisymmetric and periodic deformations is investigated. The flow is characterised by the Rossby number, which relates the axial to the circumferential flow velocity:

$$\varepsilon = U/2R\Omega' = U_R/2\Omega. \tag{1.2}$$

It is found that for flows with certain values of Rossby number, the flow near the wall is "blocked". At those critical values of Rossby number, no flow solution can be found to satisfy the boundary conditions. What happens physically is visualised by studying the flow at a Rossby number close to a critical one: $\varepsilon \to \varepsilon_c$. Fig. 1 shows that the streamlines become parallel with the pipe, and the fluid near the wall is almost stagnant. This phenomenon of blocking is characteristic of stratified fluid flow over obstacles and is discussed in detail, along with analogies to rotating fluid, by Yih (1965).

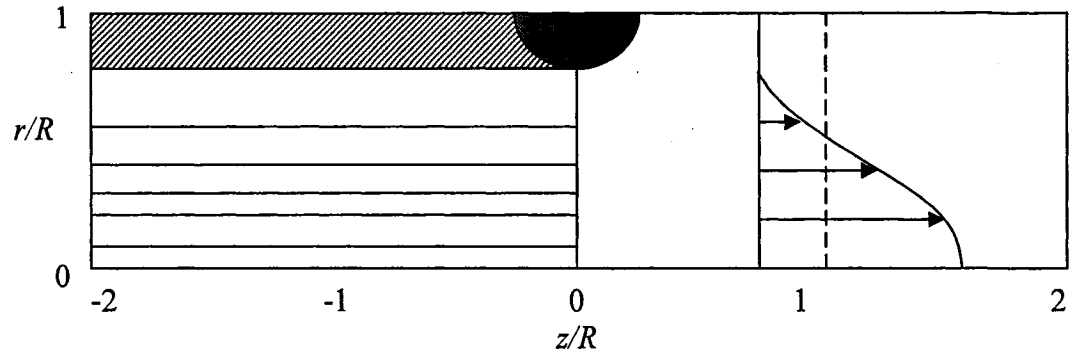

Fig. 1. First blocking encountered for swirling flow in a tube with large axysimmetric periodic wall deformation. [Figure inspired by Chow (1969)]

Lai and Chow (1973) cite Chow (1969) when their fluid solution is introduced and they make mention of the flow near the wall being blocked under certain conditions. It seems that the interpretation Lai and Chow make of flow blocking may not be correct. Could flow blocking have something to do with the region of no solution in the parameter space found by Cortelezzi et al. (2004)? This is discussed in Chapter 5.

Making use of the equations developed by Howard and Gupta (1962) for inviscid flow subjected to non-axisymmetric disturbances, Maslowe (1974) studies the stability of the particular case of rotating Poiseuille flow for an arbitrary Rossby number, ε. It is found that the growth rate of the most unstable helical perturbation is proportional to ε, provided that $\varepsilon \ll 1$, but it then decreases for larger values of ε. In the limit $\varepsilon \to 0$, the flow is stable as it tends towards a purely rotating flow, and in the limit $\varepsilon \to \infty$, the flow is stable again as it tends towards a pure Poiseuille flow.

1.1.3 Shear-flow-structure interaction

Dowell (1971) obtains a theoretical solution to the problem of a flexible plate subjected to a shear flow. A horizontal rectangular plate of finite dimensions is subjected to a horizontal compressible flow with a fully developed shear velocity profile. Through a nonlinear flutter analysis of the flexible plate, its stability is examined and the effects of the shear flow are studied. The direct effects of viscosity are neglected in the perturbation flow, and viscosity enters only through the effect of the mean flow on the perturbation

flow. The mean flow profile respects a no-slip boundary condition *at the mean position* of the oscillating plate and models a boundary layer of constant thickness. The inviscid perturbation flow is solved by applying a free-slip boundary condition at the instantaneous position of the plate. This is an important detail because normally, in the framework of linear aerodynamic theory, the boundary conditions are applied on the fixed reference surface. Dowell shows that by applying the conditions on the mean position of the surface, the stabilising effect of the boundary layer is overestimated as a result of the fact that the mean velocity is zero at the mean wall position. In order to apply the boundary condition on the instantaneous body surface, a nonzero value of displacement of the plate z_w is assumed and the flutter analysis is performed to determine the stability of that system for that range of motion. In other words, instead of applying the impermeability condition at $z = 0$ where the undeformed plate lies, it is applied at an assumed position just off the plate $z = z_w$. The pressure of the fluid acting on the plate is also taken at $z = z_w$ instead of $z = 0$.

Implicit in this analysis is the assumption that the boundary layer of the mean flow is unaffected by the panel motion. As Dowell mentions, this is a reasonable assumption when the panel amplitude is small compared to the boundary layer thickness. As it turns out, that is when the shear flow has its most significant effect. On the other hand, when the boundary layer thickness is of the same scale or smaller than the panel amplitude, the assumption is not valid.

Païdoussis et al. (1985) study the stability of clamped-clamped coaxial shells conveying viscous fluid. To study this problem, the shell-vibration-dependent fluid forces are determined by means of inviscid, potential-flow theory, whereas the viscous forces are determined separately in a time-averaged sense. This time-averaged effect of the viscous forces is introduced in the system as a pre-stress on the shells. Flügge's standard thin-shell equations [see Leissa (1973)] are rederived taking into account the steady pressure head loss and the shear stresses caused by the mean viscous flow. The equations of motion of the prestressed shells are then coupled with the time-varying equations describing the inviscid flow. The steady viscous forces have for effect the pressurisation and tensioning of the shell. Viscous damping is not accounted for.

El Chebair et al. (1990) theoretically study the stability of coaxial shells subjected to viscous inner flow in the shell and to annular flow. The novelty in this study is that here both the mean and the unsteady forces of the viscous flow on the shells are taken into account. The mean viscous forces are accounted for by using the equations of motion of shells subjected to viscous flow developed by Païdoussis et al. (1985). Then, instead of coupling these equations with an inviscid time-dependent flow solution as was done by Païdoussis et al., they are coupled to an unsteady solution of the Navier-Stokes equation written using nonprimitive variables, namely the flow potential and a velocity perturbation vector which represents the viscous perturbations. The point in using these nonprimitive variables is to separate the viscous and non-viscous effects in the flow into different equations so that they can be solved for independently. These independent solutions of the inviscid and viscous effects are then recombined in the linearised Navier-Stokes equation to lead to the pressure and shear caused on the shell by the flow. In order to solve for the flow, a mean velocity profile has to be assumed. Although it is not mentioned in El Chebair et al. (1990), from El Chebair (1988) it can be learnt that a power law profile [see Schlicting (1979)] was used to model the entire flow, despite its weaknesses near the wall and near the centreline.

El Chebair et al. encountered problems in applying the boundary conditions on the flow at the fluid-solid interface. In viscous theory, the no-slip condition must be applied at the wall: the velocity of the fluid at the wall must be equal to that of the wall. This requires that the mean flow velocity must be zero on the wall. It is argued that, in the absence of mean flow velocity on the wall, the centrifugal forces responsible for the static instability in the physical system vanish. This issue is similar to what Dowell (1971) encountered for the problem of the flat plate in shear flow. In order to recover the centrifugal forces, two methods are tested: (i) allow a slip condition at the wall and assume that an average velocity is acting at the wall, and (ii) apply the boundary condition at a distance from the wall equivalent to the radial shell deformation. Both methods give similar results. It is shown, by comparing results obtained using the aforementioned theory, with results from the inviscid theory that the unsteady viscous effects are insignificant on the stability of the system for internal flow and annular flow with a large gap between the shells.

Similar problems, related to the application of the boundary conditions on the shell wall, were encountered by Nguyen et al. (1994), who produced a fully coupled CFD solution for a cantilevered shell subjected to viscous annular flow with a rigid-pipe outer containment, These problems were resolved in a similar manner as in El Chebair et al. [see Païdoussis (2003, Section 11.7.2)].

1.1.4 Numerical solutions for pipe flow

Many different methods are employed to obtain numerical solutions for various types of pipe-flows in cylindrical coordinates.

Sadeghi and Higgins (1991) and Sadeghi (1991) study the linear stability of sliding Couette-Poisseuille flow in an annulus through the use of the compound matrix method. This method involves combining the continuity and the three momentum equations into two third-order equations by eliminating the pressure and a velocity component, to later convert this system into a system of six first-order equations. The minors of this system of equations are integrated in space by means of an appropriate Runge-Kutta method, making use of the boundary condition at the lower bound of integration. An iterative procedure is required to find the eigenvalues which will satisfy the boundary conditions at the upper bound. Once the eigenvalues are found, the equations relating the minors to the solution are integrated numerically in space to obtain the eigenfunctions. The main advantage of the compound matrix method is its ease of implementation; its obvious drawback is that iterations are required to find the eigenvalues, and the initial guess must be close to the actual value in order for the method to converge.

Maslowe (1973) studies the stability of rigidly rotating inviscid flows subjected to non-axisymmetric disturbances. Because the case being studied is inviscid, it is possible by linearization to obtain a single second-order differential equation to define the radial velocity of the flow with respect to the radial position r. This equation can be integrated along the radial direction by making use of an explicit finite-difference scheme, i.e. a Runge-Kutta procedure. To deal with the singularity at the centre of the flow, the

differential equation is expanded about this point by the method of Frobenius to find the values of the radial velocity and its r-derivative at the lowest bound of integration. The integration does not start from r=0, because, according to the Frobenius expansion, the velocity and its derivative are both zero at this point, which leads to a trivial solution. The integration is therefore started at a point just off the centre. The major disadvantage of this scheme is that iterations are necessary in order to find the correct real and imaginary frequencies which allow for the flow solution to satisfy the impermeability boundary condition on the wall. For each iteration, the entire flow has to be integrated over again.

Soh and Goodrich (1988) introduced a technique based on the finite-difference method, using a time-marching scheme with artificial compressibility to solve the incompressible Navier-Stokes equations. The momentum equations are discretised in physical time and are then written in a continuous pseudo-time derivative form. The continuity equation is preconditioned with a pseudo-time derivative of the pressure. In order to find the flow solution at each time step, the system of equations with artificial compressibility is marched in pseudo-time until the pseudo-time steady-state solution is reached. At this point the artificial compressibility and pseudo-time terms vanish and a solution is attained for the physical time-step. This scheme is repeated for every physical time-step. In effect, this pseudo-time marching is nothing but a clever way to introduce an iterative process. This scheme is used successfully by Nguyen, Païdoussis and Misra (1994) to study the dynamics of cantilevered coaxial cylindrical shells conveying fluid. To do this they solve the unsteady viscous flow between the coaxial shells in cylindrical coordinates. This method of solution allows studying the dynamics of the system really well but, on the other hand, a time-marching scheme is less efficient than an eigenvalue analysis for studying stability.

Verzicco and Orlandi (1995) introduce a new time-dependent finite-difference scheme for solving the Navier-Stokes equations for the case of three-dimensional incompressible flows in cylindrical coordinates. The novelty of their study is the introduction of the radial flux on a staggered mesh, which simplifies the treatment of the region near the axis. The radial flux is equal to the radial velocity component times the radial position. In their study, because of the staggered grid, only the radial flux is defined at the centre of the flow and it is zero by definition.

Harlow and Welch (1965) study transient viscous flows with a free surface. One key point of this work is the introduction of a staggered grid on which the Navier-Stokes and the continuity equations are discretised. The two-dimensional problem is solved in Cartesian coordinates where the velocity components and the pressure are defined on an Eulerian mesh of cells covering the computational region. For each cell, the local field variables are centred as shown in Fig. 2. Moreover, the x- and y-momentum equations are differenced, respectively, about the points where the x- and y- components of the velocity are defined. The continuity equation is differenced about the points where the pressure is defined. The scheme makes use of averages of adjacent values to evaluate the velocity components at points on the mesh where they are not defined. At first glance, this choice of grid might seem a little arbitrary, considering that no reason is given by the authors to justify their disposition of the variables on the mesh. On the other hand, their computational experiments do show "considerable numerical stability" for their computing technique. Patankar (1980) brings a possible explanation to this stability feature. On a grid which is not staggered (or which is staggered differently), the central pressure difference in the momentum equations and the central velocity differences in the continuity equation are evaluated using two alternate grid points instead of two adjacent ones. This not only diminishes the accuracy of the scheme but it also allows for a "zig-zag field" where the values of the field variables oscillate from one grid point to the next. This numerical phenomenon is also referred to as "odd-even decoupling" or "sawtooth mode" [see Kallinderis (1992)]. Patankar (1980) also notes that these troublesome hurdles seem to be associated with the first derivatives, while the second derivatives are always well behaved and create no difficulties.

Bélanger (1991), Mateescu et al. (1994a), Mekanik (1994) and Mateescu et al. (1996) adapted the staggered grid of Harlow and Welch (1965) to cylindrical coordinates to solve their problems.

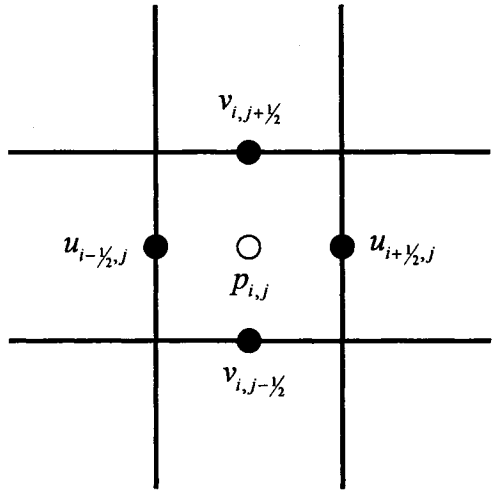

Fig. 2. Field variable value placement about a computational cell. Velocities are defined at the cell boundaries while pressures are defined at cell centres. [Figure inspired from Harlow and Welch (1965).]

Vinokur (1982) studies the stretching functions employed for finite-difference calculations. In order to make a finite difference scheme more efficient, stretching functions are used to concentrate more grid points in the regions of higher gradients. This technique is especially useful for problems with moving walls or problems including boundary layer effects. Bélanger (1991), Mateescu et al. (1994a), Mekanik (1994) and Mateescu et al. (1996) use the grid stretching functions of Vinokur (1982).

1.2. Aims and overview of the thesis

This thesis aims at developing a model to study the effects of viscosity on the stability of a rotating thin cylindrical shell conveying a co-rotating viscous flow. Building upon the discovery made by Cortelezzi et al. (2004) that the inviscid model is flawed, it is believed that the added realism brought by the introduction of viscosity in the model will lead to a successful model.

The objectives of this thesis are quadruple: (i) rederive the inviscid model developed by Lai and Chow, to set a benchmark for the viscous model and to explain further the results of Cortelezzi et al.; (ii) develop a model considering the interaction between the viscous fluid and the structure, while paying special attention to the interface

between the fluid and the structure; (iii) develop an original numerical method to solve the viscous flow; (iv) characterise the linear behaviour of the system.

The objectives of the thesis are met in the following 6 chapters: the shell equations are introduced and the inviscid fluid model is rederived in Chapter 2; the viscous model is derived in Chapter 3; the numerical scheme to solve the viscous model is explained in Chapter 4; the results obtained with the inviscid theory are presented in Chapter 5; the results obtained with the viscous theory and the numerical scheme utilized are presented in Chapter 6; the thesis is concluded in Chapter 7.

Chapter 2

Formulation of inviscid model

2.1. Formulation of the structural part of the problem

Consider a cylindrical shell of radius R', thickness h', of infinite length, containing an axial fluid flow. The whole system is in a frame of reference rotating about the axis of the cylinder at rate Ω' as illustrated in Fig. 3. In other words the fluid-shell assembly is undergoing solid body rotation. The system is described with the orthogonal dimensional coordinates r', θ, z', respectively in the radial, circumferential and axial directions. Along these coordinates are defined the unit vectors $\vec{e}_r$, $\vec{e}_\theta$ and $\vec{e}_z$. The equations of motion for the coupled fluid-structure system can be found by summing the forces in the three directions z', θ, r'. This sum of forces can be written in matrix form, where the dynamics of both the structure and the fluid can be accounted for by a matrix linear differential operator:

$$[\mathcal{L}']\begin{Bmatrix} u' \\ v' \\ w' \end{Bmatrix} = \{0\}, \tag{2.1}$$

where u', v' and w' are the orthogonal time-dependent components of displacement in the z', θ and r' directions, respectively. These components of displacement are functions of the independent variables θ and z'.

Note that to differentiate dimensional variables from dimensionless ones, the dimensional quantities are marked with a prime, $(\ )'$.

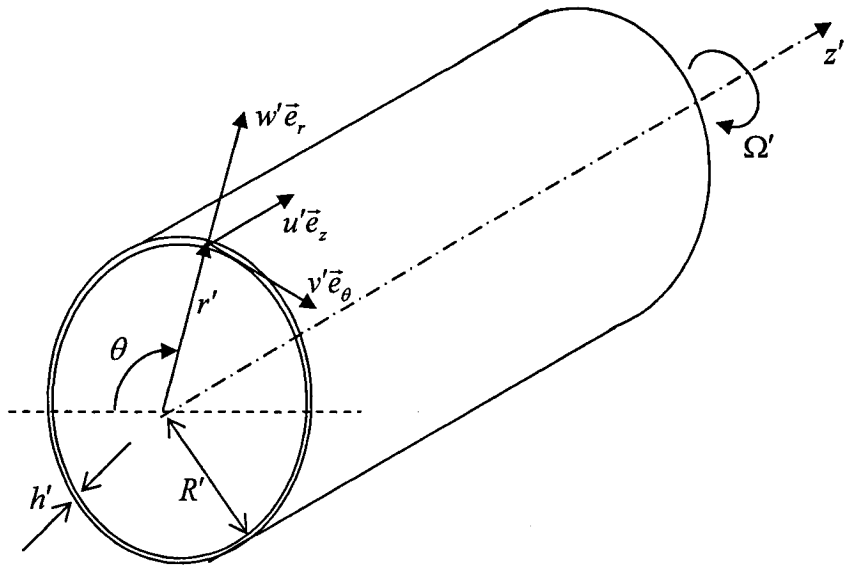

Fig. 3. Schematic of the system.

The deformation of a cylindrical shell of radius R', thickness h', Young's modulus E' and Poisson's ratio ν can be modelled using the Donnell-Mushtari theory. The derivation of this shell theory can be found in many reference textbooks, such as Leissa (1973), Soedel (2004), Kraus (1967) and many others. Using the Donnell-Mushtari theory, the structural rigidity of a thin cylindrical shell is governed by three force intensity (force per unit area) equations associated with the longitudinal, circumferential and radial directions of the shell:

$$\frac{E'h'}{1-\nu^2}\left[\frac{\partial^2 u'}{\partial z'^2}+\frac{1-\nu}{2R'^2}\frac{\partial^2 u'}{\partial \theta^2}+\frac{1+\nu}{2R'}\frac{\partial^2 v'}{\partial z'\partial\theta}+\frac{\nu}{R'}\frac{\partial w'}{\partial z'}\right]=-q'_z, \tag{2.2}$$

$$\frac{E'h'}{1-\nu^2}\left[\frac{1+\nu}{2R'}\frac{\partial^2 u'}{\partial z'\partial\theta}+\frac{1-\nu}{2}\frac{\partial^2 v'}{\partial z'^2}+\frac{1}{R'^2}\frac{\partial^2 v'}{\partial\theta^2}+\frac{1}{R'^2}\frac{\partial w'}{\partial\theta}\right]=-q'_\theta, \tag{2.3}$$

$$-\frac{E'h'}{1-\nu^2}\left[\frac{\nu}{R'}\frac{\partial u'}{\partial z'}+\frac{1}{R'^2}\frac{\partial v'}{\partial\theta}+\frac{w'}{R'^2}+\frac{h'^2}{12}\nabla'^2\nabla'^2 w'\right]=-q'_r, \tag{2.4}$$

where

$$\nabla'^2\equiv\frac{\partial^2}{\partial z'^2}+\frac{1}{R'^2}\frac{\partial^2}{\partial\theta^2} \tag{2.5}$$

and q_z', q_θ' and q_r' are the force intensity components accounting for all body and surface force intensities acting on the shell. The Donnell-Mushtari thin cylindrical shell equation is based on the following assumptions: the thickness of the shell is small compared with its radius, which implies among other things that shear deformation is negligible; strains and displacements are sufficiently small for quantities of second- and higher-order magnitude in the strain-displacement relations to be neglected in comparison with the first-order terms; the radial normal stress is small compared with the other two normal stress components and may be neglected; at every location on the shell, the normal to the underformed middle surface remains aligned in the same direction and normal to the deformed middle surface as the shell deforms (this assumption, which is also referred to as the Kirchhoff hypothesis, represents an extension to the case of a thin elastic shell of the familiar Euler-Bernoulli- hypothesis of beam theory which states that "plane sections remain plane"; the assumption of the preservation of the normal implies, among other things, that all of the strain components in the direction of the normal to the reference surface vanish); in the changes in curvature and in the twist of the midsurface, the tangential displacements and their derivatives are neglected (from this simplification, the stretch of the shell only depends on the strain and the transverse displacement); Hooke's law is the constitutive law obeyed by the material; shell material is isotropic; symmetry of the stress tensor (neglect body couples). The interested reader is referred to Leissa (1973) for more information relative to the derivation of these shell equations.

We can express the position of an arbitrary element of the undeformed shell with the following position vector:

$$\vec{r}_0' = R'\vec{e}_r + z'\vec{e}_z . \tag{2.6}$$

This same arbitrary element of the deformed shell is then located at

$$\vec{r}_1' = \left(R' + w'\right)\vec{e}_r + v'\vec{e}_\theta + \left(z' + u'\right)\vec{e}_z . \tag{2.7}$$

Because the radius of the shell is much larger than its thickness, we can neglect the effect of rotary inertia; therefore, the only body force intensity acting on the shell in this problem is the d'Alembert force caused by the translatory inertia measured in the rotating frame of reference. The absolute acceleration of a shell element located at $\vec{r}_1'$ is given by

$$\vec{a}' = \vec{a}'_{rel} + \Omega'\vec{e}_z \times \left(\Omega'\vec{e}_z \times \vec{r}_1'\right) + 2\Omega'\vec{e}_z \times \vec{v}'_{rel}, \tag{2.8}$$

where the relative velocity with respect to the rotating frame of reference is given by

$$\vec{v}'_{rel} = \frac{\partial}{\partial t'}\begin{Bmatrix} u' \\ v' \\ w' \end{Bmatrix}, \tag{2.9}$$

and the relative acceleration by

$$\vec{a}'_{rel} = \frac{\partial^2}{\partial t'^2}\begin{Bmatrix} u' \\ v' \\ w' \end{Bmatrix}. \tag{2.10}$$

The three components of the absolute acceleration can then be written as

$$a'_z = \frac{\partial^2 u'}{\partial t'^2}, \tag{2.11}$$

$$a'_\theta = \frac{\partial^2 v'}{\partial t'^2} - \Omega'^2 v' + 2\Omega'\frac{\partial w'}{\partial t'}, \tag{2.12}$$

$$a'_r = \frac{\partial^2 w'}{\partial t'^2} - 2\Omega'\frac{\partial v'}{\partial t'} - \Omega'^2 w' - R'\Omega'^2. \tag{2.13}$$

The d'Alembert force intensity created by the acceleration of a shell element is proportional to its density ρ'_s multiplied by its thickness (the mass of a unit surface area)

$$\vec{F}'_{DA} = -\rho'_s h' \vec{a}'. \tag{2.14}$$

The only surface force intensity acting on the shell is caused by the interaction of the shell with the fluid at the interface:

$$\vec{F}'_f = \begin{Bmatrix} F'_{f,z} \\ F'_{f,\theta} \\ F'_{f,r} \end{Bmatrix}, \tag{2.15}$$

where $F'_{f,z}$, $F'_{f,\theta}$ and $F'_{f,r}$ are, respectively, the longitudinal, circumferential and radial components of the force intensity caused by the fluid on the wall.

The total force intensities acting on the shell surface are then (i) the d'Alembert force intensity of eq. (2.14), which can be evaluated using the acceleration components of eqs. (2.11)-(2.13), and (ii) the fluid force intensities of eq. (2.15):

$$q'_z = -\rho'_s h' \left[\frac{\partial^2 u'}{\partial t'^2} \right] + F'_{f,z}, \tag{2.16}$$

$$q'_\theta = -\rho'_s h' \left[\frac{\partial^2 v'}{\partial t'^2} - \Omega'^2 v' + 2\Omega' \frac{\partial w'}{\partial t'} \right] + F'_{f,\theta}, \tag{2.17}$$

$$q'_r = -\rho'_s h' \left[\frac{\partial^2 w'}{\partial t'^2} - 2\Omega' \frac{\partial v'}{\partial t'} - \Omega'^2 w' - R'\Omega'^2 \right] + F'_{f,r}. \tag{2.18}$$

By substituting eqs. (2.16)-(2.18) into eqs. (2.2)-(2.4), the structural part of the problem can be expressed in one linear matrix operator:

$$[\mathcal{L}'_S] \begin{Bmatrix} u' \\ v' \\ w' \end{Bmatrix} = \rho'_s h' \begin{Bmatrix} 0 \\ 0 \\ R'\Omega'^2 \end{Bmatrix} - \begin{Bmatrix} F'_{f,z} \\ F'_{f,\theta} \\ -F'_{f,r} \end{Bmatrix}, \tag{2.19}$$

where

$$\frac{1-\nu^2}{E'h'}[\mathcal{L}'_S] =$$

$$\begin{bmatrix} \left[\frac{\partial^2}{\partial z'^2} + \frac{1-\nu}{2R'^2} \frac{\partial^2}{\partial \theta^2} - \rho'_s \frac{1-\nu^2}{E'} \frac{\partial^2}{\partial t'^2} \right] & \frac{1+\nu}{2R'} \frac{\partial^2}{\partial z' \partial \theta} & \frac{\nu}{R'} \frac{\partial}{\partial z'} \\ \frac{1+\nu}{2R'} \frac{\partial^2}{\partial z' \partial \theta} & \left[\frac{1-\nu}{2} \frac{\partial^2}{\partial z'^2} + \frac{1}{R'^2} \frac{\partial^2}{\partial \theta^2} - \rho'_s \frac{1-\nu^2}{E'} \left(\frac{\partial^2}{\partial t'^2} - \Omega'^2 \right) \right] & \left[\frac{1}{R'^2} \frac{\partial}{\partial \theta} - 2\Omega' \rho'_s \frac{1-\nu^2}{E'} \frac{\partial}{\partial t'} \right] \\ \frac{\nu}{R'} \frac{\partial}{\partial z'} & \left[\frac{1}{R'^2} \frac{\partial}{\partial \theta} - 2\Omega' \rho'_s \frac{1-\nu^2}{E'} \frac{\partial}{\partial t'} \right] & \left[\frac{1}{R'^2} + \frac{h'^2}{12} \nabla'^2 \nabla'^2 + \rho'_s \frac{1-\nu^2}{E'} \left(\frac{\partial^2}{\partial t'^2} - \Omega'^2 \right) \right] \end{bmatrix}. \tag{2.20}$$

One can notice that the signs of the radial components of eq. (2.19) are reversed as compared with eq. (2.4). The sign change was made to preserve the symmetry of the matrix linear operator. As pointed out in Leissa (1973), nonsymmetric equations of motion can yield imaginary vibration frequencies.

The following quantities are introduced to make the analysis dimensionless, namely the timescale, the thickness ratio and the density ratio:

$$\gamma' \equiv R'\sqrt{\rho_s' \frac{1-\nu^2}{E'}}, \quad h \equiv \frac{h'}{R'}, \quad \Gamma \equiv \frac{\rho_s'}{\rho'}, \tag{2.21}$$

which lead to dimensionless quantities of time, rotation rate, position, force intensity and deformation:

$$t = \frac{t'}{\gamma'}, \quad \Omega = \gamma'\Omega', \quad r = \frac{r'}{R'}, \quad z = \frac{z'}{R'}, \quad \vec{F}_f = \frac{\gamma'^2}{\rho' R'^2}\vec{F}_f',$$
$$\begin{Bmatrix} F_{f,z} \\ F_{f,\theta} \\ F_{f,r} \end{Bmatrix} = \frac{\gamma'^2}{\rho' R'^2}\begin{Bmatrix} F_{f,z}' \\ F_{f,\theta}' \\ F_{f,r}' \end{Bmatrix}, \quad \begin{Bmatrix} u \\ v \\ w \end{Bmatrix} = \frac{1}{R'}\begin{Bmatrix} u' \\ v' \\ w' \end{Bmatrix}. \tag{2.22}$$

With the quantities of eqs. (2.22), the undeformed and deformed position vectors (2.6) and (2.7) can be made dimensionless:

$$\vec{r}_0 = \vec{e}_r + z\vec{e}_z, \tag{2.23}$$

$$\vec{r}_1 = (1+w)\vec{e}_r + v\vec{e}_\theta + (z+u)\vec{e}_z. \tag{2.24}$$

Eq. (2.19) can then be rewritten in dimensionless form:

$$[\mathcal{L}_S]\begin{Bmatrix} u \\ v \\ w \end{Bmatrix} - \begin{Bmatrix} 0 \\ 0 \\ \Omega^2 \end{Bmatrix} = \frac{-1}{h\Gamma}\begin{Bmatrix} F_{f,z} \\ F_{f,\theta} \\ -F_{f,r} \end{Bmatrix}, \tag{2.25}$$

where the dimensionless structural operator take this form:

$$[\mathcal{L}_S] = \begin{bmatrix} \frac{\partial^2}{\partial z^2} + \frac{1-\nu}{2}\frac{\partial^2}{\partial \theta^2} - \frac{\partial^2}{\partial t^2} & \frac{1+\nu}{2}\frac{\partial^2}{\partial z \partial \theta} & \nu\frac{\partial}{\partial z} \\ \frac{1+\nu}{2}\frac{\partial^2}{\partial z \partial \theta} & \frac{1-\nu}{2}\frac{\partial^2}{\partial z^2} + \frac{\partial^2}{\partial \theta^2} + \Omega^2 - \frac{\partial^2}{\partial t^2} & \frac{\partial}{\partial \theta} - 2\Omega\frac{\partial}{\partial t} \\ \nu\frac{\partial}{\partial z} & \frac{\partial}{\partial \theta} - 2\Omega\frac{\partial}{\partial t} & 1 + \frac{h^2}{12}\nabla^2\nabla^2 - \Omega^2 + \frac{\partial^2}{\partial t^2} \end{bmatrix}. \tag{2.26}$$

In eq. (2.25) the Ω^2 term accounts for the static centrifugal force acting on the shell introduced by the steady rotation. Its effect is not accounted for in this stability analysis as it only induces a static deformation. The interested reader can refer to

Païdoussis et al. (1985) to understand how the static forces can be accounted for in the model.

To investigate the stability of the shell to travelling waves, we assume a solution of the following form:

$$\begin{Bmatrix} u \\ v \\ w \end{Bmatrix} \equiv \begin{Bmatrix} \bar{u} \\ \bar{v} \\ \bar{w} \end{Bmatrix} \exp\left(-ikz - in\theta + i\omega t\right) = \begin{Bmatrix} \bar{u} \\ \bar{v} \\ \bar{w} \end{Bmatrix} \exp\left(i\alpha\right), \tag{2.27}$$

where ω, k and n are the dimensionless frequency, axial wavenumber and circumferential wavenumber and where $\bar{u}$, $\bar{v}$ and $\bar{w}$ are the initial dimensionless amplitudes much smaller than 1. Substituting the solution of eq. (2.27) in eq. (2.25) leads to:

$$\left[L_\alpha\right] \begin{Bmatrix} \bar{u} \\ \bar{v} \\ \bar{w} \end{Bmatrix} \exp\left(-ikz - in\theta + i\omega t\right) - \begin{Bmatrix} 0 \\ 0 \\ \Omega^2 \end{Bmatrix} = \frac{-1}{h\Gamma} \begin{Bmatrix} F_{f,z} \\ F_{f,\theta} \\ -F_{f,r} \end{Bmatrix}, \tag{2.28}$$

where

$$\left[L_\alpha\right] = \begin{bmatrix} -k^2 - \frac{1-\nu}{2}n^2 + \omega^2 & -\frac{1+\nu}{2}kn & -i\nu k \\ -\frac{1+\nu}{2}kn & -\frac{1-\nu}{2}k^2 - n^2 + \Omega^2 + \omega^2 & -in - i2\Omega\omega \\ -i\nu k & -in - i2\Omega\omega & 1 + \frac{h^2}{12}\left(k^2 + n^2\right)^2 - \Omega^2 - \omega^2 \end{bmatrix} \tag{2.29}$$

The objective now is to eventually express eq. (2.28) in the form

$$\left[L\right] \begin{Bmatrix} u \\ v \\ w \end{Bmatrix} = 0, \tag{2.30}$$

where $\left[L\right]$ is a 3×3 matrix accounting for both the structural and the fluid forces of the system. By rewriting the force balance as an eigenvalue problem, we can obtain a dispersion relation (a relation between ω, k, n, and Ω) by expanding $\det\left[L\right] = 0$. For this, we first need to reformulate the fluid forces acting on the shell in the same form as eq. (2.27).

2.2. Formulation of the inviscid fluid model

The fluid force intensities acting on the shell and defined in eq. (2.15) are the projection of the fluid stress tensor on the interface

$$\vec{F}'_f = \begin{Bmatrix} F'_{f,z} \\ F'_{f,\theta} \\ F'_{f,r} \end{Bmatrix} = -\begin{Bmatrix} \sigma'_{rz} \\ \sigma'_{r\theta} \\ \sigma'_{rr} \end{Bmatrix}_{\vec{r}'=\vec{r}'_1}, \tag{2.31}$$

where σ'_{rz}, $\sigma'_{r\theta}$ and σ'_{rr} are respectively the shear stresses and the radial stress in the fluid and where $\vec{r}'_1$ is the position of the deformed wall defined in eq. (2.7). Notice that here we make the approximation that the difference between the position of the middle and the inner surface of the shell is negligible. This approximation, which only influences the calculations of the effect of the fluid on the shell, is acceptable for very thin shells, as is the case here. It is usual to make this simplification in fluid-structure interaction studies with shells and it was also made by Lai and Chow (1973) and El Chebair et al. (1990).

With the quantities of eqs. (2.21), we can define the dimensionless stresses in the fluid

$$\begin{Bmatrix} \sigma_{rz} \\ \sigma_{r\theta} \\ \sigma_{rr} \end{Bmatrix} = \frac{\gamma'^2}{\rho' R'^2} \begin{Bmatrix} \sigma'_{rz} \\ \sigma'_{r\theta} \\ \sigma'_{rr} \end{Bmatrix}. \tag{2.32}$$

By assuming inviscid flow, the shear components of the fluid stress can be set to zero:

$$\sigma_{rz} = \sigma_{r\theta} = 0 \tag{2.33}$$

and the radial component is simply the pressure:

$$\sigma_{rr} = -P. \tag{2.34}$$

In order to find the effect of the fluid on the shell, all that must be found is the pressure P at position $\vec{r}_1$.

Consider an incompressible inviscid fluid of density ρ' bounded by a cylindrical surface of infinite length and radius R'. The whole undergoes solid body rotation about the axis of the cylinder at rate Ω', and the dynamics is studied in a frame of reference rotating at the same rate Ω'. The fluid flows axially with a velocity $\bar{U}'$, constant across

the section of the cylinder. The system is described with the same orthogonal dimensional coordinates defined for the structural problem in Section 2.1; namely r', θ, z' which are respectively in the radial, circumferential and axial directions. Along these coordinates are defined the unit vectors $\vec{e}_r$, $\vec{e}_\theta$ and $\vec{e}_z$. Recall that the dimensional variables are marked with a prime, $(\ )'$, as opposed to the dimensionless variables. The general behaviour of the inviscid flow of an incompressible fluid with constant density obeys Euler's equation and continuity:

$$\rho'\left[\frac{\partial \vec{V}'}{\partial t'}+\left(\vec{V}'\cdot\vec{\nabla}'\right)\vec{V}'\right]=-\vec{\nabla}'P'+\rho'\vec{Q}', \tag{2.35}$$

$$\vec{\nabla}'\cdot\vec{V}'=0. \tag{2.36}$$

In order to nondimensionalize the equations of motion of the fluid (eqs. (2.35)-(2.36)), a scaling velocity has to be introduced. The reduced velocity scales the average mean flow velocity with respect to the structural timescale and size scale (eqs. (2.21)):

$$\bar{U}_R=\frac{\bar{U}'\gamma'}{R'}\equiv\bar{U}'\sqrt{\rho_s'\frac{\left(1-\nu^2\right)}{E'}}, \tag{2.37}$$

where $\bar{U}'$ is the average dimensional flow velocity in the cylinder. Some authors utilize the Strouhal number – strictly the inverse of the reduced velocity – to nondimensionalize their equations. We also introduce the dimensionless pressure, fluid particle velocity and external force

$$P\equiv\frac{P'\gamma'^2}{\rho'R'^2},\quad \vec{V}\equiv\frac{\vec{V}'\gamma'}{R'},\quad \vec{Q}\equiv\frac{\vec{Q}'\gamma'^2}{R'}. \tag{2.38}$$

Making use of the quantities defined in eqs. (2.21), (2,22) and (2.38), eqs. (2.35) and (2.36) can be rewritten in dimensionless form:

$$\frac{\partial \vec{V}}{\partial t}+\left(\vec{V}\cdot\vec{\nabla}\right)\vec{V}=-\vec{\nabla}P+\vec{Q}, \tag{2.39}$$

$$\vec{\nabla}\cdot\vec{V}=0. \tag{2.40}$$

We consider the fluid in a frame of reference rotating at the same rate as the solid body rotation the shell-fluid assembly is subjected to. The effect of the solid body rotation on the fluid can be expressed as a force field:

$$\vec{Q} = \Omega^2 r \vec{e}_r . \tag{2.41}$$

If we introduce the dimensionless velocity components in the radial, circumferential and axial directions

$$\vec{V} = \begin{Bmatrix} V_r \\ V_\theta \\ V_z \end{Bmatrix}, \tag{2.42}$$

the dimensionless Euler equation (2.39) can be rewritten in cylindrical coordinates in scalar form:

$$\begin{aligned}
&\frac{\partial V_r}{\partial t} - 2\Omega V_\theta + V_r \frac{\partial V_r}{\partial r} + \frac{V_\theta}{r}\frac{\partial V_r}{\partial \theta} - \frac{V_\theta^2}{r} + V_z \frac{\partial V_r}{\partial z} - \Omega^2 r = -\frac{\partial P}{\partial r}, \\
&\frac{\partial V_\theta}{\partial t} + 2\Omega V_r + V_r \frac{\partial V_\theta}{\partial r} + \frac{V_\theta}{r}\frac{\partial V_\theta}{\partial \theta} + \frac{V_r V_\theta}{r} + V_z \frac{\partial V_\theta}{\partial z} = -\frac{1}{r}\frac{\partial P}{\partial \theta}, \\
&\frac{\partial V_z}{\partial t} + V_r \frac{\partial V_z}{\partial r} + \frac{V_\theta}{r}\frac{\partial V_z}{\partial \theta} + V_z \frac{\partial V_z}{\partial z} = -\frac{\partial P}{\partial z}.
\end{aligned} \tag{2.43}$$

In eqs. (2.43) the Coriolis terms arise from the rotating frame of reference. The continuity equation (2.40) in cylindrical coordinates is as follows:

$$\frac{1}{r}\frac{\partial}{\partial r}(rV_r) + \frac{1}{r}\frac{\partial V_\theta}{\partial \theta} + \frac{\partial V_z}{\partial z} = 0 . \tag{2.44}$$

Because the present study is linear, we make the assumption that the normal to the underformed shell surface remains unchanged as the shell deforms. Because of this simplification, we make the implicit assumption that only the radial displacement w (eq. (2.27)) of the shell influences the flow (not the circumferential and the axial displacements u and v). This is inevitable, as an inviscid fluid cannot transmit shear.

Since we assume that the normal vector to the shell surface does not change as the shell deforms, the impermeability condition is applied in the direction of the normal to the surface and free slip is allowed in the parallel directions. Knowing that the normal to the undeformed cylindrical shell wall is in the radial direction, in order to satisfy the no penetration boundary condition, the radial velocity of the flow has to match the radial velocity of the shell wall:

$$V_r\big|_{\vec{r}=\vec{r}_1} = \left.\frac{Dw}{Dt}\right|_{\vec{r}=\vec{r}_1}, \tag{2.45}$$

in which

$$\frac{D}{Dt} = V_r \frac{\partial}{\partial r} + \frac{V_\theta}{r}\frac{\partial}{\partial \theta} + V_z \frac{\partial}{\partial z} + \frac{\partial}{\partial t}, \tag{2.46}$$

and where w is defined in eq. (2.27) and $\vec{r}_1$ in eq. (2.24). Eq. (2.46) is substituted into eq. (2.45), yielding

$$V_r\big|_{\vec{r}=\vec{r}_1} = \left[V_r \frac{\partial w}{\partial r} + \frac{V_\theta}{r}\frac{\partial w}{\partial \theta} + V_z \frac{\partial w}{\partial z} + \frac{\partial w}{\partial t} \right]_{\vec{r}=\vec{r}_1}. \tag{2.47}$$

The derivatives of w can be evaluated by making use of the definition of eq. (2.27)

$$V_r\big|_{\vec{r}=\vec{r}_1} = \left[w\left(-in\frac{V_\theta}{r} - ikV_z + i\omega \right) \right]_{\vec{r}=\vec{r}_1}. \tag{2.48}$$

In view of eq. (2.27), we can apply a perturbation scheme with a travelling wave solution of the following form :

$$\begin{aligned}
P = \;& P_0(r) + p(r)\exp(-ikz - in\theta + i\omega t) && = P_0(r) + p(r)e^{i\alpha}, \\
V_r = \;& v_r(r)\exp(-ikz - in\theta + i\omega t) && = v_r(r)e^{i\alpha}, \\
V_\theta = \;& v_\theta(r)\exp(-ikz - in\theta + i\omega t) && = v_\theta(r)e^{i\alpha}, \\
V_z = \;& \bar{U}_R + v_z(r)\exp(-ikz - in\theta + i\omega t) && = \bar{U}_R + v_z(r)e^{i\alpha}.
\end{aligned} \tag{2.49}$$

The perturbation solution (2.49) is then substituted into eq. (2.48) ; thus,

$$\left[v_r e^{i\alpha} \right]_{\vec{r}=\vec{r}_1} = \left[w\left(i\omega - in\frac{v_\theta}{r} w - ik\left\{ \bar{U}_R + v_z w \right\} \right) \right]_{\vec{r}=\vec{r}_1}. \tag{2.50}$$

Because the boundary condition (2.50) is exclusively composed of perturbation terms, the difference between evaluating it at the instantaneous shell position $\vec{r}_1$ or at the mean position of the shell $\vec{r}_0$ is of second order, hence negligible. This is further discussed in Appendix A. By neglecting second-order terms as well as the difference between evaluating eq. (2.50) at $\vec{r}_0$ instead of $\vec{r}_1$, the first-order approximation of the radial velocity at the boundary can be written as

$$v_r\big|_{r=1} = i\left(\omega - k\bar{U}_R\right)\bar{w} \text{ or } V_r\big|_{r=1} = i\left(\omega - k\bar{U}_R\right)w, \tag{2.51}$$

where the definitions of eqs. (2.27) and (2.49) are used to relate the two versions of eq. (2.51). The no-penetration boundary condition obtained in eq. (2.51) is identical to what Lai and Chow (1973) obtained. In the circumferential and longitudinal directions, the fluid is subjected to a free-slip boundary condition.

We can find the steady pressure distribution by substituting the perturbation scheme of eqs. (2.49) into the first of eqs. (2.43) and setting all perturbation terms equal to zero. This gives

$$-\Omega^2 r = -\frac{\partial P_0}{\partial r}. \tag{2.52}$$

By integrating we get

$$P_0(r) = P_R - \tfrac{1}{2}\Omega^2\left(1-r^2\right), \tag{2.53}$$

where P_R is the constant pressure at the shell-fluid interface. This term, which leads to a static deformation, can be used to model the pressurisation of the shell, but its effect cannot be accounted for with the current form of this linear stability analysis. This issue is similar to what is discussed just after eq. (2.26) for the Ω^2 term of eq. (2.25). The pressure in the flow can be found by substituting the steady pressure from eq. (2.53) into the perturbation solution of eqs. (2.49)

$$P = P_R - \tfrac{1}{2}\Omega^2\left(1-r^2\right) + p(r)e^{i\alpha}. \tag{2.54}$$

We substitute the perturbation scheme of eqs. (2.49) into the three components of Euler's equation (2.43) and the continuity equation (2.44), making use of eq. (2.52) to remove the steady pressure terms; thus we get

$$i\left(\omega - \bar{U}_R k\right)v_r - 2\Omega v_\theta = -\frac{\partial p}{\partial r}, \tag{2.55}$$

$$2\Omega v_r + i\left(\omega - \bar{U}_R k\right)v_\theta = \frac{in}{r}p, \tag{2.56}$$

$$\left(\omega - \bar{U}_R k\right)v_z = kp, \tag{2.57}$$

$$\frac{v_r}{r} + \frac{\partial v_r}{\partial r} - \frac{in}{r}v_\theta - ikv_z = 0. \tag{2.58}$$

The reader might be interested in having a look at the partial differential equation system obtained by introducing a simple perturbation scheme into eqs. (2.43)-(2.44) and have a careful look at the linearization of the system of equations. This is done in Appendix B.

By making use of eqs. (2.49), (2.55) and (2.56), after some manipulation the boundary condition of eq. (2.51) can be reformulated as a pressure boundary condition:

$$\left[\frac{\partial p}{\partial r}-n\frac{2\Omega}{\omega-k\bar{U}_R}\frac{p}{r}\right]_{r=1}=\left(\omega-k\bar{U}_R\right)^2\left(1-\left(\frac{2\Omega}{\omega-k\bar{U}_R}\right)^2\right)\bar{w}. \tag{2.59}$$

We now define a dimensionless parameter relating the rate of rotation to the difference between the travelling-wave velocity and the axial flow rate:

$$\Lambda\equiv\frac{2\Omega}{\omega-k\bar{U}_R}. \tag{2.60}$$

This dimensionless parameter can be thought of as the inverse of the pitch of the flow: it counts how many rotations a flow particle undergoes during its axial travel between two crests of amplitude of a travelling wave. To relate to the work of Chow (1969) and Maslowe (1974), the quantity $1/k\Lambda$ can be thought of as a modified Rossby number, where $\bar{U}_R-\omega/k$ is the velocity of the flow relative to the travelling waves in the shell. The Rossby number was defined in eq. (2) of Chapter 1 as $\varepsilon=\bar{U}_R/2\Omega$.

With some manipulations, eqs. (2.55)-(2.58) can be combined with eq. (2.60), to reduce the system of four equations and four variable to an ODE of the perturbation pressure:

$$\frac{\partial^2 p}{\partial r^2}+\frac{1}{r}\frac{\partial p}{\partial r}-\left[\frac{n^2}{r^2}+k^2\left(1-\Lambda^2\right)\right]p=0. \tag{2.61}$$

Eq. (2.61) is a variant of Bessel's equation. It can be solved with different functions depending on the value of Λ. The solution is completely determined by satisfying the boundary condition of eq. (2.59).

Three solutions are obtained:

for $\Lambda^2>1$

$$p(r)=\frac{\left(\omega-k\bar{U}_R\right)^2\left(1-\Lambda^2\right)\mathrm{J}_n\left(rk\sqrt{\Lambda^2-1}\right)}{k\sqrt{\Lambda^2-1}\mathrm{J}_{n-1}\left(k\sqrt{\Lambda^2-1}\right)-n(\Lambda+1)\mathrm{J}_n\left(k\sqrt{\Lambda^2-1}\right)}\bar{w}; \tag{2.62}$$

for $\Lambda^2<1$

$$p(r)=\frac{\left(\omega-k\bar{U}_R\right)^2\left(1-\Lambda^2\right)\mathrm{I}_n\left(rk\sqrt{1-\Lambda^2}\right)}{k\sqrt{1-\Lambda^2}\mathrm{I}_{n-1}\left(k\sqrt{1-\Lambda^2}\right)-n(\Lambda+1)\mathrm{I}_n\left(k\sqrt{1-\Lambda^2}\right)}\bar{w}; \tag{2.63}$$

for $\Lambda^2=1$ and $n\neq 0$

$$p(r)=\left(\omega-k\bar{U}_R\right)^2\frac{2}{|n|}r^{|n|}\bar{w}; \tag{2.64}$$

and for $\Lambda^2=1$ and $n=0$, no solution other than the trivial solution is found.

Eqs. (2.62) and (2.63) are equivalent to the perturbation pressure found by Lai and Chow (1973). However, eq. (2.64) differs slightly from the solution of Lai and Chow[†]. Little information is given by Lai and Chow (1973) or even Lai (1972) relative to the algebraic manipulations leading to their perturbation pressure solution. In any case, the solution of eq. (2.64) is only valid for two straight lines on the $\omega-\bar{U}_R$ parameter space.

2.3. Coupling of fluid and structure

The pressure exerted by the fluid on the shell surface can be expressed linearly by expanding it around the mean wall position and neglecting the second order terms of a Taylor expansion:

$$P\big|_{\vec{r}=\vec{r}_1}=P\big|_{\vec{r}=\vec{r}_0}+w\frac{\partial P}{\partial r}\bigg|_{\vec{r}=\vec{r}_0}+v\frac{1}{r}\frac{\partial P}{\partial\theta}\bigg|_{\vec{r}=\vec{r}_0}+u\frac{\partial P}{\partial z}\bigg|_{\vec{r}=\vec{r}_0}+O\left(u^2\right)+O\left(v^2\right)+O\left(w^2\right). \tag{2.65}$$

We substitute the pressure given by eq. (2.54) into the expansion of eq. (2.65) and neglect second order terms. Recalling that the mean position of the wall $\vec{r}_0$ is given in eq. (2.23), the pressure at the wall can then be written as a linear function of the wall displacement

$$P\big|_{\vec{r}=\vec{r}_1}\simeq P_R+\left[p\big|_{\vec{r}=\vec{r}_0}+\Omega^2\bar{w}\right]e^{i\alpha}. \tag{2.66}$$

Substituting eq. (2.66) into eq. (2.34) and making use of eqs. (2.33), the fluid stresses acting on the shell wall are found to be

$$\begin{Bmatrix}\sigma_{rz}\\ \sigma_{r\theta}\\ \sigma_{rr}\end{Bmatrix}_{\vec{r}=\vec{r}_1}=\begin{Bmatrix}0\\ 0\\ P_R+\left[p\big|_{\vec{r}=\vec{r}_0}+\Omega^2\bar{w}\right]e^{i\alpha}\end{Bmatrix}. \tag{2.67}$$

[†] In Lai and Chow, for $\Lambda^2=1$, $p(r)=\dfrac{8(n+1)\bar{w}\Omega^2r^n}{n(n+1)+k^2}=\left(\omega-k\bar{U}_R\right)^2\dfrac{2}{n}r^n\bar{w}\dfrac{n(n+1)}{(n+1)+k^2}$ was obtained as opposed to eq. (2.64) here.

In order to substitute eq. (2.67) back into the fluid-structure problem eq. (2.28), we introduce the following quantity, which can be thought of as a pressure influence coefficient relating the pressure exerted at the wall with the amplitude of the wall deflection:

$$\pi \equiv \frac{p\big|_{\vec{r}=\vec{r}_0}}{\overline{w}}. \tag{2.68}$$

Using eq. (2.68), eq. (2.67) can be substituted back into the fluid-structure problem eq. (2.28) to give

$$[L_\alpha]\begin{Bmatrix} u \\ v \\ w \end{Bmatrix} - \frac{1}{\chi\Gamma}\begin{bmatrix} 0 & 0 & 0 \\ 0 & 0 & 0 \\ 0 & 0 & \pi+\Omega^2 \end{bmatrix}\begin{Bmatrix} u \\ v \\ w \end{Bmatrix} = \frac{1}{h\Gamma}\begin{Bmatrix} 0 \\ 0 \\ P_R \end{Bmatrix} + \begin{Bmatrix} 0 \\ 0 \\ \Omega^2 \end{Bmatrix}. \tag{2.69}$$

One notices that the terms on the left-hand-side of eq. (2.69) are all perturbation terms proportional to *u, v, w,* while on the right-hand-side the terms are of zeroth order. These zeroth order terms cause static deformation of the shell. As discussed just after eqs. (2.26) and (2.53), the method of solution used here does not allow taking into consideration static deformation. If one drops these static terms of the right-hand-side, eq. (2.69) can be rewritten in the desired form of eq. (2.30), where the linear matrix accounting for the dynamics of the coupled system is given by

$$[L] = \begin{bmatrix} -k^2 - \frac{1-\nu}{2}n^2 + \omega^2 & -\frac{1+\nu}{2}kn & -i\nu k \\ -\frac{1+\nu}{2}kn & \left[-\frac{1-\nu}{2}k^2 - n^2 + \Omega^2 + \omega^2\right] & -in - i2\Omega\omega \\ -i\nu k & -in - i2\Omega\omega & \left[1+\frac{h^2}{12}\left(k^2+n^2\right)^2 - \Omega^2 - \omega^2 - \frac{1}{h\Gamma}\left(\pi+\Omega^2\right)\right] \end{bmatrix}. \tag{2.70}$$

Eq. (2.30) with matrix $[L]$ given by eq. (2.70) can be solved by taking its determinant equal to zero. A sixth order polynomial of variable ω is then obtained. Two methods are used to obtain the dispersion relation and be able to plot curves of ω versus $\bar{U}_R$. The first is an iterative numerical root-finding method, which consists of finding the pair of roots closest to zero, and then following their values as the flow velocity is incremented. The second is a zero-level contour method. For a given domain of ω and $\bar{U}_R$, the dispersion relation is evaluated and a zero-level contour plot is realized with this data. More information about these methods can be found in Pong (2000).

Chapter 3

Formulation of viscous model

In the formulation of the structural part of the inviscid model in Chapter 2, no assumptions were made regarding the flow which interacts with the shell. The shell model developed in Section 2.1 can therefore be used in the formulation of the viscous theory model as well. Eq. (29) from Section 2.1 gives the summation of forces in the three directions:

$$[L_\alpha]\begin{Bmatrix}\bar{u}\\ \bar{v}\\ \bar{w}\end{Bmatrix}\exp(-ikz-in\theta+i\omega t)-\begin{Bmatrix}0\\ 0\\ \Omega^2\end{Bmatrix}=\frac{-1}{h\Gamma}\begin{Bmatrix}F_{f,z}\\ F_{f,\theta}\\ -F_{f,r}\end{Bmatrix}, \tag{3.1}$$

where on the left-hand side of eq. (3.1) are the shell-related terms with the matrix $[\mathcal{L}_\alpha]$ defined in eq. (2.29), and where on the right-hand side of the equation is the vector of the force intensities produced by the fluid on the shell wall.

From eq.(2.31), recall that the dimensionless fluid force intensities acting on the shell are written as the fluid stresses evaluated at the deformed position of the shell

$$\vec{F}_f=\begin{Bmatrix}F_{f,z}\\ F_{f,\theta}\\ F_{f,r}\end{Bmatrix}=-\begin{Bmatrix}\sigma_{rz}\\ \sigma_{r\theta}\\ \sigma_{rr}\end{Bmatrix}_{\vec{r}=\vec{r}_1}. \tag{3.2}$$

One has to be careful with the signs of the three fluid stresses. Recall that in eq.(3.1), every term in the radial direction was made negative to preserve the symmetry of the matrix $[\mathcal{L}_\alpha]$. As in Chapter 2, we aim to get a flow solution which allows us to write the problem in the desired form, i.e.,

$$[L]\begin{Bmatrix}u\\ v\\ w\end{Bmatrix}=0. \tag{3.3}$$

3.1. Equations of motion of the viscous fluid

Consider an incompressible viscous fluid of density ρ' and viscosity μ', bounded by a cylindrical surface of infinite length and radius R'. The whole undergoes solid body rotation about the axis of the cylinder at rate Ω', and the dynamics is studied in a frame of reference rotating at the same rate Ω'. The fluid flows axially with a fully developed velocity profile $U'(r')$. The system is described with the same orthogonal dimensional coordinates defined for the structural problem in Section 2.1; namely r', θ, z', which are respectively in the radial, circumferential, and axial directions. Along these coordinates are defined the unit vectors $\vec{e}_r$, $\vec{e}_\theta$ and $\vec{e}_z$. Recall that the dimensional variables are marked with a prime, $(\ )'$, as opposed to the dimensionless variables. The equations of motion governing an incompressible viscous flow are the Navier-Stokes and the continuity equations:

$$\rho'\left[\frac{\partial \vec{V}'}{\partial t'}+\left(\vec{V}'\cdot\vec{\nabla}'\right)\vec{V}'\right]=-\vec{\nabla}'P'+\mu'\left[\nabla'^2\vec{V}'\right]+\rho'\vec{Q}', \tag{3.4}$$

$$\vec{\nabla}'\cdot\vec{V}'=0, \tag{3.5}$$

where $\vec{V}'$ is the fluid velocity and $\vec{Q}'$ is an external force acting on the fluid. In order to nondimensionalise the equations of motion of the fluid, we recall the timescale defined in eqs. (22) of Chapter 2:

$$\gamma' \equiv R'\sqrt{\rho_s'\frac{1-\nu^2}{E'}}.$$

With this timescale, we can define the reduced velocity $U_R(r)$ and the average reduced velocity $\bar{U}_R$ which scale the mean flow velocity $U(r)$ and the mean flow velocity averaged across the section of the cylinder $\bar{U}$ with respect to the structure time and size scales:

$$U_R(r)=\frac{U'(r')\gamma'}{R'}\equiv U'(r')\sqrt{\rho_s'\frac{1-\nu^2}{E'}}, \tag{3.6}$$

$$\bar{U}_R=\frac{\bar{U}'\gamma'}{R'}\equiv \bar{U}'\sqrt{\rho_s'\frac{1-\nu^2}{E'}}, \tag{3.7}$$

where $\bar{U}'$ is the average dimensional flow velocity across the section of the cylindrical shell. We also introduce the dimensionless pressure, fluid particle velocity and external force, defined as follows:

$$P \equiv \frac{P'\gamma'^2}{\rho' R'^2}, \quad \vec{V} \equiv \frac{\vec{V}'\gamma'}{R'}, \quad \vec{Q} \equiv \frac{\vec{Q}'\gamma'^2}{R'}. \tag{3.8}$$

The Reynolds number relates the inertial forces to the viscous forces in the flow:

$$\mathrm{Re} \equiv \frac{2\bar{U}'R'\rho'}{\mu'}. \tag{3.9}$$

Making use of the definitions of eqs. (3.7)-(3.9), the Navier-Stokes equation (3.4) and the continuity equation (3.5) can be rewritten in a dimensionless fashion:

$$\frac{\partial \vec{V}}{\partial t} + \left(\vec{V}\cdot\vec{\nabla}\right)\vec{V} = -\vec{\nabla}P + \frac{2\bar{U}_R}{\mathrm{R_e}}\left[\nabla^2\vec{V}\right] + \vec{Q}, \tag{3.10}$$

$$\vec{\nabla}\cdot\vec{V} = 0. \tag{3.11}$$

Here, the rotating frame of reference leads to the following external body force:

$$\vec{Q} = \Omega^2 r\vec{e}_r. \tag{3.12}$$

If we introduce the dimensionless flow velocity components in the radial, circumferential and axial directions,

$$\vec{V} = \begin{Bmatrix} V_r \\ V_\theta \\ V_z \end{Bmatrix}, \tag{3.13}$$

the dimensionless Navier-Stokes equation (3.10) can be rewritten in cylindrical coordinates in scalar form:

$$\begin{aligned} &\frac{\partial V_r}{\partial t} - 2\Omega V_\theta + V_r\frac{\partial V_r}{\partial r} + \frac{V_\theta}{r}\frac{\partial V_r}{\partial \theta} - \frac{V_\theta^2}{r} + V_z\frac{\partial V_r}{\partial z} - \Omega^2 r \\ &= -\frac{\partial P}{\partial r} + \frac{2\bar{U}_R}{\mathrm{Re}}\left[\frac{\partial}{\partial r}\left(\frac{1}{r}\frac{\partial}{\partial r}\left(rV_r\right)\right) + \frac{1}{r^2}\frac{\partial^2 V_r}{\partial \theta^2} + \frac{\partial^2 V_r}{\partial z^2} - \frac{2}{r^2}\frac{\partial V_\theta}{\partial \theta}\right], \end{aligned} \tag{3.14}$$

$$\begin{aligned} &\frac{\partial V_\theta}{\partial t} + 2\Omega V_r + V_r\frac{\partial V_\theta}{\partial r} + \frac{V_\theta}{r}\frac{\partial V_\theta}{\partial \theta} + \frac{V_r V_\theta}{r} + V_z\frac{\partial V_\theta}{\partial z} \\ &= -\frac{1}{r}\frac{\partial P}{\partial \theta} + \frac{2\bar{U}_R}{\mathrm{Re}}\left[\frac{\partial}{\partial r}\left(\frac{1}{r}\frac{\partial}{\partial r}\left(rV_\theta\right)\right) + \frac{1}{r^2}\frac{\partial^2 V_\theta}{\partial \theta^2} + \frac{\partial^2 V_\theta}{\partial z^2} + \frac{2}{r^2}\frac{\partial V_r}{\partial \theta}\right], \end{aligned} \tag{3.15}$$

$$\frac{\partial V_z}{\partial t}+V_r\frac{\partial V_z}{\partial r}+\frac{V_\theta}{r}\frac{\partial V_z}{\partial \theta}+V_z\frac{\partial V_z}{\partial z}$$
$$=-\frac{\partial P}{\partial z}+\frac{2\bar{U}_R}{\mathrm{Re}}\left[\frac{1}{r}\frac{\partial}{\partial r}\left(r\frac{\partial V_z}{\partial r}\right)+\frac{1}{r^2}\frac{\partial^2 V_z}{\partial \theta^2}+\frac{\partial^2 V_z}{\partial z^2}\right]. \tag{3.16}$$

In eqs. (3.14) and (3.15), the Coriolis terms arise from the rotating frame of reference. The continuity equation (3.11) in cylindrical coordinates written with respect to the velocity components of eq. (3.13), is

$$\frac{1}{r}\frac{\partial}{\partial r}(rV_r)+\frac{1}{r}\frac{\partial V_\theta}{\partial \theta}+\frac{\partial V_z}{\partial z}=0. \tag{3.17}$$

Consistently with the assumptions made to derive the Donnell-Mushtari shell equations, we make the assumption that the normal vector to the shell surface does not change as the shell deforms; this is conventional in a linear analysis. Hence, for a no-slip boundary condition, the velocity of the fluid at the wall is simply the velocity of the wall:

$$V_r\big|_{\vec{r}=\vec{r}_1}=\left.\frac{Dw}{Dt}\right|_{\vec{r}=\vec{r}_1},$$
$$V_\theta\big|_{\vec{r}=\vec{r}_1}=\left.\frac{Dv}{Dt}\right|_{\vec{r}=\vec{r}_1}, \tag{3.18}$$
$$V_z\big|_{\vec{r}=\vec{r}_1}=\left.\frac{Du}{Dt}\right|_{\vec{r}=\vec{r}_1},$$

where u, v, w are the three shell perturbation quantities defined in eq. (2.27):

$$\begin{Bmatrix}u\\v\\w\end{Bmatrix}\equiv\begin{Bmatrix}\bar{u}\\\bar{v}\\\bar{w}\end{Bmatrix}\exp(-ikz-in\theta+i\omega t)=\begin{Bmatrix}\bar{u}\\\bar{v}\\\bar{w}\end{Bmatrix}\exp(i\alpha). \tag{3.19}$$

The material derivative is given by

$$\frac{D}{Dt}=\frac{\partial}{\partial t}+V_r\frac{\partial}{\partial r}+\frac{V_\theta}{r}\frac{\partial}{\partial \theta}+V_z\frac{\partial}{\partial z}. \tag{3.20}$$

Making use of the definitions of eqs. (3.19) and (3.20), the boundary conditions of eqs. (3.18) can be rewritten as

$$
\begin{aligned}
V_r\big|_{\vec{r}=\vec{r}_1} &= w\left[i\omega - \frac{in}{r}V_\theta - ikV_z \right]_{\vec{r}=\vec{r}_1}, \\
V_\theta\big|_{\vec{r}=\vec{r}_1} &= v\left[i\omega - \frac{in}{r}V_\theta - ikV_z \right]_{\vec{r}=\vec{r}_1}, \\
V_z\big|_{\vec{r}=\vec{r}_1} &= u\left[i\omega - \frac{in}{r}V_\theta - ikV_z \right]_{\vec{r}=\vec{r}_1}.
\end{aligned}
\tag{3.21}
$$

One quickly notices the added complexity when comparing eqs. (3.21) with eq. (2.51), the boundary conditions of the inviscid theory; under the free-slip and impermeability conditions, only the transverse displacement w affects the flow, as shear cannot be transmitted by inviscid flow. With the inclusion of viscosity in the model, all three shell perturbation components have an influence on the flow. So, now, we are dealing with a system subjected to not one but three perturbations. The idea to be developed in what follows, is to superpose three different fluid solutions, each proportional to one of the three perturbations.

3.2. Triple perturbation scheme

Similarly to what is done in the inviscid model, the velocity of the fluid is decomposed in two distinct parts, namely the steady mean flow velocityand the unsteady perturbation velocity:

$$
\vec{V}(r,\theta,z,t) = \vec{V}_0(r) + \vec{v}(r)e^{i\alpha}, \tag{3.22}
$$

where the perturbation velocity bears a travelling-wave form identical to eq. (3.19). Since the perturbation of the flow is due to the three deflections of the shell, the perturbation velocity is expanded as a power series of the amplitude of these deflections

$$
\begin{aligned}
\vec{v}(r) = \vec{\hat{v}}_w(r)\overline{w} + \vec{\hat{v}}_v(r)\overline{v} + \vec{\hat{v}}_u(r)\overline{u} + \frac{1}{2!}\Big[& \vec{\hat{v}}_{ww}(r)\overline{w}^2 + \vec{\hat{v}}_{vv}(r)\overline{v}^2 + \vec{\hat{v}}_{uu}(r)\overline{u}^2 \\
& + 2\vec{\hat{v}}_{vw}(r)\overline{v}\,\overline{w} + 2\vec{\hat{v}}_{uv}(r)\overline{u}\,\overline{v} + 2\vec{\hat{v}}_{uw}(r)\overline{u}\,\overline{w} \Big] + \ldots,
\end{aligned}
\tag{3.23}
$$

where the vectors $\vec{\hat{v}}_x(r)$ are velocity "influence functions" which relate the fluid velocity at location r caused by one or more perturbation indicated in the subscript. These velocity influence functions are not small; the amplitude of the shell deflections, on the other

hand, is assumed in the derivation of the shell equations to be arbitrarily small. Since this is a linear study, we consider only first-order terms,

$$\vec{v}(r) = \vec{\hat{v}}_w(r)\overline{w} + \vec{\hat{v}}_v(r)\overline{v} + \vec{\hat{v}}_u(r)\overline{u}\,. \tag{3.24}$$

The perturbation velocity vector of eq. (3.24) can be written in component/matrix form:

$$\begin{Bmatrix} v_z \\ v_\theta \\ v_r \end{Bmatrix} = \begin{bmatrix} \hat{v}_{z,u}(r) & \hat{v}_{z,v}(r) & \hat{v}_{z,w}(r) \\ \hat{v}_{\theta,u}(r) & \hat{v}_{\theta,v}(r) & \hat{v}_{\theta,w}(r) \\ \hat{v}_{r,u}(r) & \hat{v}_{r,v}(r) & \hat{v}_{r,w}(r) \end{bmatrix} \begin{Bmatrix} \overline{u} \\ \overline{v} \\ \overline{w} \end{Bmatrix}. \tag{3.25}$$

Since the only mean flow velocity component is along the axis and is given by eq. (3.6), eq. (3.22) can be rewritten in component form by making use of eq. (3.25):

$$\begin{Bmatrix} V_z(r,\theta,z,t) \\ V_\theta(r,\theta,z,t) \\ V_r(r,\theta,z,t) \end{Bmatrix} = \begin{Bmatrix} U_R(r) \\ 0 \\ 0 \end{Bmatrix} + \begin{bmatrix} \hat{v}_{z,u}(r) & \hat{v}_{z,v}(r) & \hat{v}_{z,w}(r) \\ \hat{v}_{\theta,u}(r) & \hat{v}_{\theta,v}(r) & \hat{v}_{\theta,w}(r) \\ \hat{v}_{r,u}(r) & \hat{v}_{r,v}(r) & \hat{v}_{r,w}(r) \end{bmatrix} \begin{Bmatrix} \overline{u} \\ \overline{v} \\ \overline{w} \end{Bmatrix} e^{i\alpha}. \tag{3.26}$$

Through the Navier-Stokes equations (3.14)-(3.16), the perturbation velocity causes a perturbation pressure in the fluid, which takes a similar form as eq. (3.22),

$$P(r,\theta,z,t) = P_R + P_0(r,z) + p(r)e^{i\alpha}\,. \tag{3.27}$$

Similarly to the flow velocity influence functions of eq. (3.24), we introduce the pressure influence functions which are the superposed pressure perturbations caused by the three distinct perturbation amplitudes:

$$p(r) = \hat{p}_u(r)\overline{u} + \hat{p}_v(r)\overline{v} + \hat{p}_w(r)\overline{w}\,. \tag{3.28}$$

We then combine eqs. (3.27) and (3.28):

$$P(r,\theta,z,t) = P_R + P_0(r,z) + \left[\hat{p}_u(r)\overline{u} + \hat{p}_v(r)\overline{v} + \hat{p}_w(r)\overline{w}\right]e^{i\alpha}\,. \tag{3.29}$$

The introduction of the velocity and pressure influence functions is necessary in this solution scheme because of the nature of the problem we are solving. Since we are solving an eigenvalue problem (a linear problem), the amplitude of oscillation of the shell is unknown and arbitrary; it cannot be solved for. In analytical studies such as Lai and Chow (1973), the amplitude is explicitly kept throughout the derivation of the equations of motion, and it is cancelled out in the end when the equations of the shell and the fluid are coupled back together. It is impossible to do this here. Since we use numerical methods to solve the fluid we must solve for floating point values. The values we solve

for numerically cannot contain the arbitrary amplitude; this is why we shall solve for the velocity and pressure influence functions in order to obtain a solution for the flow.

3.3. Mean flow solutions

Two different mean flows are presented here: the laminar mean flow derived from the leading order terms of the Navier-Stokes equations and the turbulent mean flow based on empirical relationships.

3.3.1. Laminar mean flow

The steady solution to the problem of rotating viscous pipe-flow can be found by applying the perturbation scheme of eqs. (3.26) and (3.29) to eqs. (3.14) and (3.16) while keeping only the leading order terms:

$$-\Omega^2 r = -\frac{\partial P_0}{\partial r}, \tag{3.30}$$

$$0 = -\frac{\partial P_0}{\partial z} + \frac{2\bar{U}_R}{\mathrm{Re}}\left[\frac{1}{r}\frac{\partial}{\partial r}\left(r\frac{\partial}{\partial r}U_R(r)\right)\right]. \tag{3.31}$$

Since the flow is fully developed, we can assume that the steady pressure solution has the following form:

$$P_0(r,z) = \psi(r) + \zeta(z). \tag{3.32}$$

We substitute this solution back into eq.(3.30):

$$\frac{\partial \psi}{\partial r} = \Omega^2 r, \tag{3.33}$$

and by integrating we obtain

$$\psi(r) = \tfrac{1}{2}\Omega^2\left(r^2 - 1\right). \tag{3.34}$$

Then we substitute eq. (3.32) into eq. (3.31) and separate the z-dependant term from the r-dependant terms:

$$\frac{\partial \zeta}{\partial z} = \frac{2\bar{U}_R}{\mathrm{Re}}\left[\frac{1}{r}\frac{\partial}{\partial r}\left(r\frac{\partial}{\partial r}U_R(r)\right)\right] = \text{const.}, \tag{3.35}$$

which when integrated leads to the steady axial flow velocity profile:

$$U_R(r) = C_1 r^2 + C_2 \ln(r) + C_3 . \tag{3.36}$$

Since the velocity profile has to be finite for $0 \le r \le 1$, the logarithmic term must vanish; i.e., $C_2 = 0$.

Introducing the perturbation scheme of eq. (3.26) into the longitudinal boundary condition (3.18) and keeping only the zeroth-order term leads to the mean no-slip boundary condition

$$U_R(r)\big|_{r=1} = 0 . \tag{3.37}$$

Substituting eq. (3.37) in eq. (3.36), one finds that $C_3 = -C_1$. All that is missing to completely define the flow profile is a scaling constant. Since the average flow velocity $\bar{U}_R$ is already present in the equations of motion, it will be employed to scale the flow profile:

$$\bar{U}_R = \int_0^1 \left(C_1 r^2 - C_1\right) dr = -\frac{2}{3} C_1 . \tag{3.38}$$

We can then express the velocity flow profile as

$$U_R(r) = \frac{3}{2} \bar{U}_R \left(1 - r^2\right) . \tag{3.39}$$

This is the typical laminar Poisseuille or parabolic velocity profile. Inserting the velocity profile of eq. (3.39) in eq. (3.35), the axial pressure distribution can be found to be

$$\zeta = -12 \frac{\bar{U}_R^{\,2}}{\mathrm{Re}} z . \tag{3.40}$$

Substituting the axial and the radial pressure distributions of eqs. (3.34) and (3.40) into eq. (3.32), the steady static pressure in the flow is then given by

$$P_0(r,z) = \tfrac{1}{2} \Omega^2 \left(r^2 - 1\right) - 12 \frac{\bar{U}_R^{\,2}}{\mathrm{Re}} z , \tag{3.41}$$

where the first term is the pressure term accounting for the centrifugal force field in the fluid and the second term accounts for the change of pressure along the length of the cylinder due to the viscous friction with the walls.

3.3.2. Turbulent mean flow

The turbulent mean flow used here is based on widely adopted empirical relationships, namely the venerable $1/7^{th}$ power-law profile, the empirical law of the wall and Colebrook's equation.

From Munson et al. (2002), the $1/7^{th}$ empirical power-law velocity profile is

$$U_R(r) = U_C(1-r)^{1/7}, \tag{3.42}$$

where U_C is the centreline reduced velocity. By integrating eq. (3.42) over r from 0 to 1, we can replace the centreline velocity for the average mean velocity in the equation:

$$U_R(r) = \frac{8}{7}\bar{U}_R(1-r)^{1/7}. \tag{3.43}$$

The power-law profile has a flaw at the wall (at r=1): its slope is infinite. For this reason the law of the wall is employed to evaluate the slope of the profiles at the wall. This slope is calculated using Colebrook's equation to find the friction factor for a rough pipe. From Munson et al. (2002), the law of the wall is given by

$$U'(r') = (R'-r')\frac{\tau'_w}{\mu'}, \tag{3.44}$$

where the shear on the wall can be found in terms of the pressure drop along the length of the axis of the cylinder:

$$\tau'_w = -\frac{R'}{2}\frac{dP'_0}{dz'}, \tag{3.45}$$

and where the pressure drop is function of the Darcy friction factor f:

$$\frac{dP'_0}{dz'} = -f\frac{\rho'\bar{U}'^2}{4R'}. \tag{3.46}$$

The Darcy friction factor is found by solving the transcendental equation of Colebrook

$$\frac{1}{\sqrt{f}} = -2\log\left(\frac{\varepsilon'}{7.4R'} + \frac{2.51}{\mathrm{Re}\sqrt{f}}\right), \tag{3.47}$$

where ε' is the equivalent roughness of the surface of the wall. Introducing the dimensionless equivalent roughness

$$\varepsilon = \varepsilon'/R', \tag{3.48}$$

eq. (3.47) can be rewritten as

$$\frac{1}{\sqrt{f}} = -2\log\left(\frac{\varepsilon}{7.4} + \frac{2.51}{\mathrm{Re}\sqrt{f}}\right). \tag{3.49}$$

The roughness of the surface has for effect to increase the slope of the profile at the wall. The rougher the pipe, the more "square" the profile is.

We combine and nondimensionalize eqs. (3.44)-(3.46) using the quantities of eqs. (2.22), (3.6)-(3.9) :

$$U_R(r) = (1-r)\frac{f}{16}\mathrm{Re}\bar{U}_R, \tag{3.50}$$

$$\frac{dP_0}{dz} = -f\frac{\bar{U}_R^2}{4}. \tag{3.51}$$

Over the cross-section of the cylinder, the profile is then the minimum of eqs. (3.43) and (3.50):

$$U_R(r) = \min\left[\left\{(1-r)\frac{f}{16}\mathrm{Re}\bar{U}_R\right\}, \left\{\frac{8}{7}\bar{U}_R(1-r)^{1/7}\right\}\right], \tag{3.52}$$

which when plotted for a Reynolds number of 10^6 gives the profile plotted in Fig. 4. Because of the law of the wall, the slope of the velocity profile at the wall varies with the Reynolds number. On the other hand, the core of the flow is invariant with the Reynolds number. The exponent of the power law model should really be a weak function of the Reynolds number, but for sake of simplicity it is taken constant at 1/7 here. One could also argue that the power-law profile is not valid at the centreline of the flow cross-section since $dU_R/dr \neq 0$ at $r = 0$. It is nevertheless a reasonable approximation and, since the location where the profile is not valid is farthest from the wall, its effect on the shell is diminished.

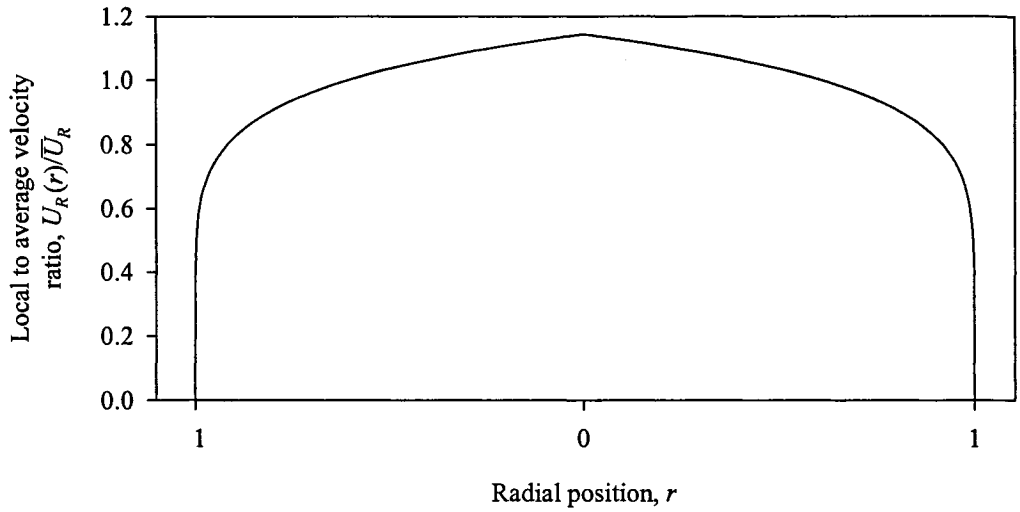

Fig. 4. Power-law / law of the wall velocity profile for a Re=10^6.

Assuming a fully developed flow, from eqs. (3.30) and (3.51), the mean pressure distribution in the flow is

$$P_0(r,z) = \tfrac{1}{2}\Omega^2\left(r^2-1\right) - f\frac{\overline{U}_R^2}{4}z\,. \tag{3.53}$$

3.4. Perturbation flow solution

Although the dynamics of the three perturbations of eq. (3.19) is coupled through the equations of motion (3.1), since they are three linearly independent perturbations, the introduction of the triple perturbation scheme of eqs. (3.26) and (3.29) into the equations of motion (3.14)-(3.17) leads to three distinct superimposed flow solutions. By introducing the scheme of eqs. (3.26) and (3.29) into the equations of motion (3.14)-(3.17) and keeping only the first-order terms, one finds the following three sets of four equations:

$$i\omega\hat{v}_{r,x}(r) - 2\Omega\hat{v}_{\theta,x}(r) - ikU_R(r)\hat{v}_{r,x}(r) = -\frac{\partial\hat{p}_x(r)}{\partial r} +$$
$$\frac{2\overline{U}_R}{\mathrm{Re}}\left[\frac{\partial}{\partial r}\left(\frac{1}{r}\frac{\partial}{\partial r}\left(r\hat{v}_{r,x}(r)\right)\right) - n^2\frac{1}{r^2}\hat{v}_{r,x}(r) - k^2\hat{v}_{r,x}(r) + in\frac{2}{r^2}\hat{v}_{\theta,x}(r)\right] \text{ for } x = u,v,w, \tag{3.54}$$

$$i\omega\hat{v}_{\theta,x}(r)+2\Omega\hat{v}_{r,x}(r)-ikU_R(r)\hat{v}_{\theta,x}(r)=in\frac{1}{r}\hat{p}_x(r)+$$
$$\frac{2\bar{U}_R}{\mathrm{Re}}\left[\frac{\partial}{\partial r}\left(\frac{1}{r}\frac{\partial}{\partial r}\left(r\hat{v}_{\theta,x}(r)\right)\right)-n^2\frac{1}{r^2}\hat{v}_{\theta,x}(r)-k^2\hat{v}_{\theta,x}(r)-in\frac{2}{r^2}\hat{v}_{r,x}(r)\right] \text{ for } x=u,v,w, \quad (3.55)$$

$$i\omega\hat{v}_{z,x}(r)+\frac{\partial U_R(r)}{\partial r}\hat{v}_{r,x}(r)-ikU_R(r)\hat{v}_{z,x}(r)=ik\hat{p}_x(r)+$$
$$\frac{2\bar{U}_R}{\mathrm{Re}}\left[\frac{1}{r}\frac{\partial}{\partial r}\left(r\frac{\partial\hat{v}_{z,x}(r)}{\partial r}\right)-n^2\frac{1}{r^2}\hat{v}_{z,x}(r)-k^2\hat{v}_{z,x}(r)\right] \quad \text{for } x=u,v,w, \quad (3.56)$$

$$\frac{1}{r}\frac{\partial}{\partial r}\left(r\hat{v}_{r,x}(r)\right)-in\frac{1}{r}\hat{v}_{\theta,x}(r)-ik\hat{v}_{z,x}(r)=0 \text{ for } x=u,v,w, \quad (3.57)$$

where $x=u,v,w$ refers to the three superimposed solutions associated with the three perturbations in the triple perturbation scheme of eqs. (3.26) and (3.29). The reader might be interested in having a look at the partial differential equation system obtained by introducing a simple perturbation scheme into eqs. (3.14)-(3.17) and have a careful look at the linearization of the system of equations. This is done in Appendix C.

Since we are seeking a linear solution, we do a first-order approximation and neglect the non-linear coupling in the fluid between the effect of one perturbation and that of another. This coupling is obviously of second order since it has to be proportional to the product of two perturbations. It is important to emphasise that the non-linear coupling between the effects of the different perturbations is neglected, but as we shall see in eq. (3.83) the linear coupling arising in the force summation of the shell equations (3.1) is enhanced, as the three deformations produce forces in all three directions in the fluid. Therefore, in this linear analysis, it is reasonable (and inevitable) to neglect the non-linear coupling and simply consider, three distinct linear flow solutions superimposed on one another.

3.5. Boundary conditions of the viscous fluid

Because of the triple perturbation scheme, we obtained three sets of equations of motion (3.54)-(3.57) and we can also expect three sets of boundary conditions. The triple

perturbation scheme of eqs. (3.26) and (3.29) is substituted into eqs. (3.21) and the terms of second order are neglected; thusm

$$\left[\hat{v}_{r,w}(r)w+\hat{v}_{r,v}(r)v+\hat{v}_{r,u}(r)u\right]_{\vec{r}=\vec{r}_1}=\left[i\omega w-ikU_R(r)w\right]_{\vec{r}=\vec{r}_1}, \tag{3.58}$$

$$\left[\hat{v}_{\theta,w}(r)w+\hat{v}_{\theta,v}(r)v+\hat{v}_{\theta,u}(r)u\right]_{\vec{r}=\vec{r}_1}=\left[i\omega v-ikU_R(r)v\right]_{\vec{r}=\vec{r}_1}, \tag{3.59}$$

$$\left[U_R(r)+\hat{v}_{z,w}(r)w+\hat{v}_{z,v}(r)v+\hat{v}_{z,u}(r)u\right]_{\vec{r}=\vec{r}_1}=\left[i\omega u-ikU_R(r)u\right]_{\vec{r}=\vec{r}_1}. \tag{3.60}$$

Eqs. (3.58) and (3.59) contain only first-order quantities, as explained in Appendix A; they can be evaluated at the mean position of the wall instead of the instantaneous position of the wall without introducing a significant error:

$$\left[\hat{v}_{r,w}(r)\overline{w}+\hat{v}_{r,v}(r)\overline{v}+\hat{v}_{r,u}(r)\overline{u}\right]_{\vec{r}=\vec{r}_0}e^{i\alpha}=\left[i\omega\overline{w}-ikU_R(r)\overline{w}\right]_{\vec{r}=\vec{r}_0}e^{i\alpha}, \tag{3.61}$$

$$\left[\hat{v}_{\theta,w}(r)\overline{w}+\hat{v}_{\theta,v}(r)\overline{v}+\hat{v}_{\theta,u}(r)\overline{u}\right]_{\vec{r}=\vec{r}_0}e^{i\alpha}=\left[i\omega\overline{v}-ikU_R(r)\overline{v}\right]_{\vec{r}=\vec{r}_0}e^{i\alpha}. \tag{3.62}$$

On the other hand, eq. (3.60) contains a leading order term dependent on r, so its evaluation at the instantaneous position of the wall can be done by expanding about the mean position of wall and keeping only first order terms:

$$\begin{aligned}&\left[U_R(r)+\hat{v}_{z,w}(r)\overline{w}+\hat{v}_{z,v}(r)\overline{v}+\hat{v}_{z,u}(r)\overline{u}\right]_{\vec{r}=\vec{r}_0}e^{i\alpha}+w\left[\frac{\partial U_R(r)}{\partial r}\right]_{\vec{r}=\vec{r}_0}+O\left(w^2\right)\\&=\left[i\omega\overline{u}-ikU_R(r)\overline{u}\right]_{\vec{r}=\vec{r}_0}e^{i\alpha}.\end{aligned} \tag{3.63}$$

The mean velocity boundary condition (3.37) can be subtracted from eq. (3.63),

$$\left[\hat{v}_{z,w}(r)\overline{w}+\hat{v}_{z,v}(r)\overline{v}+\hat{v}_{z,u}(r)\overline{u}\right]_{\vec{r}=\vec{r}_0}e^{i\alpha}=\left[i\omega\overline{u}-ikU_R(r)\overline{u}-\frac{\partial U_R(r)}{\partial r}\overline{w}\right]_{\vec{r}=\vec{r}_0}e^{i\alpha}. \tag{3.64}$$

We have thus obtained three equations (eqs. (3.61), (3.62) and (3.64)) describing the boundaries. Since $\overline{u}$, $\overline{v}$ and $\overline{w}$ are three independent perturbation amplitudes, the three boundary condition equations (3.61), (3.62) and (3.64) must be satisfied for any arbitrary combinations of $\overline{u}$, $\overline{v}$ and $\overline{w}$. We say that $\overline{u}$, $\overline{v}$ and $\overline{w}$ are linearly independent and eqs. (3.61), (3.62) and (3.64) lead to 3 sets of 3 boundary conditions

$$\begin{aligned}&\hat{v}_{z,u}(r)\big|_{r=1}=i\omega-ikU_R(r)\big|_{r=1},\\&\hat{v}_{\theta,u}(r)\big|_{r=1}=0,\\&\hat{v}_{r,u}(r)\big|_{r=1}=0,\end{aligned} \tag{3.65}$$

$$\hat{v}_{z,v}(r)\big|_{r=1} = 0,$$
$$\hat{v}_{\theta,v}(r)\big|_{r=1} = i\omega - ikU_R(r)\big|_{r=1}, \tag{3.66}$$
$$\hat{v}_{r,v}(r)\big|_{r=1} = 0,$$

$$\hat{v}_{z,w}(r)\big|_{r=1} = \left.\frac{\partial U_R(r)}{\partial r}\right|_{r=1},$$
$$\hat{v}_{\theta,w}(r)\big|_{r=1} = 0, \tag{3.67}$$
$$\hat{v}_{r,w}(r)\big|_{r=1} = i\omega - ikU_R(r)\big|_{r=1}.$$

3.6. Coupling fluid and structure

As written in eq. (3.2), the effect of the fluid on the shell comes from the fluid stresses acting on the wall of the shell. From Munson et al. (2002) the viscous fluid stresses acting on a surface perpendicular to the radial direction in cylindrical coordinates take the following dimensional form:

$$\sigma'_{rz} = \mu\left[\frac{\partial V'_r}{\partial' z} + \frac{\partial V'_z}{\partial r'}\right], \tag{3.68}$$

$$\sigma'_{r\theta} = \mu\left[r'\frac{\partial}{\partial r'}\left(\frac{V'_\theta}{r'}\right) + \frac{1}{r'}\frac{\partial V'_r}{\partial \theta'}\right], \tag{3.69}$$

$$\sigma'_{rr} = \left[-P' + 2\mu\frac{\partial V'_r}{\partial r'}\right], \tag{3.70}$$

where V'_r, V'_θ and V'_z are the dimensional components of the flow velocity. Eqs. (3.68) to (3.70) can be put into dimensionless form by using eqs. (3.7)-(3.9) and (2.32):

$$\sigma_{rz} = 2\frac{\bar{U}_R}{\mathrm{Re}}\left[\frac{\partial V_r}{\partial z} + \frac{\partial V_z}{\partial r}\right], \tag{3.71}$$

$$\sigma_{r\theta} = 2\frac{\bar{U}_R}{\mathrm{Re}}\left[r\frac{\partial}{\partial r}\left(\frac{V_\theta}{r}\right) + \frac{1}{r}\frac{\partial V_r}{\partial \theta}\right], \tag{3.72}$$

$$\sigma_{rr} = \left[-P + 4\frac{\bar{U}_R}{\mathrm{Re}}\frac{\partial V_r}{\partial r}\right]. \tag{3.73}$$

We then substitute the perturbation scheme of eqs. (3.26) and (3.29) into eqs. (3.71)-(3.73):

$$\sigma_{rz} = 2\frac{\bar{U}_R}{\mathrm{Re}}\Bigg[-ik\left\{\hat{v}_{r,w}(r)w+\hat{v}_{r,v}(r)v+\hat{v}_{r,u}(r)u\right\} + \frac{\partial U_R(r)}{\partial r}+\frac{\partial \hat{v}_{z,w}(r)}{\partial r}w+\frac{\partial \hat{v}_{z,v}(r)}{\partial r}v+\frac{\partial \hat{v}_{z,u}(r)}{\partial r}u\Bigg], \tag{3.74}$$

$$\sigma_{r\theta} = 2\frac{\bar{U}_R}{\mathrm{Re}}\Bigg[\frac{\partial \hat{v}_{\theta,w}(r)}{\partial r}w+\frac{\partial \hat{v}_{\theta,v}(r)}{\partial r}v+\frac{\partial \hat{v}_{\theta,u}(r)}{\partial r}u -\frac{1}{r}\left\{\hat{v}_{\theta,w}(r)w+\hat{v}_{\theta,v}(r)v+\hat{v}_{\theta,u}(r)u\right\}-\frac{in}{r}\left\{\hat{v}_{r,w}(r)w+\hat{v}_{r,v}(r)v+\hat{v}_{r,u}(r)u\right\}\Bigg], \tag{3.75}$$

$$\sigma_{rr} = \Bigg[-P_R-P_0(r,z)-\hat{p}_w(r)w-\hat{p}_v(r)v-\hat{p}_u(r)u +4\frac{\bar{U}_R}{\mathrm{Re}}\left\{\frac{\partial \hat{v}_{r,w}(r)}{\partial r}w+\frac{\partial \hat{v}_{r,v}(r)}{\partial r}v+\frac{\partial \hat{v}_{r,u}(r)}{\partial r}u\right\}\Bigg]. \tag{3.76}$$

The fluid forces acting on the shell are given by evaluating eqs. (3.74)-(3.76) as in eq. (3.2):

$$F_{f,z} = -2\frac{\bar{U}_R}{\mathrm{Re}}\Bigg[-ik\left\{\hat{v}_{r,w}(r)w+\hat{v}_{r,v}(r)v+\hat{v}_{r,u}(r)u\right\} + \frac{\partial U_R(r)}{\partial r}+\frac{\partial \hat{v}_{z,w}(r)}{\partial r}w+\frac{\partial \hat{v}_{z,v}(r)}{\partial r}v+\frac{\partial \hat{v}_{z,u}(r)}{\partial r}u\Bigg]_{\bar{r}=\bar{r}_1}, \tag{3.77}$$

$$F_{f,\theta} = -2\frac{\bar{U}_R}{\mathrm{Re}}\Bigg[\frac{\partial \hat{v}_{\theta,w}(r)}{\partial r}w+\frac{\partial \hat{v}_{\theta,v}(r)}{\partial r}v+\frac{\partial \hat{v}_{\theta,u}(r)}{\partial r}u -\frac{1}{r}\left\{\hat{v}_{\theta,w}(r)w+\hat{v}_{\theta,v}(r)v+\hat{v}_{\theta,u}(r)u\right\}-\frac{in}{r}\left\{\hat{v}_{r,w}(r)w+\hat{v}_{r,v}(r)v+\hat{v}_{r,u}(r)u\right\}\Bigg]_{\bar{r}=\bar{r}_1}, \tag{3.78}$$

$$F_{f,r} = -\Bigg[-P_R-P_0(r,z)-\hat{p}_w(r)w-\hat{p}_v(r)v-\hat{p}_u(r)u +4\frac{\bar{U}_R}{\mathrm{Re}}\left\{\frac{\partial \hat{v}_{r,w}(r)}{\partial r}w+\frac{\partial \hat{v}_{r,v}(r)}{\partial r}v+\frac{\partial \hat{v}_{r,u}(r)}{\partial r}u\right\}\Bigg]_{\bar{r}=\bar{r}_1}. \tag{3.79}$$

As explained in Appendix A, because eqs. (3.77) and (3.79) contain terms of leading order, their evaluation at the instantaneous position of the wall can be done by expanding about the mean position of the wall and keeping only first-order terms; while eq. (3.78)

contains only first order quantities, so it can be evaluated at the mean position of the wall instead of the instantaneous position of the wall without introducing a significant error:

$$F_{f,z} = -2\frac{\bar{U}_R}{\mathrm{Re}}\Bigg[-ik\left\{\hat{v}_{r,w}(r)w+\hat{v}_{r,v}(r)v+\hat{v}_{r,u}(r)u\right\} + \frac{\partial U_R(r)}{\partial r}+\frac{\partial \hat{v}_{z,w}(r)}{\partial r}w+\frac{\partial \hat{v}_{z,v}(r)}{\partial r}v+\frac{\partial \hat{v}_{z,u}(r)}{\partial r}u\Bigg]_{\vec{r}=\vec{r}_0} - 2\frac{\bar{U}_R}{\mathrm{R_e}}w\frac{\partial^2 U_R(r)}{\partial r^2}\Bigg|_{\vec{r}=\vec{r}_0}, \tag{3.80}$$

$$F_{f,\theta} = -2\frac{\bar{U}_R}{\mathrm{Re}}\Bigg[\frac{\partial \hat{v}_{\theta,w}(r)}{\partial r}w+\frac{\partial \hat{v}_{\theta,v}(r)}{\partial r}v+\frac{\partial \hat{v}_{\theta,u}(r)}{\partial r}u -\frac{1}{r}\left\{\hat{v}_{\theta,w}(r)w+\hat{v}_{\theta,v}(r)v+\hat{v}_{\theta,u}(r)u\right\}-\frac{in}{r}\left\{\hat{v}_{r,w}(r)w+\hat{v}_{r,v}(r)v+\hat{v}_{r,u}(r)u\right\}\Bigg]_{\vec{r}=\vec{r}_0}, \tag{3.81}$$

$$F_{f,r} = -\Bigg[-P_R-P_0(r,z)-\hat{p}_w(r)w-\hat{p}_v(r)v-\hat{p}_u(r)u +4\frac{\bar{U}_R}{\mathrm{Re}}\left\{\frac{\partial \hat{v}_{r,w}(r)}{\partial r}w+\frac{\partial \hat{v}_{r,v}(r)}{\partial r}v+\frac{\partial \hat{v}_{r,u}(r)}{\partial r}u\right\}\Bigg]_{\vec{r}=\vec{r}_0} + w\frac{\partial P_0(r,z)}{\partial r}\Bigg|_{\vec{r}=\vec{r}_0} + u\frac{\partial P_0(r,z)}{\partial z}\Bigg|_{\vec{r}=\vec{r}_0}. \tag{3.82}$$

Rewriting eqs. (3.80)-(3.82) in vector form, we get

$$\begin{Bmatrix}F_{f,z}\\F_{f,\theta}\\F_{f,r}\end{Bmatrix} = -\begin{Bmatrix}2\dfrac{\bar{U}_R}{\mathrm{Re}}\dfrac{\partial U_R}{\partial r}\Big|_{\vec{r}=\vec{r}_0}\\0\\-P_R-P_0|_{\vec{r}=\vec{r}_0}\end{Bmatrix} - \begin{bmatrix}\pi_{z,u} & \pi_{z,v} & \pi_{z,w}+2\dfrac{\bar{U}_R}{\mathrm{Re}}\dfrac{\partial^2 U_R}{\partial r^2}\Big|_{\vec{r}=\vec{r}_0}\\ \pi_{\theta,u} & \pi_{\theta,v} & \pi_{\theta,w}\\ \pi_{r,u}-\dfrac{\partial P_0}{\partial z}\Big|_{\vec{r}=\vec{r}_0} & \pi_{r,v} & \pi_{r,w}-\dfrac{\partial P_0}{\partial r}\Big|_{\vec{r}=\vec{r}_0}\end{bmatrix}\begin{Bmatrix}u\\v\\w\end{Bmatrix}, \tag{3.83}$$

where the force influence coefficients are defined as

$$\begin{Bmatrix}\pi_{z,x}\\\pi_{\theta,x}\\\pi_{r,x}\end{Bmatrix} = \frac{2\bar{U}_R}{\mathrm{Re}}\begin{Bmatrix}\dfrac{\partial \hat{v}_{z,x}}{\partial r}-ik\hat{v}_{r,x}\\ \dfrac{\partial \hat{v}_{\theta,x}}{\partial r}-\dfrac{\hat{v}_{\theta,x}}{r}-\dfrac{in}{r}\hat{v}_{r,x}\\ 2\dfrac{\partial \hat{v}_{r,x}}{\partial r}-\dfrac{\mathrm{Re}}{2\bar{U}_R}\hat{p}_x\end{Bmatrix}_{r=1}, \text{ for } x=u,v,w, \tag{3.84}$$

where the (r) indicating that the velocity influence functions $\hat{v}$ are functions of r, as in eqs. (3.80)-(3.82), have been dropped for conciseness.

The forces of eq. (3.83) can be substituted back into the fluid-structure problem eq. (3.1), yielding

$$[L_\alpha]\begin{Bmatrix} u \\ v \\ w \end{Bmatrix} + \frac{1}{h\Gamma}\begin{bmatrix} -\pi_{z,u} & -\pi_{z,v} & -\pi_{z,w} - 2\dfrac{\bar{U}_R}{\mathrm{Re}}\dfrac{\partial^2 U_R}{\partial r^2}\Big|_{\vec{r}=\vec{r}_0} \\ -\pi_{\theta,u} & -\pi_{\theta,v} & -\pi_{\theta,w} \\ \pi_{r,u} - \dfrac{\partial P_0}{\partial z}\Big|_{\vec{r}=\vec{r}_0} & \pi_{r,v} & \pi_{r,w} - \dfrac{\partial P_0}{\partial r}\Big|_{\vec{r}=\vec{r}_0} \end{bmatrix}\begin{Bmatrix} u \\ v \\ w \end{Bmatrix} = \begin{Bmatrix} 0 \\ 0 \\ \Omega^2 \end{Bmatrix} + \frac{1}{h\Gamma}\begin{Bmatrix} 2\dfrac{\bar{U}_R}{\mathrm{Re}}\dfrac{\partial U_R}{\partial r}\Big|_{\vec{r}=\vec{r}_0} \\ 0 \\ -P_R - P_0\big|_{\vec{r}=\vec{r}_0} \end{Bmatrix}. \tag{3.85}$$

One notices that the terms on the left-hand-side of eq. (3.85) are all perturbation terms proportional to *u, v, w,* while on the right-hand-side the terms are of zeroth order. These zeroth order terms cause static deformation of the shell. As discussed in Chapter 2, the method of solution used here does not allow taking into consideration static deformation. If one drops these static terms of the right-hand side, eq. (3.85) can be rewritten in the desired form of eq. (3.3) where the linear matrix accounting for the dynamics of the coupled system is given by

$$[L] = \begin{bmatrix} \left[-k^2 - \dfrac{1-\nu}{2}n^2 + \omega^2 - \dfrac{\pi_{z,u}}{h\Gamma}\right] & -\dfrac{1+\nu}{2}kn - \dfrac{\pi_{z,v}}{h\Gamma} & \left[-i\nu k - \dfrac{\pi_{z,w}}{h\Gamma} - \dfrac{2}{h\Gamma}\dfrac{\bar{U}_R}{\mathrm{Re}}\dfrac{\partial^2 U_R}{\partial r^2}\Big|_{\vec{r}=\vec{r}_0}\right] \\ -\dfrac{1+\nu}{2}kn - \dfrac{\pi_{\theta,u}}{h\Gamma} & \left[-\dfrac{1-\nu}{2}k^2 - n^2 + \Omega^2 + \omega^2 - \dfrac{\pi_{\theta,v}}{h\Gamma}\right] & -in - i2\Omega\omega - \dfrac{\pi_{\theta,w}}{h\Gamma} \\ \left[-i\nu k + \dfrac{\pi_{r,u}}{h\Gamma} - \dfrac{1}{h\Gamma}\dfrac{\partial P_0}{\partial z}\Big|_{\vec{r}=\vec{r}_0}\right] & -in - i2\Omega\omega + \dfrac{\pi_{r,v}}{h\Gamma} & \left[1 + \dfrac{h^2}{12}\left(k^2+n^2\right)^2 - \Omega^2 - \omega^2 + \dfrac{\pi_{r,w}}{h\Gamma} - \dfrac{1}{h\Gamma}\dfrac{\partial P_0}{\partial r}\Big|_{\vec{r}=\vec{r}_0}\right] \end{bmatrix}. \tag{3.86}$$

Eq. (3.3) with its matrix $[L]$ given by eq. (3.86) can be solved by taking its determinant equal to zero. In order to do so, the π-coefficients which depend on ω, k, n, Ω, Re and $\bar{U}_R$ which express the fluid force intensities acting on the shell must be found using a numerical method. This is discussed in the next chapter. For a given prescribed mode of oscillation of the shell, the flow is solved and its reaction is imposed on the shell in this strong-coupling FSI analysis.

However, despite the careful derivation of the equations, early tests done with the boundary conditions derived in Section 3.5 demonstrated a failure of the model. Modifications to the boundary conditions therefore proved necessary. This is discussed in the following sections.

3.7 Effect on the stability of the classical no-slip boundary conditions

In fluid-structure interactions, the interface between the fluid and the solid is critical. Both the fluid and the solid models must exchange information in order to achieve the desired coupling. The problem with linear shear-flow/structure interactions is that this information exchange is compromised. In the inviscid model, there are two terms in the fluid boundary conditions which transmit the structure's slope (or position) $-ikw$ and its velocity $i\omega w$; the linear boundary condition given by eq. (2.51) is the following:

$$V_r\big|_{r=1} = i\omega w - ik\bar{U}_R w. \tag{3.87}$$

Information about the velocity and the position of the wall is transmitted to the fluid. This makes possible centrifugal (added stiffness), Coriolis and added mass forces among others acting on the structure. But for the linear boundary conditions of viscous flow, since the mean flow velocity is zero at the wall for both the laminar and the turbulent velocity profiles, the position-dependent term disappears from eqs. (3.65)-(3.67), as $U_R(r)\big|_{r=1} = 0$. There is a position-dependent term in the axial direction component of eq. (3.67), but it does not take into account the slope of the wall since it has no k-dependence. Because all effects relative to the slope of the wall are removed, the dynamics of the

system is greatly impoverished. In fact, the model simply does not predict the dynamics properly; hence this is why the classical viscous model (see subsection 3.8.1) is extremely stable for laminar flow and extremely unstable for turbulent flow, as shown in the results of Section 6.1. Dowell (1971) had found that the approximation of applying the boundary conditions at the undeformed position of the wall, instead of its instantaneous position overestimates the stabilizing effect of the boundary layer, as a result of the fact that the mean velocity at the undeformed position of the wall is zero.

The disappearance of the slope of the wall in the boundary conditions is an artefact of linearization due to the application of the boundary conditions at the mean position of the wall instead of its instantaneous deformed position.

One possible way to correct this problem would be to do a large amplitude analysis and apply the boundary conditions at the deformed position of the wall. A large deformation analysis would require a non-linear model. There seems to be no elegant or formally derivable solution or correction to the linear problem in this framework of solution methods. For additional discussion, the reader is referred to Paidoussis (2003, Section 11.5.2(f)).

To overcome this problem, three corrections to the linear formulation of the problem are attempted here. The first one consists of forgetting about the no-slip boundary condition altogether and applying a slip condition on the viscous model which reinstates the position-related terms in the radial boundary conditions, while also getting rid of the velocity profile. The second attempt involves the modification of the perturbation no-slip boundary conditions by allowing a non-zero mean velocity acting on the wall, even though the steady velocity profile has zero-flow velocity on the wall, in the manner of El Chebair et al. (1990). The third attempt is inspired by Dowell (1971), and it was also implemented by El Chebair et al. (1990): instead of applying the boundary conditions at $r = 1$ at the undeformed shell position, it is applied at an assumed position just off the shell mean position.

3.8. The viscous models

Four models are presented in the following subsections: (i) the classical viscous model, (ii) the slip model, (iii) the average velocity model, (iv) the delta model.

3.8.1. The classical viscous model

The classical viscous model has been carefully derived in Sections 3.1-3.6, utilizing the conventional no-slip boundary conditions. The equations of motion (3.54)-(3.57) must be solved three times, once for each of the three perturbations u, v, w using each set of boundary conditions given in eqs. (3.65), (3.66) and (3.67). The fluid forces are given in eqs. (3.83)-(3.84). In the laminar regime, the mean pressure solution is of the form of eq. (3.41) and the parabolic flow profile is as given in eq. (3.39). For the turbulent regime, the mean pressure solution is of the form of eq. (3.53) and the turbulent flow profile is as given in eq. (3.52).

3.8.2. The slip model

If we substitute the requirement of no-slip on the wall for a slip boundary condition, the velocity profile becomes "square". We then obtain a model with effectively no velocity profile, where viscosity affects the flow solution only through shear stress and dissipation. Although this model has very limited realism, we have reasons to believe that the dissipative effect of viscosity is a necessary component for a rotating flow model. The other motivation for using this scheme is that it allows to test and to validate the solution methods for viscous flow. In the case of vanishing viscosity, the results with this model should tend toward those obtained with the inviscid model. In the slip model, the radial velocity boundary condition is identical to the one given by eq. (2.51) for the inviscid model:

$$V_r\big|_{r=1} = i\omega w - ik\bar{U}_R w. \tag{3.88}$$

For the other two directions, a certain slip is allowed. Therefore, the boundary condition is applied on the second r-derivative of the circumferential and axial velocities,

$$\left.\frac{\partial^2 V_\theta}{\partial r^2}\right|_{r=1} = 0, \tag{3.89}$$

$$\left.\frac{\partial^2 V_z}{\partial r^2}\right|_{r=1} = 0. \tag{3.90}$$

These are not free-slip conditions since they concern the second derivatives; free-slip boundary conditions are concerned with the first derivatives with respect to the coordinate normal to the surface of the velocity components parallel to the surface. It is thought that a condition on the second derivative is a little more constraining than a free-slip condition, hence a little more realistic.

Because of the form of the boundary conditions of eqs. (3.88)-(3.90), the flow solution obtained with the slip model depends only on the w-perturbation. The triple perturbation scheme is therefore not necessary here, and the u and v velocity and pressure influence functions can be set to zero; thus,

$$\hat{v}_{r,u} = \hat{v}_{\theta,u} = \hat{v}_{z,u} = \hat{v}_{r,v} = \hat{v}_{\theta,v} = \hat{v}_{z,v} = \hat{p}_u = \hat{p}_v = 0. \tag{3.91}$$

Applying the solution scheme of eq. (3.26) on the boundary conditions (3.88)-(3.90) while utilizing eq. (3.91), we obtain

$$\hat{v}_r\big|_{r=1} = i\omega - ik\bar{U}_R, \tag{3.92}$$

$$\left.\frac{\partial^2 \hat{v}_\theta}{\partial r^2}\right|_{r=1} = 0, \tag{3.93}$$

$$\left.\frac{\partial^2 \hat{v}_z}{\partial r^2}\right|_{r=1} = 0, \tag{3.94}$$

and

$$U_R(r) = \bar{U}_R. \tag{3.95}$$

Because the reduced velocity flow profile of eq. (3.95) is constant across the section, the term related to the viscous friction with the walls in the mean pressure solution of eq. (3.41) vanishes, leading to

$$P_0(r) = \tfrac{1}{2}\Omega^2\left(r^2 - 1\right). \tag{3.96}$$

With the simplification of eq. (3.91), it is only necessary to solve eqs. (3.54)-(3.57) for the *w*-perturbation. The fluid forces acting on the shell are given by eq. (3.83) where, because only one flow solution is required, the force influence coefficients of eq. (3.84) simplify to:

$$\frac{\mathrm{Re}}{2\bar{U}_R}\begin{bmatrix}\pi_{z,u} & \pi_{z,v} & \pi_{z,w}\\ \pi_{\theta,u} & \pi_{\theta,v} & \pi_{\theta,w}\\ \pi_{r,u} & \pi_{r,v} & \pi_{r,w}\end{bmatrix}=\begin{bmatrix}0 & 0 & \dfrac{\partial\hat{v}_{z,w}}{\partial r}-ik\hat{v}_{r,w}\\ 0 & 0 & \dfrac{\partial\hat{v}_{\theta,w}}{\partial r}-\dfrac{\hat{v}_{\theta,w}}{r}-\dfrac{in}{r}\hat{v}_{r,w}\\ 0 & 0 & 2\dfrac{\partial\hat{v}_{r,w}}{\partial r}-\dfrac{\mathrm{Re}}{2\bar{U}_R}\hat{p}_w\end{bmatrix}_{r=1}. \tag{3.97}$$

3.8.3. The average-velocity model

Although this solution can be considered to be not rigorous, it will be seen (in Chapter 6) to work acceptably well and it incorporates all the aspects of the real physical system: boundary layer, velocity flow profile, and a non-vanishing centrifugal force. The idea here is to use the boundary conditions of eqs. (3.65), (3.66) and (3.67), but to utilize the averaged mean flow velocity $\bar{U}_R$, instead of $U_R(r)$ which evaluated at $r=1$ is zero. This gives

$$\begin{aligned}&\hat{v}_{z,u}(r)\big|_{r=1}=i\omega-ik\bar{U}_R,\\ &\hat{v}_{\theta,u}(r)\big|_{r=1}=0,\\ &\hat{v}_{r,u}(r)\big|_{r=1}=0,\end{aligned} \tag{3.98}$$

$$\begin{aligned}&\hat{v}_{z,v}(r)\big|_{r=1}=0,\\ &\hat{v}_{\theta,v}(r)\big|_{r=1}=i\omega-ik\bar{U}_R,\\ &\hat{v}_{r,v}(r)\big|_{r=1}=0,\end{aligned} \tag{3.99}$$

$$\begin{aligned}&\hat{v}_{z,w}(r)\big|_{r=1}=\left.\frac{\partial U_R(r)}{\partial r}\right|_{r=1},\\ &\hat{v}_{\theta,w}(r)\big|_{r=1}=0,\\ &\hat{v}_{r,w}(r)\big|_{r=1}=i\omega-ik\bar{U}_R.\end{aligned} \tag{3.100}$$

Only the perturbation boundary conditions are changed in this scheme with respect to the classical no-slip model. Despite the non-zero velocity effective at the wall, the average-velocity model presents the same velocity profiles as in the classical no-slip model. In the laminar regime, the parabolic flow profile is as given in eq. (3.39) and the mean pressure solution is of the form of eq. (3.41). For the turbulent regime, the flow profile is as given in eq. (3.52) and the mean pressure solution is of the form of eq (3.53). The fluid forces in eqs. (3.83) and (3.84) are left in the same form.

3.8.4. The delta model

The application of the average mean velocity in the boundary conditions of the average-velocity model is arbitrary. An effective velocity has to be stitched to the boundary conditions of the carefully derived classical no-slip model in order to obtain acceptable results. A more justifiable approach for applying a non-zero effective mean velocity in the boundary conditions is attempted here with the delta model. This model was introduced by Dowell (1971) for flow over flat plates and it was later applied to flows in cylindrical shells by El Chebair et al. (1990). It consists of applying the boundary conditions at a position off the mean undeformed position of the wall,

$$r = 1 - \delta, \tag{3.101}$$

rather than at the undeformed position of the wall $r = 1$ as in the classical no-slip model; δ is equivalent to the shell deformation in the radial direction. The flow is solved over the interval $0 \le r \le 1 - \delta$ and the forces produced by the fluid acting on the shell are evaluated at $r = 1 - \delta$. As $\delta \to 0$ the classical viscous model is recovered. The boundary conditions of eqs. (3.65)-(3.67) can then be rewritten as

$$\begin{aligned} \hat{v}_{z,u}(r)\big|_{r=1-\delta} &= i\omega - ikU_R(r)\big|_{r=1-\delta}, \\ \hat{v}_{\theta,u}(r)\big|_{r=1-\delta} &= 0, \\ \hat{v}_{r,u}(r)\big|_{r=1-\delta} &= 0, \end{aligned} \tag{3.102}$$

$$\hat{v}_{z,v}(r)\big|_{r=1-\delta} = 0,$$
$$\hat{v}_{\theta,v}(r)\big|_{r=1-\delta} = i\omega - ikU_R(r)\big|_{r=1-\delta}, \tag{3.103}$$
$$\hat{v}_{r,v}(r)\big|_{r=1-\delta} = 0,$$

$$\hat{v}_{z,w}(r)\big|_{r=1-\delta} = \left.\frac{\partial U_R(r)}{\partial r}\right|_{r=1-\delta},$$
$$\hat{v}_{\theta,w}(r)\big|_{r=1-\delta} = 0, \tag{3.104}$$
$$\hat{v}_{r,w}(r)\big|_{r=1-\delta} = i\omega - ikU_R(r)\big|_{r=1-\delta}.$$

The model still bears the same velocity profiles as in the classical no-slip model. In the laminar regime, the parabolic flow profile is as given in eq. (3.39) and the mean pressure solution is of the form of eq. (3.41). For the turbulent regime, the flow profile is as given in eq. (3.52) and the mean pressure solution is of the form of eq (3.53). Eqs. (3.54)-(3.57) must be solved for all three perturbations *u*, *v*, *w* over the domain $0 \le r \le 1-\delta$, and the fluid forces in eqs. (3.83) and (3.84) are evaluated at $r = 1-\delta$. Thus, in eqs. (3.83) and (3.84), the position vector is taken to be

$$\vec{r}_0 = (1-\delta)\vec{e}_r + z\vec{e}_z. \tag{3.105}$$

Chapter 4

Numerical Solution of Viscous Equations

4.1. Finite difference scheme

Many different methods are employed to numerically solve pipe-flows in cylindrical coordinates. From the literature (see section 1.1.4), the ideal approach which would maximise both simplicity and efficiency would thus make use of flux quantities and a staggered grid to avoid iterating, get rid of the singularity at the centre of the flow and maximise the accuracy for the number of grid points.

In Section 3.7, four different viscous models are presented. These four models obey the same equations of motion (3.54)-(3.57), but have different boundary conditions, different domains of integration and require a different number of solutions of the equations of motion. The following numerical method is derived for the classical viscous model of Section 3.7.1; it is then adapted for the different models in Section 4.6.

The equations of motion (3.54)-(3.57) relate the different components of velocity influence functions and the pressure influence functions. For brevity, in this chapter they will simply be referred to as pressure and velocity.

4.2. From physical boundaries to numerical boundaries

The physical boundary conditions in this fluid problem are clear: the fluid domain has very large (infinite) axial length, on the wall the velocity of the fluid is dictated by the no-slip boundary condition and the pressure is unknown (this is in part what we are looking for in order to couple the fluid with the shell). Mathematically, because we introduced the travelling-wave solution for the perturbation quantities, the solution to the time-dependent three-dimensional flow takes the form of a sinusoidal fluctuation in θ, z and t of the solution along the radius. The numerical domain is then limited to one

dimension going from r=0 to r=1. Consequently, boundary conditions have to be imposed at both boundaries of the domain, although *a priori* nothing is known about the flow at its centre. Add to this that the equations of motion of the flow (eqs. (3.54)-(3.57)) have a common singularity at r=0: the four equations blow up at r=0. It must be emphasised that this singularity is a mathematical artefact; it is not physical: the velocities and the pressure of the flow at the centre of a pipe are finite. In the literature, different schemes are used to get around this singularity, as discussed in Section 1.1.4.

In order to solve the equations of motion (eqs . (3.54)-(3.57)) over the numerical domain, we need eight boundary conditions: the three velocity components and the pressure at r=0 and r=1; but we only have three: the three velocity components on the wall. Since the nature of the boundary at r=0 is more mathematical than physical, it seems logical that a condition for that boundary could be introduced in the same way. Verzicco and Orlandi (1996) showed that making a change of variable by introducing the flux of a quantity allows imposing a homogeneous boundary condition at r=0. The trick has been adopted here and we introduce the pressure flux influence function which we will refer to as simply the pressure flux:

$$\hat{q}_x = r\hat{p}_x, \tag{4.1}$$

and by definition $\hat{q}_x\big|_{r=0} \equiv 0$. This modifies the equations of motion into:

$$\begin{aligned} &i\omega\hat{v}_r - 2\Omega\hat{v}_\theta - ikU_R(r)\hat{v}_r = -\frac{\partial}{\partial r}\left(\frac{1}{r}\hat{q}\right) + \\ &\frac{2\bar{U}_R}{\mathrm{Re}}\left[\frac{\partial}{\partial r}\left(\frac{1}{r}\frac{\partial}{\partial r}(r\hat{v}_r)\right) - n^2\frac{1}{r^2}\hat{v}_r - k^2\hat{v}_r + in\frac{2}{r^2}\hat{v}_\theta\right], \end{aligned} \tag{4.2}$$

$$\begin{aligned} &i\omega\hat{v}_\theta + 2\Omega\hat{v}_r - ikU_R(r)\hat{v}_\theta = in\frac{1}{r^2}\hat{q} + \\ &\frac{2\bar{U}_R}{\mathrm{Re}}\left[\frac{\partial}{\partial r}\left(\frac{1}{r}\frac{\partial}{\partial r}(r\hat{v}_\theta)\right) - n^2\frac{1}{r^2}\hat{v}_\theta - k^2\hat{v}_\theta - in\frac{2}{r^2}\hat{v}_r\right], \end{aligned} \tag{4.3}$$

$$\begin{aligned} &i\omega\hat{v}_z + \frac{\partial U_R(r)}{\partial r}\hat{v}_r - ikU_R(r)\hat{v}_z = \frac{ik}{r}\hat{q} + \\ &\frac{2\bar{U}_R}{\mathrm{Re}}\left[\frac{1}{r}\frac{\partial}{\partial r}\left(r\frac{\partial\hat{v}_z}{\partial r}\right) - n^2\frac{1}{r^2}\hat{v}_z - k^2\hat{v}_z\right], \end{aligned} \tag{4.4}$$

$$\frac{1}{r}\frac{\partial}{\partial r}(r\hat{v}_r) - in\frac{1}{r}\hat{v}_\theta - ik\hat{v}_z = 0, \tag{4.5}$$

where the subscript x present in every influence functions of eqs. (3.54)-(3.57) relative to the three perturbations u, v, w is dropped for conciseness. This brings the total number of boundary conditions to 4: the three velocity components on the wall and the pressure flux at the centre. Keeping in mind this limited number of boundary conditions, we proceed to the next step which involves discretising the continuity and the three momentum equations.

4.3. Staggered grid discretisation

A straightforward way to solve the problem would be to use a finite difference scheme to solve the four equations simultaneously with the limited number of boundary conditions and iterate for the missing ones. Of course the value of some of the velocity components on the axis can be deduced from the physics of the problem, depending on the circumferential wavenumber. Such a method is cumbersome but was attempted by Chaumond (2003) without much success. Instead of using iterations, we use a staggered grid similar to that of Harlow and Welch (1965) to discretise the problem and hence make our numerical model such that it only requires the information we know: the four boundary conditions.

In the same spirit as in Verzicco and Orlandi (1995), the momentum and continuity equations are discretised on a staggered grid in such a way that only the known quantities are defined on the boundaries. However, this is done in a different fashion here. The three velocity components are defined at the points $r = r_j + \frac{1}{2}\Delta r$ and the pressure flux is defined at the points $r = r_j$. The grid is shown schematically in Fig. 5 and we use a notation similar to that of Kress and Nilsson (2003):

$$\hat{v}_{r,j-\frac{1}{2}} = \hat{v}_r\left(r_j - \tfrac{1}{2}\Delta r\right),\ j = 1,\ldots,N+1,$$

$$\hat{v}_{\theta,j-\frac{1}{2}} = \hat{v}_\theta\left(r_j - \tfrac{1}{2}\Delta r\right),\ j = 1,\ldots,N+1,$$

$$\hat{v}_{z,j-\frac{1}{2}} = \hat{v}_z\left(r_j - \tfrac{1}{2}\Delta r\right),\ j = 1,\ldots,N+1,$$

$$\hat{q}_j = \hat{q}\left(r_j\right),\ j = 0,\ldots,N,$$

where $r_j = j\Delta r$ and $\Delta r = 1/\left(N+\frac{1}{2}\right)$. As in Mateescu et al. (1994b), a central differencing procedure is then applied about the velocity points $r = r_j + \frac{1}{2}\Delta r$ on the three momentum equations (4.2)-(4.4), and about the pressure flux points $r = r_j$ on the continuity equation (4.5):

$$i\omega\hat{v}_{r,j-\frac{1}{2}} - 2\Omega\hat{v}_{\theta,j-\frac{1}{2}} - ikU_R\left(r_{j-\frac{1}{2}}\right)\hat{v}_{r,j-\frac{1}{2}} = -\frac{1}{r_{j-\frac{1}{2}}}D_-\hat{q}_j + \frac{1}{r^2_{j-\frac{1}{2}}}\frac{\hat{q}_j+\hat{q}_{j-1}}{2} + \frac{2\bar{U}_R}{\mathrm{Re}}\left[D_-D_+\hat{v}_{r,j-\frac{1}{2}} + \frac{1}{r_{j-\frac{1}{2}}}D_0\hat{v}_{r,j-\frac{1}{2}} - \frac{\hat{v}_{r,j-\frac{1}{2}}}{r^2_{j-\frac{1}{2}}} - n^2\frac{1}{r^2_{j-\frac{1}{2}}}\hat{v}_{r,j-\frac{1}{2}} - k^2\hat{v}_{r,j-\frac{1}{2}} + in\frac{2}{r^2_{j-\frac{1}{2}}}\hat{v}_{\theta,j-\frac{1}{2}}\right], \tag{4.6}$$

$$i\omega\hat{v}_{\theta,j-\frac{1}{2}} + 2\Omega\hat{v}_{r,j-\frac{1}{2}} - ikU_R\left(r_{j-\frac{1}{2}}\right)\hat{v}_{\theta,j-\frac{1}{2}} = in\frac{1}{r^2_{j-\frac{1}{2}}}\frac{\hat{q}_j+\hat{q}_{j-1}}{2} + \frac{2\bar{U}_R}{\mathrm{Re}}\left[D_-D_+\hat{v}_{\theta,j-\frac{1}{2}} + \frac{1}{r_{j-\frac{1}{2}}}D_0\hat{v}_{\theta,j-\frac{1}{2}} - \frac{\hat{v}_{\theta,j-\frac{1}{2}}}{r^2_{j-\frac{1}{2}}} - n^2\frac{1}{r^2_{j-\frac{1}{2}}}\hat{v}_{\theta,j-\frac{1}{2}} - k^2\hat{v}_{\theta,j-\frac{1}{2}} - in\frac{2}{r^2_{j-\frac{1}{2}}}\hat{v}_{r,j-\frac{1}{2}}\right], \tag{4.7}$$

$$i\omega\hat{v}_{z,j-\frac{1}{2}} + \left.\frac{\partial U_R(r)}{\partial r}\right|_{r_{j-\frac{1}{2}}}\hat{v}_{r,j-\frac{1}{2}} - ikU_R\left(r_{j-\frac{1}{2}}\right)\hat{v}_{z,j-\frac{1}{2}} = \frac{ik}{r_{j-\frac{1}{2}}}\frac{\hat{q}_j+\hat{q}_{j-1}}{2} + \frac{2\bar{U}_R}{\mathrm{Re}}\left[D_-D_+\hat{v}_{z,j-\frac{1}{2}} + \frac{1}{r_{j-\frac{1}{2}}}D_0\hat{v}_{z,j-\frac{1}{2}} - n^2\frac{1}{r^2_{j-\frac{1}{2}}}\hat{v}_{z,j-\frac{1}{2}} - k^2\hat{v}_{z,j-\frac{1}{2}}\right], \tag{4.8}$$

$$D_-\hat{v}_{r,j+\frac{1}{2}} + \frac{1}{r_j}\frac{\hat{v}_{r,j+\frac{1}{2}}+\hat{v}_{r,j-\frac{1}{2}}}{2} - in\frac{1}{r_j}\frac{\hat{v}_{\theta,j+\frac{1}{2}}+\hat{v}_{\theta,j-\frac{1}{2}}}{2} - ik\frac{\hat{v}_{z,j+\frac{1}{2}}+\hat{v}_{z,j-\frac{1}{2}}}{2} = 0, \tag{4.9}$$

where the difference operators are defined as

$$D_+\hat{v}_{r,j} = \frac{\hat{v}_{r,j+1}-\hat{v}_{r,j}}{\Delta r},$$

$$D_-\hat{v}_{r,j} = \frac{\hat{v}_{r,j}-\hat{v}_{r,j-1}}{\Delta r},$$

$$D_0\hat{v}_{r,j} = \frac{\hat{v}_{r,j+1}-\hat{v}_{r,j-1}}{2\Delta r},$$

and where interpolation has been used to define the pressure flux on the velocity points and vice versa:

$$\hat{q}_{j-\frac{1}{2}} \simeq \frac{\hat{q}_j + \hat{q}_{j-1}}{2},$$

$$\hat{v}_{r,j} \simeq \frac{\hat{v}_{r,j+\frac{1}{2}} + \hat{v}_{r,j-\frac{1}{2}}}{2}.$$

The resulting scheme is second-order accurate, as shown in Appendix D.

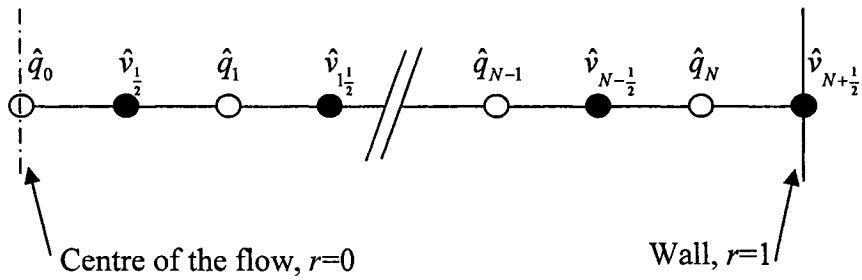

Fig. 5. Schematic of the staggered grid arrangement.

At point $j=1$, because of the boundary at $r=0$, the derivatives of the velocities in the three momentum equations require special treatment. For $j=1$, the continuity eq. (4.9) is left unchanged but the three momentum equations read

$$i\omega\hat{v}_{r,j-\frac{1}{2}} - 2\Omega\hat{v}_{\theta,j-\frac{1}{2}} - ikU_R\left(r_{j-\frac{1}{2}}\right)\hat{v}_{r,j-\frac{1}{2}} = -\frac{1}{r_{j-\frac{1}{2}}} D_{-}\hat{q}_j + \frac{1}{r^2_{j-\frac{1}{2}}}\frac{\hat{q}_j + \hat{q}_{j-1}}{2} +$$

$$\frac{2\bar{U}_R}{\mathrm{Re}}\left[D^2_{C+}\hat{v}_{r,j-\frac{1}{2}} + \frac{1}{r_{j-\frac{1}{2}}} D_{C+}\hat{v}_{r,j-\frac{1}{2}} - \frac{\hat{v}_{r,j-\frac{1}{2}}}{r^2_{j-\frac{1}{2}}} - n^2\frac{1}{r^2_{j-\frac{1}{2}}}\hat{v}_{r,j-\frac{1}{2}} - k^2\hat{v}_{r,j-\frac{1}{2}} + in\frac{2}{r^2_{j-\frac{1}{2}}}\hat{v}_{\theta,j-\frac{1}{2}} \right], \tag{4.10}$$

$$i\omega\hat{v}_{\theta,j-\frac{1}{2}} + 2\Omega\hat{v}_{r,j-\frac{1}{2}} - ikU_R\left(r_{j-\frac{1}{2}}\right)\hat{v}_{\theta,j-\frac{1}{2}} = in\frac{1}{r^2_{j-\frac{1}{2}}}\frac{\hat{q}_j + \hat{q}_{j-1}}{2} +$$

$$\frac{2\bar{U}_R}{\mathrm{Re}}\left[D^2_{C+}\hat{v}_{\theta,j-\frac{1}{2}} + \frac{1}{r_{j-\frac{1}{2}}} D_{C+}\hat{v}_{\theta,j-\frac{1}{2}} - \frac{\hat{v}_{\theta,j-\frac{1}{2}}}{r^2_{j-\frac{1}{2}}} - n^2\frac{1}{r^2_{j-\frac{1}{2}}}\hat{v}_{\theta,j-\frac{1}{2}} - k^2\hat{v}_{\theta,j-\frac{1}{2}} - in\frac{2}{r^2_{j-\frac{1}{2}}}\hat{v}_{r,j-\frac{1}{2}} \right], \tag{4.11}$$

$$i\omega\hat{v}_{z,j-\frac{1}{2}} + \left.\frac{\partial U_R(r)}{\partial r}\right|_{r_{j-\frac{1}{2}}} \hat{v}_{r,j-\frac{1}{2}} - ikU_R\left(r_{j-\frac{1}{2}}\right)\hat{v}_{z,j-\frac{1}{2}} = \frac{ik}{r_{j-\frac{1}{2}}}\frac{\hat{q}_j + \hat{q}_{j-1}}{2} +$$

$$\frac{2\bar{U}_R}{\mathrm{Re}}\left[D^2_{C+}\hat{v}_{z,j-\frac{1}{2}} + \frac{1}{r_{j-\frac{1}{2}}} D_{C+}\hat{v}_{z,j-\frac{1}{2}} - n^2\frac{1}{r^2_{j-\frac{1}{2}}}\hat{v}_{z,j-\frac{1}{2}} - k^2\hat{v}_{z,j-\frac{1}{2}} \right], \tag{4.12}$$

where the difference operators acting on the velocities are multipoint second-order accurate forward-differences:

$$D_{C+}\hat{v}_{r,j} = \frac{-\hat{v}_{j+2} + 4\hat{v}_{j+1} - 3\hat{v}_j}{2\Delta r}, \tag{4.13}$$

$$D^2_{C+}\hat{v}_{r,j} = \frac{-\hat{v}_{j+3} + 4\hat{v}_{j+2} - 5\hat{v}_{j+1} + 2\hat{v}_j}{\Delta r^2}. \tag{4.14}$$

These finite-difference operators are only used at the point $j = 1$.

The special set of eqs. (4.10), (4.11), (4.12) and (4.9) used at point $j = 1$ along with the $N-1$ set of eqs. (4.6)-(4.9) for the other $N-1$ points can be rewritten in matrix form in order to solve the problem implicitly:

$$[A]\begin{Bmatrix} \{\hat{v}\}_{\frac{1}{2}} \\ \hat{q}_1 \\ \{\hat{v}\}_{1\frac{1}{2}} \\ \vdots \\ \hat{q}_{N-1} \\ \{\hat{v}\}_{N-\frac{1}{2}} \\ \hat{q}_N \end{Bmatrix} = \begin{Bmatrix} -\{P_+\}\hat{q}_0 \\ 0 \\ \vdots \\ 0 \\ -[A_{j+}]\{\hat{v}\}_{N+\frac{1}{2}} \end{Bmatrix}, \tag{4.15}$$

where $[A]$ is the $4N \times 4N$ linear finite-difference matrix

$$[A] = \begin{bmatrix} [A_{C1}] & \{P_+\} & [A_{C2}] & 0 & [A_{C3}] & 0 & [A_{C4}] & 0 & 0 & 0 \\ [A_{j-}] & \{P_-\} & [A_j] & \{P_+\} & [A_{j+}] & 0 & 0 & 0 & 0 & 0 \\ 0 & 0 & [A_{j-}] & \{P_-\} & [A_j] & \{P_+\} & [A_{j+}] & 0 & 0 & 0 \\ 0 & 0 & 0 & 0 & \ddots & \ddots & \ddots & \ddots & 0 & 0 \\ 0 & 0 & 0 & 0 & [A_{j-}] & \{P_-\} & [A_j] & \{P_+\} & [A_{j+}] & 0 \\ 0 & 0 & 0 & 0 & 0 & 0 & [A_{j-}] & \{P_-\} & [A_j] & \{P_+\} \end{bmatrix}, \tag{4.16}$$

and where the coefficient matrices and vectors of eqs. (4.15) and (4.16) are given as

$$\left[A_j\right]=\begin{bmatrix} A_{jj} & 2\Omega+in\dfrac{2U_R}{\mathrm{Re}}\dfrac{2}{r_{j-\frac{1}{2}}^2} & 0 \\ -2\Omega-in\dfrac{2U_R}{\mathrm{Re}}\dfrac{2}{r_{j-\frac{1}{2}}^2} & A_{jj} & 0 \\ \left.\dfrac{\partial U_R(r)}{\partial r}\right|_{r_{j-\frac{1}{2}}} & 0 & A_{jj}+\dfrac{2U_R}{\mathrm{Re}}\dfrac{1}{r_{j-\frac{1}{2}}^2} \\ \dfrac{1}{2r_j}-\dfrac{1}{\Delta r} & -in\dfrac{1}{2r_j} & -\dfrac{ik}{2} \end{bmatrix}, \tag{4.17}$$

where

$$A_{jj}=-i\omega+ikU_R\left(r_{j-\frac{1}{2}}\right)-\frac{2U_R}{\mathrm{Re}}\left\{\frac{1+n^2}{r_{j-\frac{1}{2}}^2}+k^2+\frac{2}{\Delta r^2}\right\},$$

$$\left[A_{j+}\right]=\begin{bmatrix} \dfrac{2U_R}{\mathrm{Re}}\left[\dfrac{1}{\Delta r^2}+\dfrac{1}{2r_{j-\frac{1}{2}}\Delta r}\right] & 0 & 0 \\ 0 & \dfrac{2U_R}{\mathrm{Re}}\left[\dfrac{1}{\Delta r^2}+\dfrac{1}{2r_{j-\frac{1}{2}}\Delta r}\right] & 0 \\ 0 & 0 & \dfrac{2U_R}{\mathrm{Re}}\left[\dfrac{1}{\Delta r^2}+\dfrac{1}{2r_{j-\frac{1}{2}}\Delta r}\right] \\ \dfrac{1}{2r_j}+\dfrac{1}{\Delta r} & -in\dfrac{1}{2r_j} & -\dfrac{ik}{2} \end{bmatrix}, \tag{4.18}$$

$$\left[A_{j-}\right]=\begin{bmatrix} \dfrac{2U_R}{\mathrm{Re}}\left[\dfrac{1}{\Delta r^2}-\dfrac{1}{2r_{j-\frac{1}{2}}\Delta r}\right] & 0 & 0 \\ 0 & \dfrac{2U_R}{\mathrm{Re}}\left[\dfrac{1}{\Delta r^2}-\dfrac{1}{2r_{j-\frac{1}{2}}\Delta r}\right] & 0 \\ 0 & 0 & \dfrac{2U_R}{\mathrm{Re}}\left[\dfrac{1}{\Delta r^2}-\dfrac{1}{2r_{j-\frac{1}{2}}\Delta r}\right] \\ 0 & 0 & 0 \end{bmatrix}, \tag{4.19}$$

.

$$\{P_+\}=\begin{bmatrix} \dfrac{1}{2r^2_{j-\frac{1}{2}}}-\dfrac{1}{r_{j-\frac{1}{2}}\Delta r} \\ in\dfrac{1}{2r^2_{j-\frac{1}{2}}} \\ ik\dfrac{1}{2r^2_{j-\frac{1}{2}}} \\ 0 \end{bmatrix}, \{P_-\}=\begin{bmatrix} \dfrac{1}{2r^2_{j-\frac{1}{2}}}+\dfrac{1}{r_{j-\frac{1}{2}}\Delta r} \\ in\dfrac{1}{2r^2_{j-\frac{1}{2}}} \\ ik\dfrac{1}{2r^2_{j-\frac{1}{2}}} \\ 0 \end{bmatrix}, \qquad (4.20), (4.21)$$

$$[A_{C1}]=\begin{bmatrix} AC_{jj} & 2\Omega+in\dfrac{2U_R}{\mathrm{Re}}\dfrac{2}{r^2_{j-\frac{1}{2}}} & 0 \\ -2\Omega-in\dfrac{2U_R}{\mathrm{Re}}\dfrac{2}{r^2_{j-\frac{1}{2}}} & AC_{jj} & 0 \\ \left.\dfrac{\partial U_R(r)}{\partial r}\right|_{r_{j-\frac{1}{2}}} & 0 & AC_{jj}+\dfrac{2U_R}{\mathrm{Re}}\dfrac{1}{r^2_{j-\frac{1}{2}}} \\ \dfrac{1}{2r_j}-\dfrac{1}{\Delta r} & -in\dfrac{1}{2r_j} & -\dfrac{ik}{2} \end{bmatrix}, \qquad (4.22)$$

$$AC_{jj}=-i\omega+ikU_R\left(r_{j-\frac{1}{2}}\right)-\frac{2U_R}{\mathrm{Re}}\left\{\frac{3}{2r_{j-\frac{1}{2}}\Delta r}+\frac{1+n^2}{r^2_{j-\frac{1}{2}}}+k^2-\frac{2}{\Delta r^2}\right\},$$

$$[A_{C2}]=\begin{bmatrix} \dfrac{2U_R}{\mathrm{Re}}\left[\dfrac{2}{r_{j-\frac{1}{2}}\Delta r}-\dfrac{5}{\Delta r^2}\right] & 0 & 0 \\ 0 & \dfrac{2U_R}{\mathrm{Re}}\left[\dfrac{2}{r_{j-\frac{1}{2}}\Delta r}-\dfrac{5}{\Delta r^2}\right] & 0 \\ 0 & 0 & \dfrac{2U_R}{\mathrm{Re}}\left[\dfrac{2}{r_{j-\frac{1}{2}}\Delta r}-\dfrac{5}{\Delta r^2}\right] \\ \dfrac{1}{2r_j}+\dfrac{1}{\Delta r} & -in\dfrac{1}{2r_j} & -\dfrac{ik}{2} \end{bmatrix}, \qquad (4.23)$$

$$[A_{C3}]=\begin{bmatrix} \frac{2U_R}{\mathrm{Re}}\left[-\frac{1}{2r_{j-\frac{1}{2}}h}+\frac{4}{\Delta r^2}\right] & 0 & 0 \\ 0 & \frac{2U_R}{\mathrm{Re}}\left[-\frac{1}{2r_{j-\frac{1}{2}}\Delta r}+\frac{4}{\Delta r^2}\right] & 0 \\ 0 & 0 & \frac{2U_R}{\mathrm{Re}}\left[-\frac{1}{2r_{j-\frac{1}{2}}\Delta r}+\frac{4}{\Delta r^2}\right] \\ 0 & 0 & 0 \end{bmatrix}, \quad (4.24)$$

$$[A_{C4}]=\begin{bmatrix} -\frac{2U_R}{\mathrm{Re}}\frac{1}{\Delta r^2} & 0 & 0 \\ 0 & -\frac{2U_R}{\mathrm{Re}}\frac{1}{\Delta r^2} & 0 \\ 0 & 0 & -\frac{2U_R}{\mathrm{Re}}\frac{1}{\Delta r^2} \\ 0 & 0 & 0 \end{bmatrix}. \quad (4.25)$$

4.4. Coupling the fluid solution with the shell

Because of the way the grid is staggered, the value of the pressure flux on the wall is not found directly. The pressure-flux is not discretised on the wall, as seen on Fig. 5. In order to evaluate it at the wall, a second-order-accurate extrapolation is used:

$$\hat{q}_{N+\frac{1}{2}}=\frac{15\hat{q}_N-10\hat{q}_{N-1}+3\hat{q}_{N-2}}{8}. \quad (4.26)$$

The fluid stresses on the wall also depend on the r-derivative of the velocity components. It is therefore necessary to define a multipoint backward difference for the velocity with an equation analogous to eqs. (4.13):

$$D_{W\_}\hat{v}_{r,j}=\frac{3\hat{v}_{r,j}-4\hat{v}_{r,j-1}+\hat{v}_{r,j-2}}{2\Delta r}. \quad (4.27)$$

The forces produced by the fluid acting on the shell wall are modelled through the force influence coefficients of eq. (3.84). Making use of eq. (4.27), the force influence

coefficients of eq. (3.84) can be expressed as functions of the numerical solution of the flow specific to a given set of parameters ω, k, n, Ω, Re, $\bar{U}_R$:

$$\pi_z = \frac{2\bar{U}_R}{\mathrm{Re}} D_{W-}\hat{v}_{z,N+\frac{1}{2}} - ik\frac{2\bar{U}_R}{\mathrm{Re}}\hat{v}_{r,N+\frac{1}{2}}, \tag{4.28}$$

$$\pi_\theta = \frac{2\bar{U}_R}{\mathrm{Re}} D_{W-}\hat{v}_{\theta,N+\frac{1}{2}} - \frac{2\bar{U}_R}{\mathrm{Re}}\frac{1}{r_{N+\frac{1}{2}}}\hat{v}_{\theta,N+\frac{1}{2}} - in\frac{2\bar{U}_R}{\mathrm{Re}}\frac{1}{r_{N+\frac{1}{2}}}\hat{v}_{r,N+\frac{1}{2}}, \tag{4.29}$$

$$\pi_r = \frac{4\bar{U}_R}{\mathrm{Re}} D_{W-}\hat{v}_{r,N+\frac{1}{2}} - \hat{q}_{N+\frac{1}{2}}, \tag{4.30}$$

where as in the rest of this chapter the subscript x present in every influence function has been dropped for brevity.

4.5. Iterative loop

To summarise the problem, we have the summation of forces given by eq. (3.3). By setting the determinant of the matrix $[L]$ in eq. (3.3) to zero, we obtain a dispersion relation, and for a given set of parameters k, n, Ω, $\mathrm{R_e}$, $\bar{U}_R$, h, Γ, ν we can solve for the complex frequencies of the system ω. Because the fluid force influence coefficients obtained through the numerical solution of the flow in eqs. (4.28)-(4.30) depend on the complex frequency of the system ω, the dispersion relation is implicit in ω and we must iterate to find the admissible frequencies of the system.

The scheme employed to obtain the curves of the evolution of the complex frequencies versus the mean flow rate is to first find the lowest frequencies of the system with no axial flow by iterating using a Müller root-finding algorithm [see Burden and Faires (2001)]. Once these are obtained, we proceed to slowly increment the flow rate using the frequencies of the previous step as a first guess.

4.6. Numerical solutions to the viscous models

4.6.1. Numerical solution to the classical no-slip model

The classical no-slip model defined in Section 3.8.1 requires three solutions of the finite difference system of equations (4.15) over the domain $0 \le r \le 1$ with the flow profile defined in eq. (3.39) if the flow is laminar,

$$U_R(r_j) = \frac{3}{2}\bar{U}_R\left(1-r_j^2\right), \tag{4.31}$$

or the flow profile defined in eq. (3.52) if the flow is turbulent

$$U_R(r)\big|_{r_j} = \min\left[\left\{\left(1-r_j\right)\frac{f}{16}\mathrm{Re}\bar{U}_R\right\},\ \left\{\frac{8}{7}\bar{U}_R\left(1-r_j\right)^{1/7}\right\}\right], \tag{4.32}$$

for the three sets of boundary conditions

$$\begin{Bmatrix}\hat{v}_{z,u}\\ \hat{v}_{\theta,u}\\ \hat{v}_{r,u}\end{Bmatrix}_{N+\frac{1}{2}} = \begin{Bmatrix}i\omega\\ 0\\ 0\end{Bmatrix}, \tag{4.33}$$

$$\begin{Bmatrix}\hat{v}_{z,v}\\ \hat{v}_{\theta,v}\\ \hat{v}_{r,v}\end{Bmatrix}_{N+\frac{1}{2}} = \begin{Bmatrix}0\\ i\omega\\ 0\end{Bmatrix}, \tag{4.34}$$

$$\begin{Bmatrix}\hat{v}_{z,w}\\ \hat{v}_{\theta,w}\\ \hat{v}_{r,w}\end{Bmatrix}_{N+\frac{1}{2}} = \begin{Bmatrix}-3\bar{U}_R\\ 0\\ i\omega\end{Bmatrix}, \tag{4.35}$$

and by definition $\hat{q}_0 \equiv 0$ always. The fluid forces of eq. (3.83) can be substituted in the matrix $[L]$ defined in eq. (3.86) once they have been computed according to eqs. (4.28)-(4.30).

4.6.2. Numerical solution to the slip model

The slip model defined in Section 3.8.2 requires one solution of the flow for a *w*-perturbation. In order to impose the boundary conditions of the form given in eqs. (3.89)

and (3.90), we define a second-order multipoint backward difference, analogous to eq. (4.14),

$$D_{W\_}^2 \hat{v}_{r,j} = \frac{2\hat{v}_j - 5\hat{v}_{j-1} + 4\hat{v}_{j-2} - \hat{v}_{j-3}}{\Delta r^2}. \tag{4.36}$$

In the system of finite difference equations (4.15), we can then treat $\hat{v}_{\theta,N+\frac{1}{2}}$ and $\hat{v}_{z,N+\frac{1}{2}}$ as unknowns and move them from the right-hand side of the equation to the left-hand side. This requires the introduction of two more equations in the system based on eqs. (3.89), (3.90) and (4.36):

$$\frac{2\hat{v}_{\theta,N+\frac{1}{2}} - 5\hat{v}_{\theta,N-\frac{1}{2}} + 4\hat{v}_{\theta,N-1\frac{1}{2}} - \hat{v}_{\theta,N-2\frac{1}{2}}}{\Delta r^2} = 0, \tag{4.37}$$

$$\frac{2\hat{v}_{z,N+\frac{1}{2}} - 5\hat{v}_{z,N-\frac{1}{2}} + 4\hat{v}_{z,N-1\frac{1}{2}} - \hat{v}_{z,N-2\frac{1}{2}}}{\Delta r^2} = 0. \tag{4.38}$$

The other boundary condition on the wall is provided by the no-penetration condition:

$$\hat{v}_{r,N+\frac{1}{2}} = i\omega - ik\bar{U}_R. \tag{4.39}$$

The boundary conditions at the centre of the flow is by definition $\hat{q}_0 \equiv 0$. The flow can then be solved over the domain $0 \le r \le 1$ with a square flow profile

$$U_R(r_j) = \bar{U}_R, \tag{4.40}$$

$$\left.\frac{\partial U_R(r)}{\partial r}\right|_{r_j} = 0. \tag{4.41}$$

The forces the fluid produce on the shell are given in eqs. (3.83), (3.97) and can be computed according to eqs. (4.28)-(4.30).

4.6.3. Numerical solution to the average-velocity model

The numerical solution to the average-velocity model defined in Section 3.8.3 is essentially the same as that of the classical no-slip model, except that the boundary conditions at the wall are the following:

$$\begin{Bmatrix} \hat{v}_{z,u} \\ \hat{v}_{\theta,u} \\ \hat{v}_{r,u} \end{Bmatrix}_{N+\frac{1}{2}} = \begin{Bmatrix} i\omega - ik\bar{U}_R \\ 0 \\ 0 \end{Bmatrix}, \tag{4.42}$$

$$\begin{Bmatrix} \hat{v}_{z,v} \\ \hat{v}_{\theta,v} \\ \hat{v}_{r,v} \end{Bmatrix}_{N+\frac{1}{2}} = \begin{Bmatrix} 0 \\ i\omega - ik\bar{U}_R \\ 0 \end{Bmatrix}, \tag{4.43}$$

$$\begin{Bmatrix} \hat{v}_{z,w} \\ \hat{v}_{\theta,w} \\ \hat{v}_{r,w} \end{Bmatrix}_{N+\frac{1}{2}} = \begin{Bmatrix} -3\bar{U}_R \\ 0 \\ i\omega - ik\bar{U}_R \end{Bmatrix}. \tag{4.44}$$

4.6.4. Numerical solution to the delta model

The numerical solution to delta model defined in Section 3.8.4 requires three solutions of the finite difference system of equations (4.15) over the domain $0 \le r \le 1-\delta$, with the flow profile defined in eq. (3.39) if the flow is laminar,

$$U_R(r_j) = \frac{3}{2}\bar{U}_R\left(1-r_j^2\right), \tag{4.45}$$

or the flow profile defined in eq. (3.52) if the flow is turbulent

$$U_R(r)\big|_{r_j} = \min\left[\left\{\left(1-r_j\right)\frac{f}{16}\mathrm{Re}\bar{U}_R\right\}, \left\{\frac{8}{7}\bar{U}_R\left(1-r_j\right)^{1/7}\right\}\right], \tag{4.46}$$

for the three sets of boundary conditions

$$\begin{Bmatrix} \hat{v}_{z,u} \\ \hat{v}_{\theta,u} \\ \hat{v}_{r,u} \end{Bmatrix}_{N+\frac{1}{2}} = \begin{Bmatrix} i\omega - ikU_R(r)\big|_{r=1-\delta} \\ 0 \\ 0 \end{Bmatrix}, \tag{4.47}$$

$$\begin{Bmatrix} \hat{v}_{z,v} \\ \hat{v}_{\theta,v} \\ \hat{v}_{r,v} \end{Bmatrix}_{N+\frac{1}{2}} = \begin{Bmatrix} 0 \\ i\omega - ikU_R(r)\big|_{r=1-\delta} \\ 0 \end{Bmatrix}, \tag{4.48}$$

$$\begin{Bmatrix} \hat{v}_{z,w} \\ \hat{v}_{\theta,w} \\ \hat{v}_{r,w} \end{Bmatrix}_{N+\frac{1}{2}} = \begin{Bmatrix} \left.\dfrac{\partial U_R(r)}{\partial r}\right|_{r=1-\delta} \\ 0 \\ i\omega - ikU_R(r)\big|_{r=1-\delta} \end{Bmatrix}, \tag{4.49}$$

and by definition $\hat{q}_0 \equiv 0$ always. In this numerical solution $r_j = j\Delta r$ and $\Delta r = \left(1-\delta\right)/\left(N+\frac{1}{2}\right)$. The fluid forces of eq. (3.83) can be substituted in the matrix $[L]$ given by eq. (3.86) once they have been computed according to eqs. (4.28)-(4.30).

A copy of the Matlab code used to find the numerical solution to the delta model is presented in Appendix E.

Chapter 5

Inviscid theory results

In this chapter, the results to the problem formulated in Chapter 2, namely that of a cylindrical shell subjected to an internal inviscid fluid flow are presented. These results are obtained to (i) reproduce in part the work of Lai and Chow (1973), (ii) to attempt explaining further the results of Cortelezzi et al. (2004) and build upon their findings, and (iii) to establish a benchmark for the viscous theory results of the next chapter.

The calculations are performed for the case of a rubber tube carrying water flow. The values of the shell and fluid parameters employed in the analyses are given in Table 1. Lai and Chow (1973) and Cortelezzi et al. (2004) studied the same system with identical parameter values.

Parameter	Value
R' [m]	0.019
h' [m]	3.8E-4
ν	0.49
E' [Pa]	1.033E6
ρ_s' [kg/m^3]	1050
ρ_f' [kg/m^3]	1000

Table 1. Shell and fluid parameter values of the inviscid system studied

5.1. Pure axial flow

The shell is first subjected to a pure axial flow. The evolution of the frequencies of the system for increasing internal flow velocity is plotted for four different axial

wavenumbers in Fig. 6. Notice that the scale varies from plot to plot. In each of its vibrating modes, defined by its particular combination of axial and circumferential wavenumbers, the system loses stability by coupled-mode flutter when the forward and the backward travelling wave frequencies coalesce[‡]. By comparing the results of Fig. 6 (b) to those obtained by and Lai and Chow (1973), one notices that the match is exact. The only difference comes from the fact that here an iterative complex-root-finding algorithm was employed to obtain the frequencies rather than a method using only real frequencies. This allowed obtaining the post instability frequencies with the complex parts. The modes are said to be unstable when one of the imaginary frequencies becomes negative. For example, in Fig. 6 (a) for an axial wavenumber of $k = 15$, the circumferential mode $n = 0$ becomes unstable at a critical reduced flow velocity $\bar{U}_R = 0.12$; $n = 6$ becomes unstable at $\bar{U}_R = 0.13$; $n = 8$ becomes unstable at $\bar{U}_R = 0.14$. Out of the limited number of frequency evolutions shown in Fig. 6, for mode $n = 6$, $k = 5$ has the lowest critical reduced flow velocity at $\bar{U}_R = 0.105$.

The main objective of a linear stability analysis is to define precisely the critical points of the onset of instability. This is done by plotting the neutral stability curve of the system, as is done in Fig. 7. It is observed that the most unstable circumferential wavenumber depends on the axial wavenumber. For the studied circumferential wavenumbers presented in Fig. 7, $n = 0$ has the lowest critical reduced flow velocity for large axial wavenumbers $k > 10$, $n = 6$ has the lowest critical reduced flow velocity for medium axial wavenumbers $2 < k < 10$, and $n = 3$ has the lowest critical reduced flow velocity for small axial wavenumbers $k < 2$.

[‡] It is noted that, actually, before this happens, the backward travelling wave becomes a second forward travelling one, when it crosses the Real(ω)=0 line. That point has been considered to represent a form of divergence in the system.

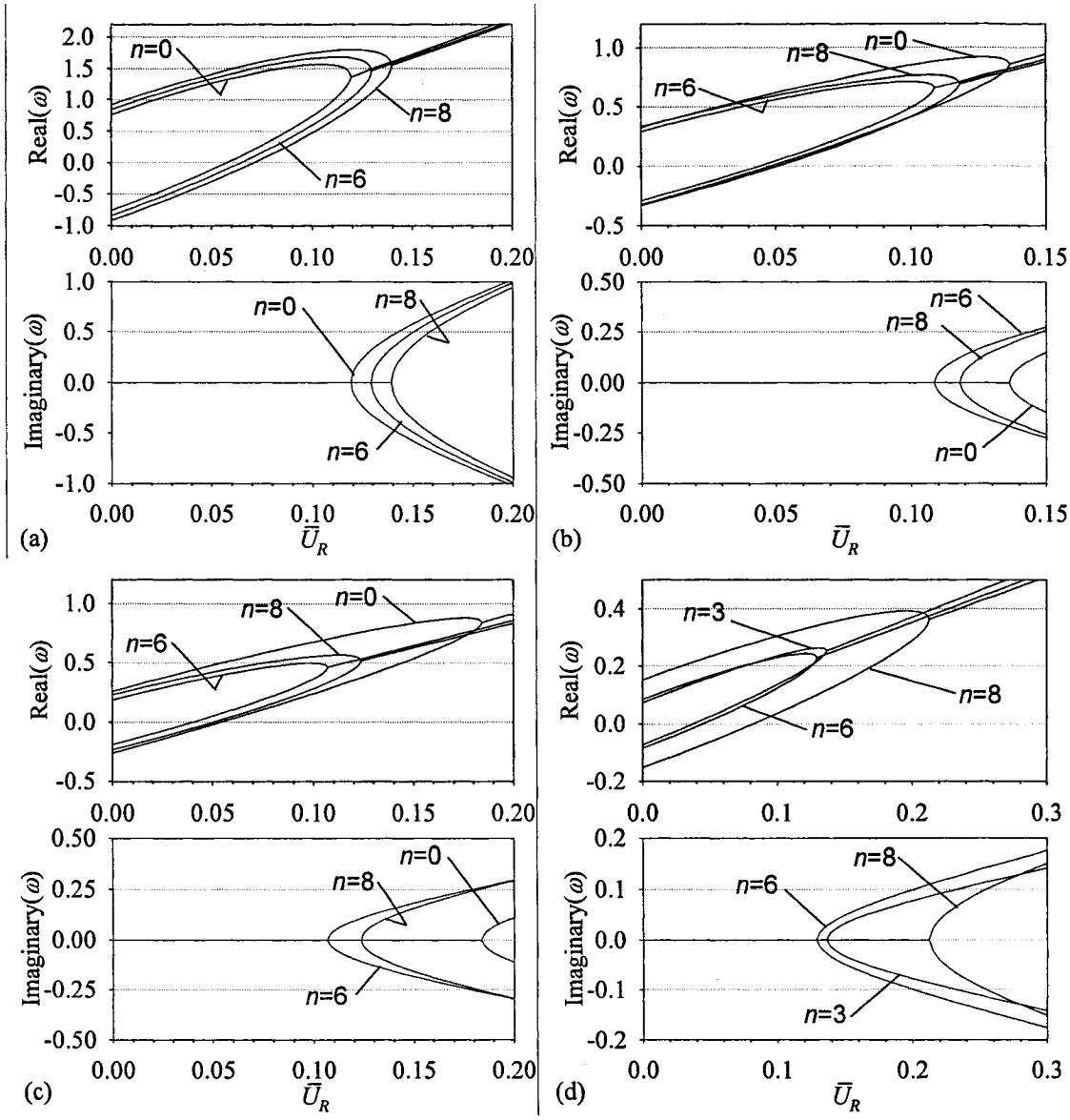

Fig. 6. Evolution of the frequencies of a non-rotating tube vibrating at dimensionless wavenumbers (a) : k=15; (b) : k=7.2; (c) : k=5; (d) : k=2

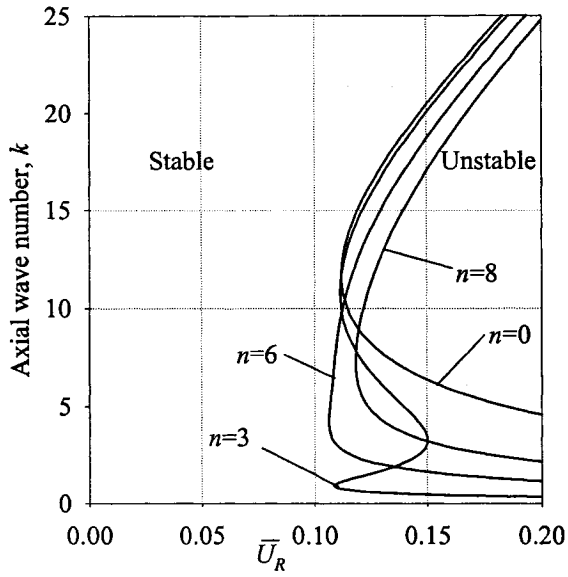

Fig. 7. Neutral stability curves of vibrating modes of non-rotating tube with flowing inviscid fluid.

5.2. Rotation

As mentioned in Chapter 1, Cortelezzi et al. (2004) found it impossible to reproduce the results of Lai and Chow (1973) when there is rotation, because of the existence of singularities. These singularities make the problem such that no solution exists. Because we know that the solution does not exist for a particular region of the parameter space, we employ the technique of the zero-level contour method described in Pong (2000) to obtain results.

The dispersion relation curve for $\Omega = 0.1$, $k = 10$ and $n = 0$ is computed and shown in Fig. 8 superimposed on the contour plot of the value of Λ, which is defined in eq. (2.60) as $\Lambda = 2\Omega/(\omega - kU_R)$. In Fig. 8 the dispersion relation is exactly the same as that obtained by Cortelezzi et al. The "islets where a solution is not feasible" described by Cortelezzi et al. really are numerous infinitely long lines that appear as islets only because of lack of resolution. These lines of no-solution are parallel to the Λ-isolines as can be seen in Fig. 8 in the region where $|\Lambda| > 1$. The breakdown of the flow solution is directly related to the value of this parameter Λ, which motivates a deeper look at the formulation of the inviscid flow solution. This is done in the next sections of this chapter.

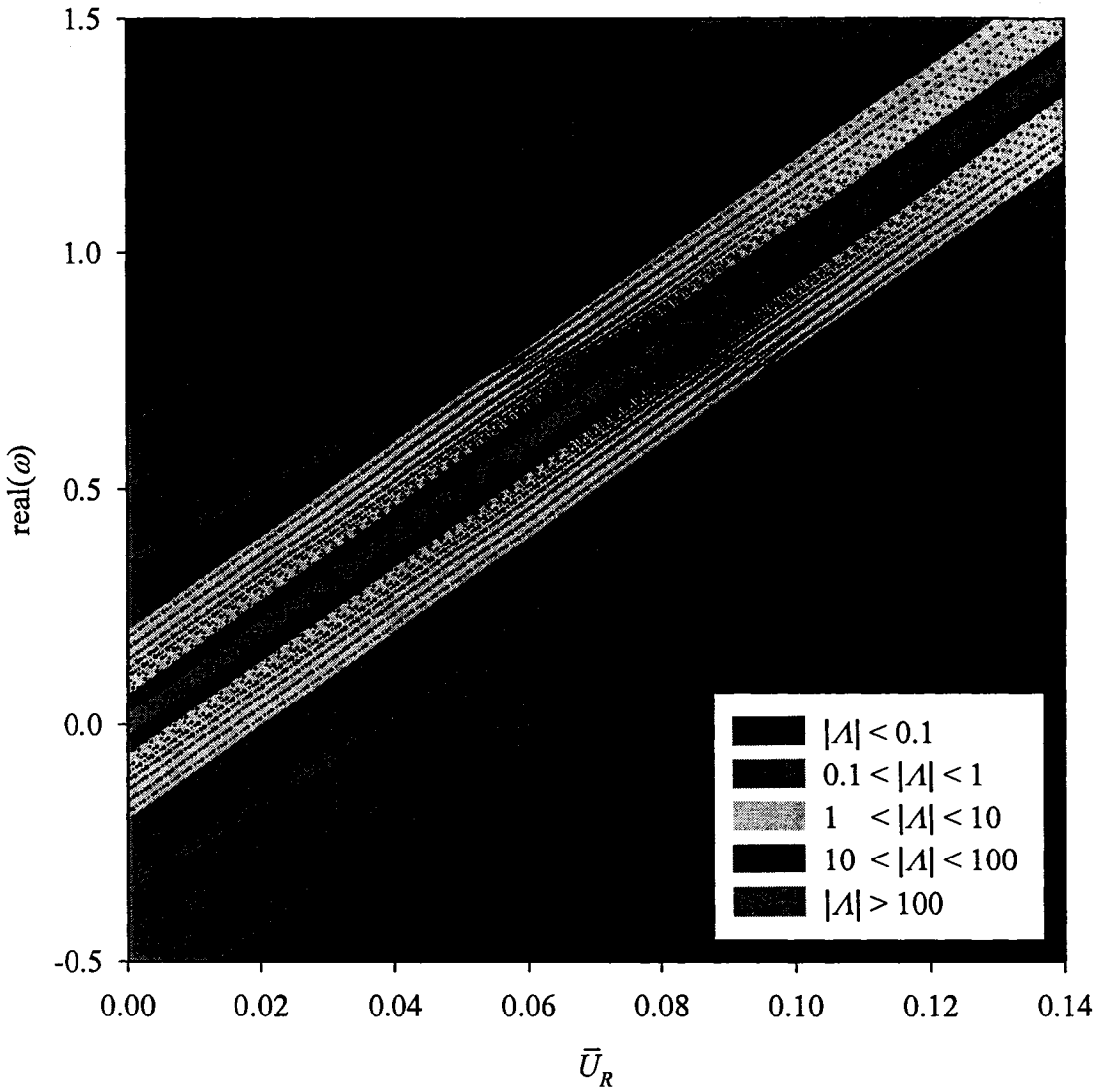

Fig. 8. Stability curve of the inviscid fluid model superimposed on the contour plot of the absolute value of Λ. The shades of grey represent the contour plot of the absolute value of Λ with which is associated the legend in the lower right corner.

5.3. Discontinuities in the pressure solution

The inviscid fluid pressure solution is given in by eqs. (2.62)-(2.64). Depending on the absolute value of Λ, the flow solution takes the form of a modified Bessel function, a Bessel function or a polynomial. As can be seen in Fig. 8 by comparing the dispersion relation with the Λ-contours, it is the Bessel function which is responsible for

these infinite lines of no-solution in the $|\Lambda| > 1$ region. A typical pressure flow solution obtained with the Bessel solution is shown in Fig. 9 for a small range of Λ. It is seen that the pressure solution has a great number of poles for various values of Λ. As pictured in the contour plot in Fig. 8, for the domain of ω of interest and $\bar{U}_R$, $|\Lambda|$ can take values ranging from almost 0 to ∞. As the Bessel function has an infinite number of roots, in the region where $|\Lambda| > 1$ the denominator of eq. (2.62) goes to zero an infinite number of times. Each time, there is no bounded solution, as Cortelezzi et al. had found, and for each critical value of Λ this leads to a line of no-solution in the dispersion relation.

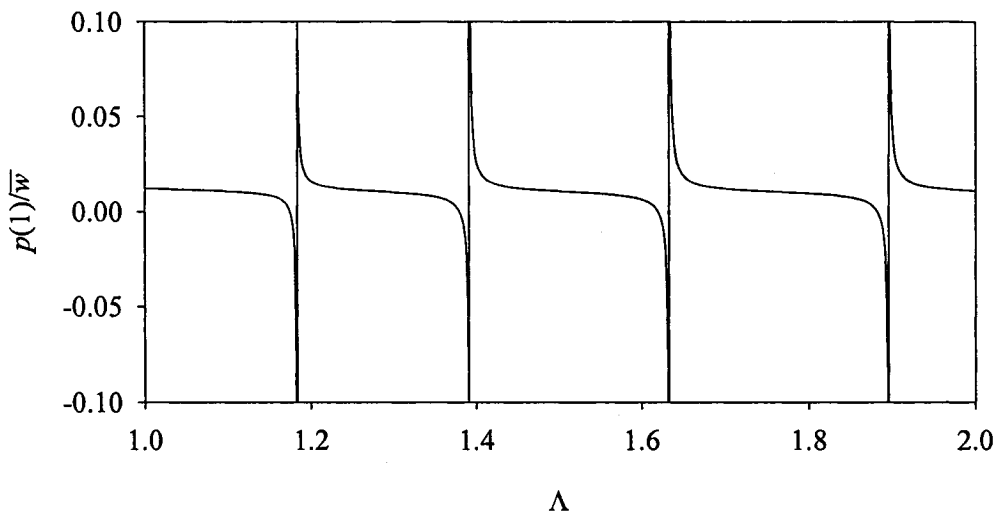

Fig. 9. Typical pressure flow solution obtained with the modified Bessel function for the parameters: k=10, n=0, Ω=0.1, U_R=0.1.

5.4. Bessel approximations

From many good mathematical textbooks, it can be found that Bessel functions may be expressed in the following infinite series form:

$$J_n(x) = \sum_{m=0}^{\infty} \frac{(-1)^m}{m!(m+n)!}\left(\frac{x}{2}\right)^{2m+n}, \tag{5.1}$$

and modified Bessel functions are given by this series:

$$I_n(x) = \sum_{m=0}^{\infty} \frac{1}{m!(m+n)!}\left(\frac{x}{2}\right)^{2m+n}. \tag{5.2}$$

Obviously when doing numerical computations, the series of eqs. (5.1) and (5.2) have to be truncated to a finite number of terms.

In eq. (2.62) the quantity of interest is $\mathrm{J}_n(x)/\left(x\mathrm{J}_{n-1}(x)-nf(x)\mathrm{J}_n(x)\right)$, where $f(x)=\sqrt{1+x^2/k^2}+1$ and $x=k\sqrt{\Lambda^2-1}$. This quantity can be approximated by a finite number of terms of eq. (5.1):

1 term

$$\frac{\mathrm{J}_n(x)}{x\mathrm{J}_{n-1}(x)-nf(x)\mathrm{J}_n(x)}\simeq\frac{1}{n\left(2-f(x)\right)}\ \text{for}\ n>0\ \text{and}\simeq\frac{-2}{x^2}\ \text{for}\ n=0, \tag{5.3}$$

2 terms

$$\frac{\mathrm{J}_n(x)}{x\mathrm{J}_{n-1}(x)-nf(x)\mathrm{J}_n(x)}\simeq\frac{(n+1)-\left(x/2\right)^2}{2(n+1)\left(n-\left(x/2\right)^2\right)-nf(x)\left((n+1)-\left(x/2\right)^2\right)}. \tag{5.4}$$

3 terms

$$\frac{\mathrm{J}_n(x)}{x\mathrm{J}_{n-1}(x)-nf(x)\mathrm{J}_n(x)}\simeq$$

$$\frac{2(n+2)\left((n+1)-\left(x/2\right)^2\right)+\left(x/2\right)^4}{2(n+2)\left(2(n+1)\left(n-\left(x/2\right)^2\right)+\left(x/2\right)^4\right)-nf(x)\left(2(n+2)\left((n+1)-\left(x/2\right)^2\right)+\left(x/2\right)^4\right)} \tag{5.5}$$

The Bessel function rather than the modified one is used as a solution only when $\Lambda^2>1$; therefore, $x>0$ and $f(x)>2$. It is then obvious that the 1-term approximation of eq. (5.3) is continuous over the range of its application. But, if we increase the number of terms, the order of the polynomial of the denominator increases and so does the number of roots. For each root of the polynomial of the denominator within the range of application ($\Lambda^2>1$), the solution has a pole and the calculated pressure is infinite. As the number of terms of the solution tends to infinity, the number of poles tends to infinity too.

In the case where $n=0$, eqs (5.3), (5.4) and (5.5) do not have poles in the range where $\Lambda^2>1$ or $x>0$; but the 4-term expansion contains a pole, and the subsequent expansions contain more and more poles. For the $n\neq 0$ cases, it is not as simple, and

poles start to appear in the 2-term expansion and become more numerous because of the $nf(x)$ term in the denominator.

In the work by Lai and Chow (1973), it is not clear how many terms they used in the expansion of the pressure solution; however, but, form the above analysis, we are led to conclude that this number was not very high. The way they succeeded in having closed curves for the dispersion relations of their different figures was most probably by using a limited number of expansion terms.

In an attempt to reproduce the results obtained by Lai & Chow (1973), eq. (2.30) is solved using various numbers of terms in the expansion of the pressure solution. The effect of the number of terms in the expansion of the pressure solution is shown in Fig. 10 for $n = 0$ and in Fig. 11 for $n = 8$.

As expected, the curves obtained with a 1-term and a 3-term expansion are perfectly continuous in Fig. 10 (a) and (b). When the number of terms is increased to four, the discontinuities appear, as shown in Fig. 10 (c) and (d).

In Fig. 11 (a) as well, the curve obtained with only 1 term is perfectly continuous, but discontinuities are readily visible as soon as two terms or more are employed in the expansion of Fig. 11 (b) and (c). The $nf(x)$ terms in the denominator of eqs (5.4) and (5.5) increase the number of poles as compared to the $n = 0$ case.

In Fig. 10 (d) and Fig. 11 (d) the Bessel functions and modified Bessel functions are computed using the Matlab functions "besselj" and "besseli". These algorithms use a high enough number of terms of the series for the value of the function to converge to 15 significant digits. The solutions offered by these Matlab functions will be referred to here as semi-infinite, as their precision is as good as the rest of the computations. With these semi-infinite expansions, the results obtained are the same as those of Cortelezzi et al. (2004) and the lines of no solution start showing. Since we only find solutions for a finite number of values of $\bar{U}_R$ and ω, the discontinuities appear as islets, but, as shown in the previous section, these discontinuities should appear as an infinite number of isolines of Λ between in the zone where $\Lambda^2 > 1$.

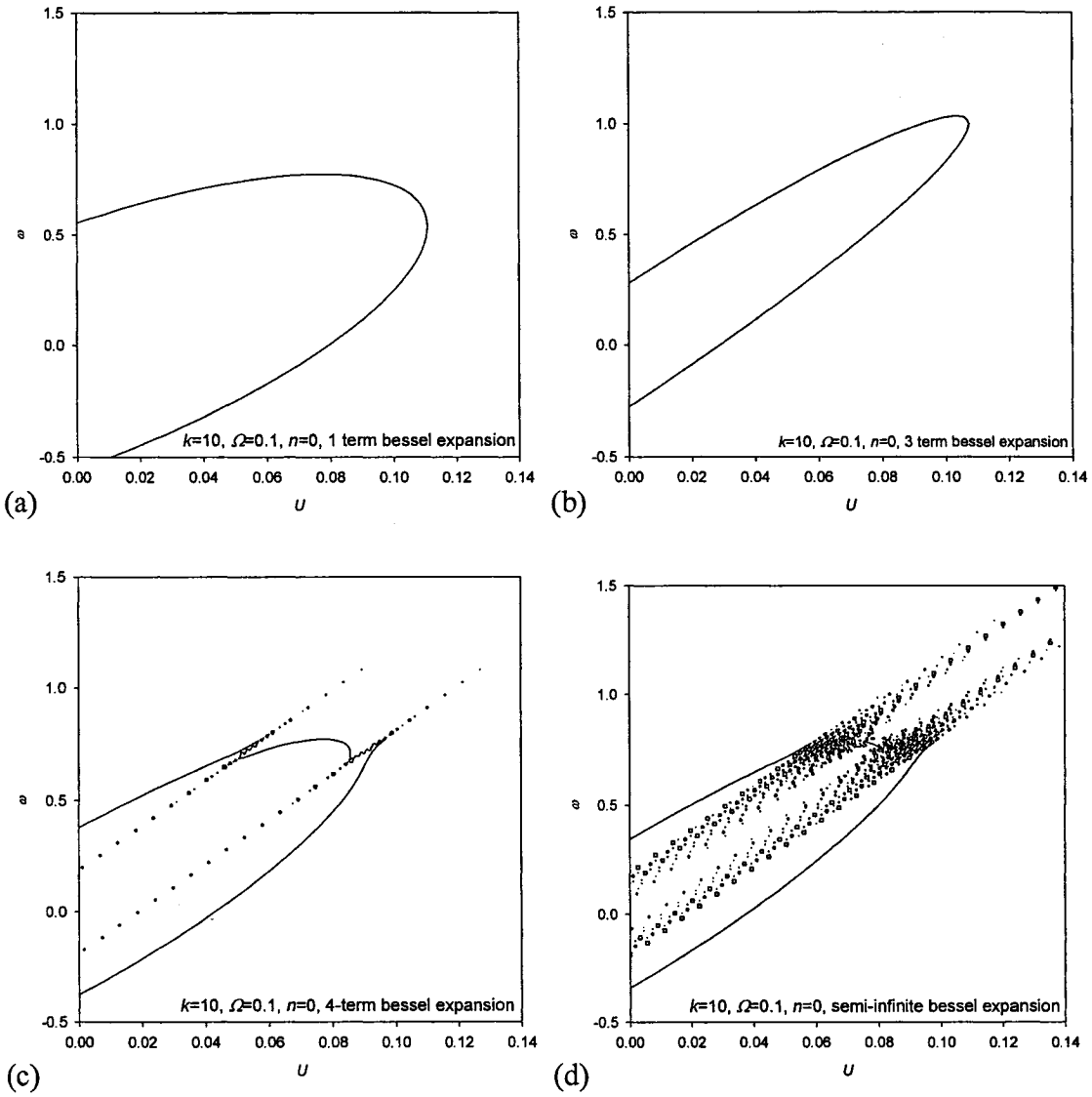

Fig. 10. Comparative study of the effect of the number of terms in the Bessel functions on the continuity of the pressure solution in the case of $n = 0$ circumferential waves and axial wavenumber $k = 10$: (a) 1-term Bessel expansion; (b) 3-term Bessel expansion; (c)43-term Bessel expansion; (d) semi-infinite Bessel expansion.

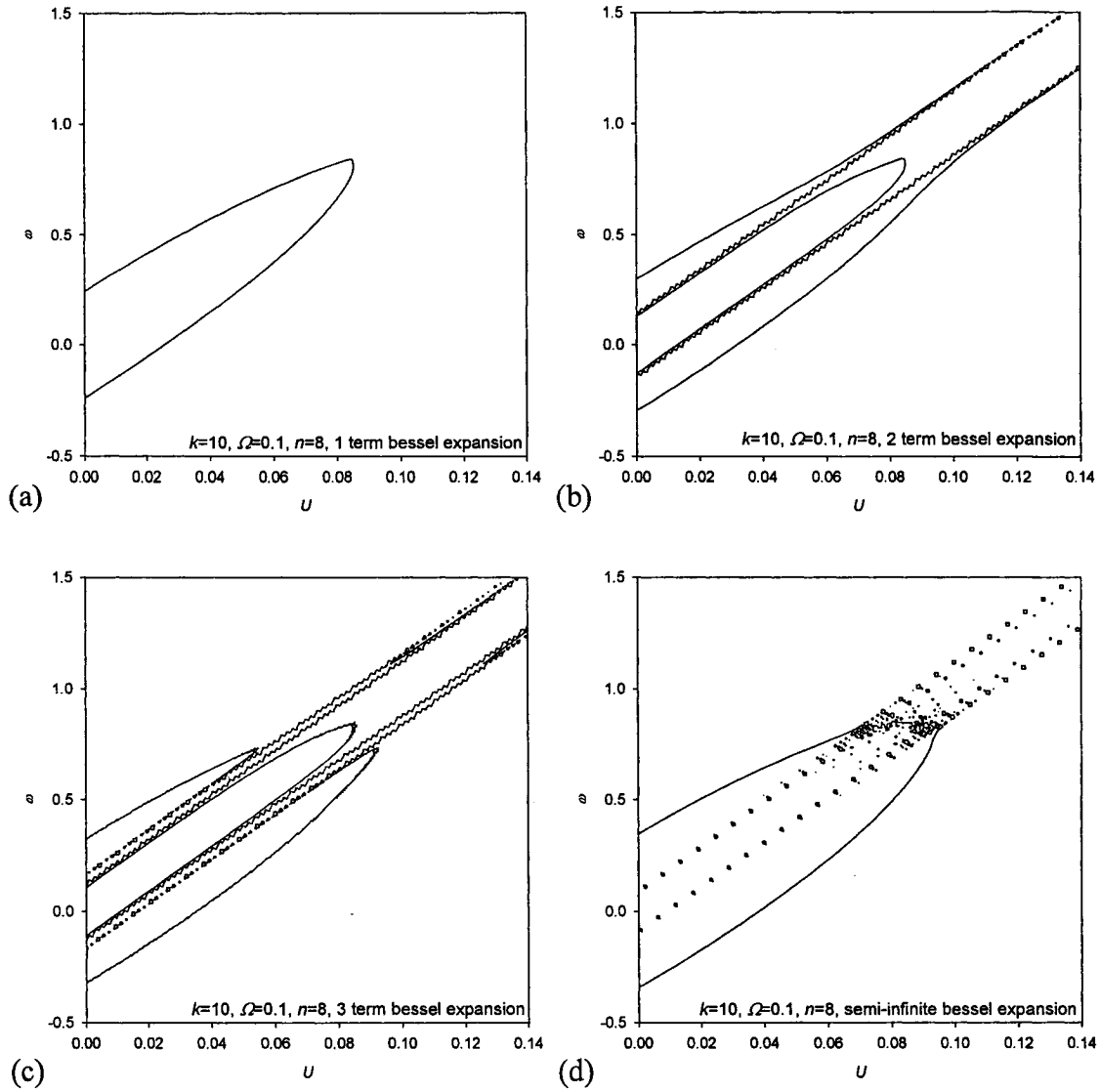

Fig. 11. Comparative study of the effect of the number of terms in the Bessel functions on the continuity of the pressure solution in the case of $n = 8$ circumferential waves and axial wavenumber $k = 10$: (a) 1-term Bessel expansion; (b) 2-term Bessel expansion; (c) 3-term Bessel expansion; (d) semi-infinite Bessel expansion.

5.5. Flow blocking

Chow (1969) investigates the swirling fluid flow in cylindrical tubes with permanent axisymmetric periodic deformations (varicose-shaped tubes). This is done by solving for the stream function in the governing equations for steady inviscid and

incompressible fluid flow. The problem studied by Chow (1969) is similar to the fluid part of the problem we are concerned with in this section; two major differences are that in Chow (1969) (i) the solution sought is a steady-state one because the boundary of the fluid is not moving and (ii) the deformations in the boundary are not necessarily small. Nevertheless, the two problems share a similar flow solution based on the Bessel functions and both have their dynamics dictated by the Rossby number (here, $1/k\Lambda$ is a modified Rossby number because of the moving walls). In Chow (1969), for critical values of the Rossby number, the system exhibits what the author calls "flow blocking". The effective radius of the pipe is diminished by an amount equal to the size of the permanent undulation of the wall and the flow near the wall becomes stagnant. This phenomenon of flow blocking is observed in stratified flow over obstacles and is discussed more in the literature review of Chapter 1. The similarities between swirling flows and stratified flows were first proposed by Rayleigh (1920) and they are discussed further with an analogy between gravitation and acceleration in Howard and Gupta (1962) and in Yih (1965, Chapter 6).

Flow blocking occurs in Chow (1969) when the fluid solution blows up at a critical Rossby number. Mathematically, something similar happens in the problem considered here when the flow solution has a pole (see sections 5.3 and 5.4). These similarities between the two systems lead us to believe that the poles in the flow studied here could possibly be related to flow blocking. However, due to the way the boundary conditions are applied –at the mean wall position instead of the instantaneous wall position– it is not possible to witness flow blocking. Possibly a non-linear flow model taking into consideration large boundary deformations could show fluid stagnation near the walls at Rossby numbers close to the critical values.

Chapter 6

Viscous theory results

The purpose of this chapter is to present the results of the investigation on the dynamical behaviour of the system defined in Chapter 3, namely that of a cylindrical shell subjected to an internal viscous flow. Because no analytical solution is available for the viscous flow equations of this particular problem, the flow is solved with a numerical method presented in Chapter 4.

The calculations are performed for the same case of the rubber tube carrying water flow studied in Chapter 5. The parameters kept constant in this study are given in Table 2.

Parameter	Value
R' [m]	0.019
h' [m]	3.8E-4
ν	0.49
E' [Pa]	1.033E6
ρ_s' [kg/m^3]	1050
ρ_f' [kg/m^3]	1000

Table 2. Shell and fluid parameter values of the viscous system studied.

6.1 Pure axial flow

The value of the Reynolds number of the flow is varied to study the effect of viscosity. One might wonder why the Reynolds number is taken to be constant for a given set of results instead of increasing as the mean flow velocity is incremented. In an experimental system, as the flow rate is increased, the Reynolds number of the flow would increase too, but here, in this theoretical study, the Reynolds number is taken to be

constant for a given frequency evolution graph. The reason the system is studied for constant values of Reynolds number rather than for a constant value of the viscosity or Stokes number is twofold. First, the entire simulation is run for a single Reynolds number which insures that the flow stays in the same regime throughout, laminar or turbulent. For values of the Reynolds number below 2000, the laminar mean flow model of Section 3.3.1 is used, while for values above 4000, the turbulent model described in Section 3.3.2 is used. Secondly, for a finite value of the Reynolds number, since the diameter and the fluid density are kept constant, as the flow velocity tends to zero, the viscosity must tend to zero too. This has as a consequence to make the damping in the system vanish as $\bar{U}_R \to 0$. For vanishingly small flow velocity, the frequencies of the system are then purely real. It is then simple to iteratively find the real frequencies of the system at close to zero flow velocity and then make use of a complex iterative method to follow the frequencies for incrementing flow velocity. For a constant value of the Reynolds number it is not possible to solve the fluid equations for zero reduced velocity. The solution is therefore obtained for close to zero flow velocity.

It has been shown [see Païdoussis (2003, section 7.2.4(b))] that an FSI model of a cylindrical shell conveying fluid using linear inviscid theory can predict acceptably well the critical reduced flow velocity of the system. Païdoussis and Denise (1972) compared the prediction of the onset of instability of their linear theory with experimental observations. From the characteristics of their experimental systems and from standard values of air viscosity, the range of the Reynolds number in their experiment can be calculated to be 0 to 29200[§]. In their experiments, depending on the boundary conditions, the error margin between the inviscid theoretical prediction of the onset of instability and the measured critical velocity was between 0 and 20%. Karagiozis (2006) has also shown

---

[§] In Païdoussis and Denise (1972), the maximal experimental critical flow velocity found is about $\bar{U}_R = 0.7$. Their dimensionless velocity is equivalent to the reduced velocity defined here in eq. (chapter 3.7). Two different tubes are used in their experiments, but the highest Reynolds number is reached for the silicone rubber tube with properties $E' = 1.48\text{E}6\,\text{Pa}$, $\rho_s' = 1030\,\text{kg/m}^3$, $\nu = 0.47$, and $R' = 0.00711\,\text{m}$. The highest critical reduced velocity is then equivalent to the dimensional flow velocity $\bar{U} = 30\,\text{m/s}$. The experiments were done using air, so assuming standard atmosphere conditions, the kinematic viscosity of air can be found from Munson et al. (2002) to be $\nu_{air} = 1.46\text{E}-5\,\text{m}^2/\text{s}$. This leads to a maximum Reynolds number of $\text{Re} = 29200$.

good agreement between his inviscid theory and his experimental observations for Reynolds number at the onset of instability ranging from 10^4 to 10^6.

Because of the limited experimental data available and because in this analysis we study an infinitely long shell and do not use physical structural boundary conditions, there are no experimental data available to reliably compare to our theoretical results. Because of the satisfactory results obtained with inviscid theory in the previously cited studies, we expect that the added realism brought in by the addition of the unsteady viscous forces in the system should not change the predicted critical flow velocities too much from those found with the inviscid theory, in the turbulent regime at least. Engineering judgement leads us to believe that as the Reynolds number becomes larger and larger, the behaviour of the system should tend towards that predicted with the inviscid theory. From the comparisons of inviscid theoretical predictions with experimental results by Païdoussis and Denise and by Karagiozis, we expect that, in the turbulent regime, the viscous predictions should match in the inviscid predictions at Reynolds numbers of the order of 10^4 and higher.

6.1.1. Classical viscous model results

The dynamics of the system predicted by the carefully derived classical viscous model detailed in Section 3.8.1 with its numerical method of solution developed in Section 4.6.1 is shown here. The frequency evolution for incrementing average reduced velocity obtained with the classical no-slip model is plotted in Fig. 12 for a laminar mean flow with a Reynolds number of 1000. On the same plots, the complex frequencies predicted by the inviscid theory are also shown. In Fig. 12 (a), for dimensionless wavenumbers k=15, and n=8, the classical no-slip model predicts that the system loses stability as the backward travelling wave flutters at $\bar{U}_R = 1.04$, while the inviscid prediction for the onset of instability by coupled-mode flutter is at $\bar{U}_R = 0.14$. In Fig. 12 (b), for k=10, n=0, the classical no-slip model critical reduced velocity is $\bar{U}_R = 1.92$, and for the inviscid theory, it is $\bar{U}_R = 0.115$; in Fig. 12 (c), for k=5, n=6, the classical no-slip model critical reduced velocity is $\bar{U}_R = 1.80$, and for the inviscid theory, it is $\bar{U}_R = 0.107$;

in Fig. 12 (d), for k=2, n=3, the classical no-slip model critical reduced velocity is $\bar{U}_R = 0.14$, and with the inviscid theory it is $\bar{U}_R = 0.137$. Except for the last case, the predictions for the onset of instability by the classical no-slip and the inviscid theories differ by as much as an order of magnitude.

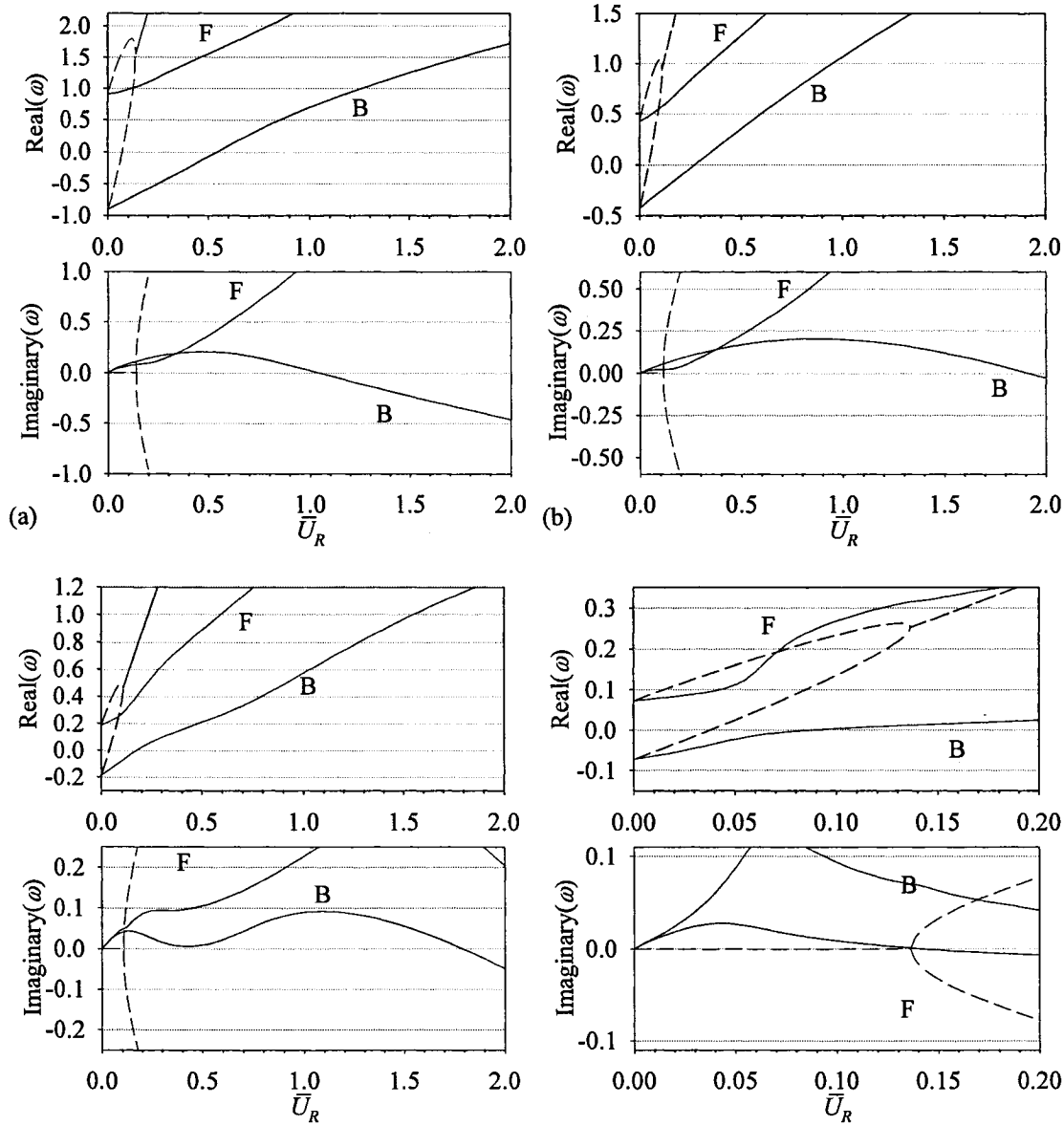

Fig. 12. Comparison of the frequency evolution of a vibrating non-rotating tube conveying laminar flow obtained with the classical no-slip model at Re=10^3 (——), and with the inviscid model (-------), for dimensionless wavenumbers (a) k=15, n=8; (b) k=10, n=0; (c) k=5, n=6; (d) k=2, n=3. The letters F and B indicate the forward and backward travelling waves.

Let us look at the effect of viscosity on the stability of short waves, i.e. large axial wavenumbers. The frequency evolution of the oscillatory mode with dimensionless

wavenumbers k=15 and n=8 is plotted in Fig. 12 (a) for a Reynolds number of 10^3; in Fig. 13 (a)-(d), the frequency evolution of the same mode is plotted for Reynolds numbers of 10^1, 10^2, 10^4, and 10^7. Note that here the parabolic profile was used to obtain all the results plotted in Fig. 12 and Fig. 13. Here when studying the system with a parabolic profile at Reynolds numbers higher than the range of the laminar regime, this is done simply to emphasise the effect of viscosity or the lack thereof. At very a very low Reynolds number of 10^1, as the reduced velocity is increased, the backward travelling wave dies out asymptotically, this could possibly be a form of divergence. For a Reynolds number of 10^2, the backward travelling wave flutters at $\bar{U}_R = 0.455$, at $\mathrm{Re} = 10^3$ it flutters at $\bar{U}_R = 1.04$, and at $\mathrm{Re} = 10^4$ the system seems stable at reduced velocities in the range $0 \le \bar{U}_R \le 2$. If the Reynolds number is increased further and further, we can see in Fig. 13 (d) that the prediction of the critical velocity of the classical no-slip model approaches that of the inviscid model. One can also notice that in Fig. 13 (b) and in Fig. 12 (a), for a Reynolds number of $10^2 - 10^3$, it is the backward travelling wave which makes the system unstable through flutter while in Fig. 13 (d), it is the forward travelling wave. Of course what the model with a parabolic profile predicts at Reynolds number of 10^4 or 10^7 is questionable, as it is outside the laminar regime.

Now looking at the effect of viscosity on a longer wave, i.e. a wave with a small axial wavenumber, the frequency evolution of the oscillatory mode with dimensionless wavenumbers k=2, n=3 is plotted in Fig. 14 (a)-(d) for values of the Reynolds number of 10^2, 10^3, 10^4, and 10^5. Similarly as for the short wave, the increase of the Reynolds number from 10^3 to 10^4 greatly delays the instability. Again as with the short wave, the increase of the Reynolds number past 10^4 makes the system lose stability earlier and earlier and it is the forward travelling wave that flutters rather than the backward one. One also notices that the agreement in the prediction of the loss of instability between the classical no-slip and the inviscid theories which was good in the case of Fig. 12 (d) deteriorates as the Reynolds number is increased. This is contrary to the notion that decreasing the viscosity will make the viscous theory tend towards the inviscid theory.

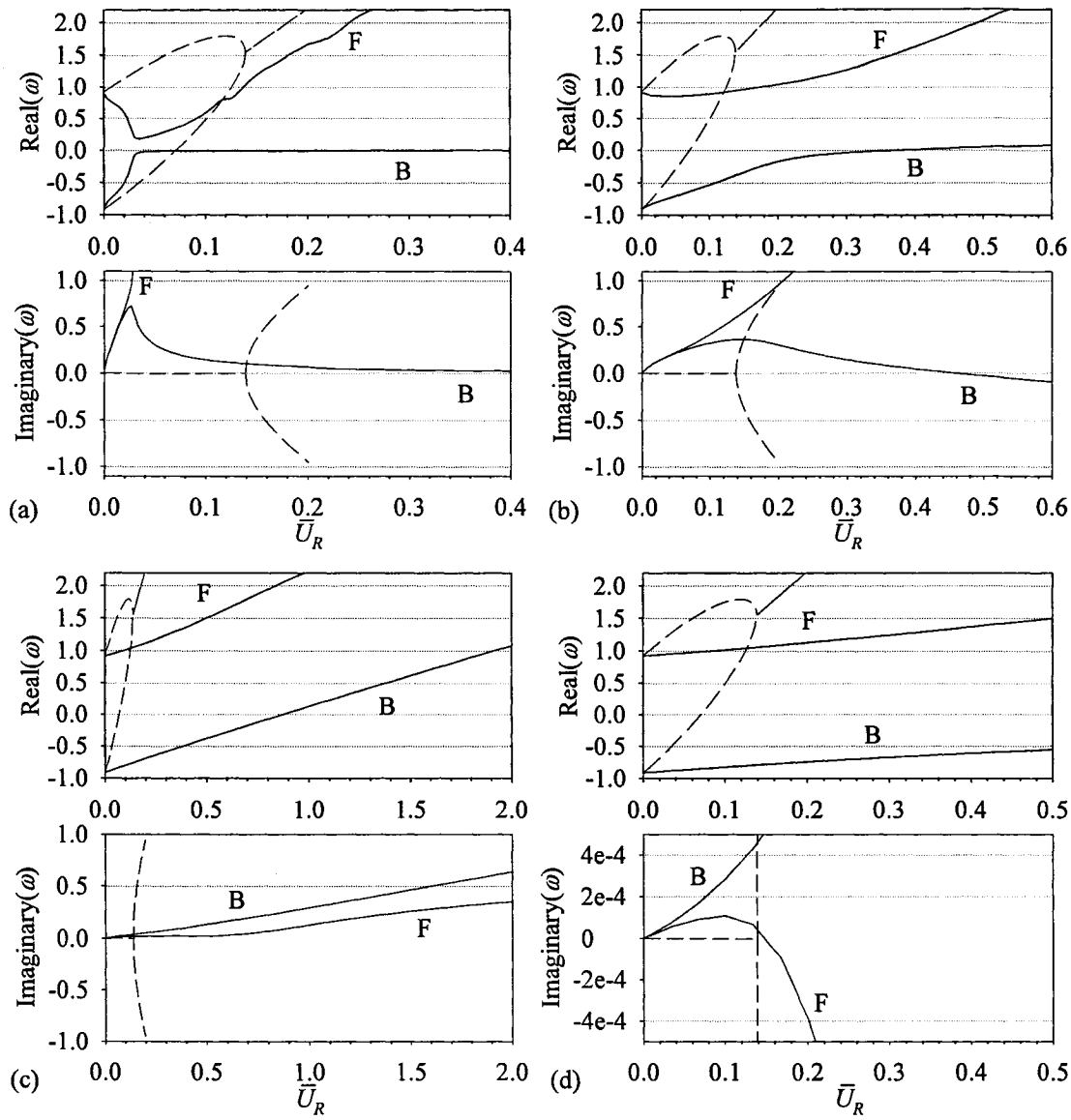

Fig. 13. Effect of the Reynolds number on the classical no-slip model prediction of the frequency evolution of a vibrating non-rotating tube conveying laminar flow for dimensionless wavenumbers k=15 and n=8 (——), for (a) Re=10^1; (b) Re=10^2; (c) Re=10^4; (d) Re=10^7. The letters F and B indicate the forward and backward travelling waves. The inviscid results are plotted for comparison (-------).

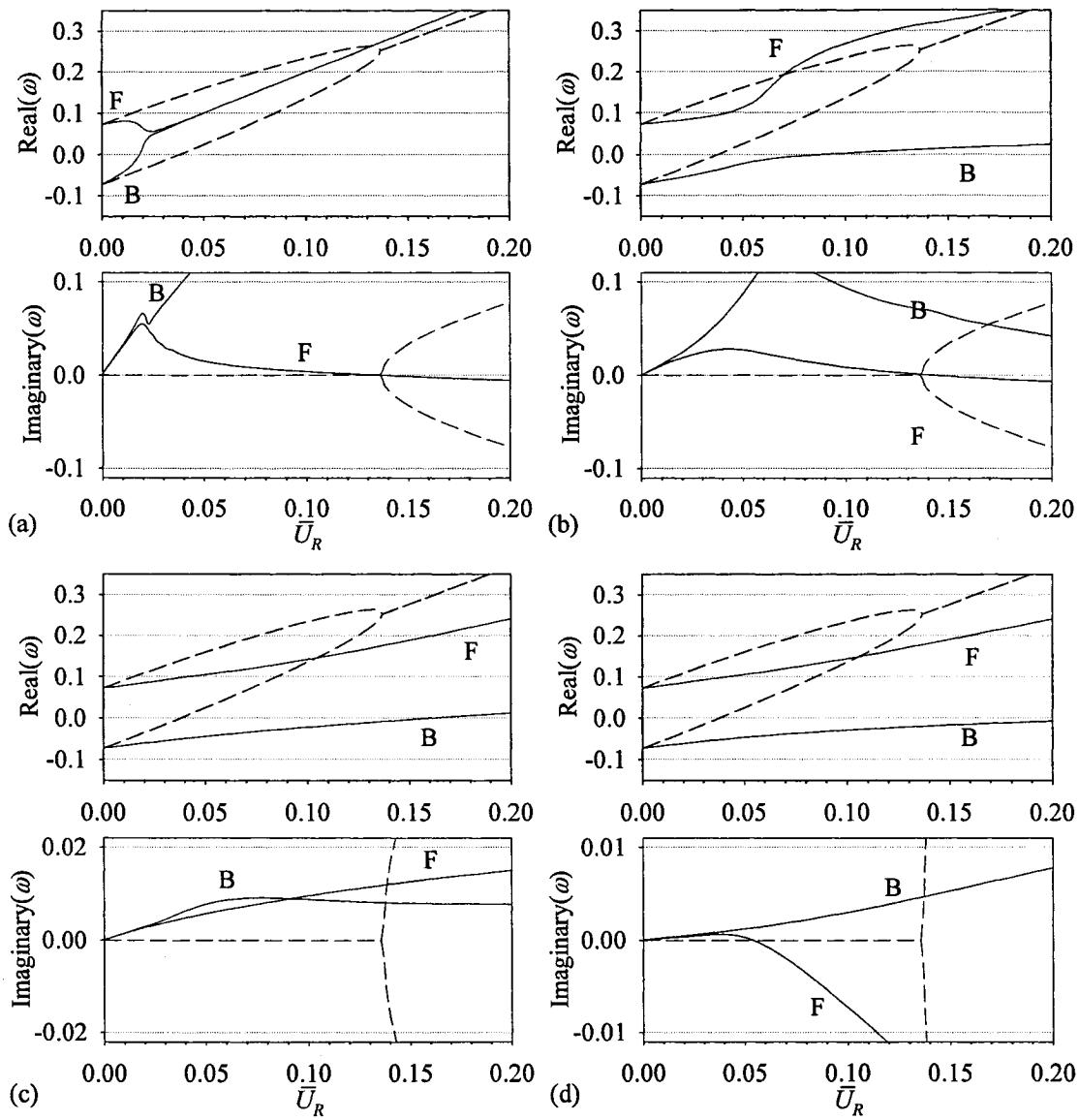

Fig. 14. Effect of the Reynolds number on the classical no-slip model prediction of the frequency evolution of a vibrating non-rotating tube conveying laminar flow for dimensionless wavenumbers k=2 and n=3 (——), for (a) Re=10^2; (b) Re=10^3; (c) Re=10^4; (d) Re=10^5. The letters F and B indicate the forward and backward travelling waves. The inviscid results are plotted for comparison (-------).

The results of Figs. 12-14 were obtained with the classical no-slip model for a laminar profile. For the turbulent regime, the profile based on the empirical power-law and the law of the wall is used. The frequency evolutions of modes k=15, n=8 and k=10, n=0 are plotted in Fig. 15. Two things are noticeable: (i) the critical velocity of both modes is very low, and (ii) a third travelling wave, the Z-wave, emanates from the origin.

Considering the low critical velocity, it seems strange that, compared to the inviscid model, the addition of viscosity, therefore dissipation, dramatically destabilises the system. The fact that the boundary conditions are applied at the undeformed position of the wall really influences the stability of the system, as discussed in Section 3.7. In the viscous model, the velocity components at the wall interface are subjected to no slip boundary conditions. This leads to two things: the perturbation velocity components at the wall match the Lagrangian velocity of the shell, and the mean velocity profile is zero on the wall. Since the mean flow velocity is zero at the wall, the position-dependent terms disappear from the perturbation velocity boundary conditions and this greatly alters the stability of the system. Three different models are presented and derived in Section 3.8 to address this issue. The results obtained with these models follow in the next subsections.

The Z-wave, which at zero flow velocity does not exist, possibly arises from the fluid in the system. Although the very low critical velocity makes the results of Fig. 15 questionable, the presence of the Z-wave is still relevant; as we shall see it is still present in some results of obtained with the delta model. It is discussed more in Section 6.1.3.

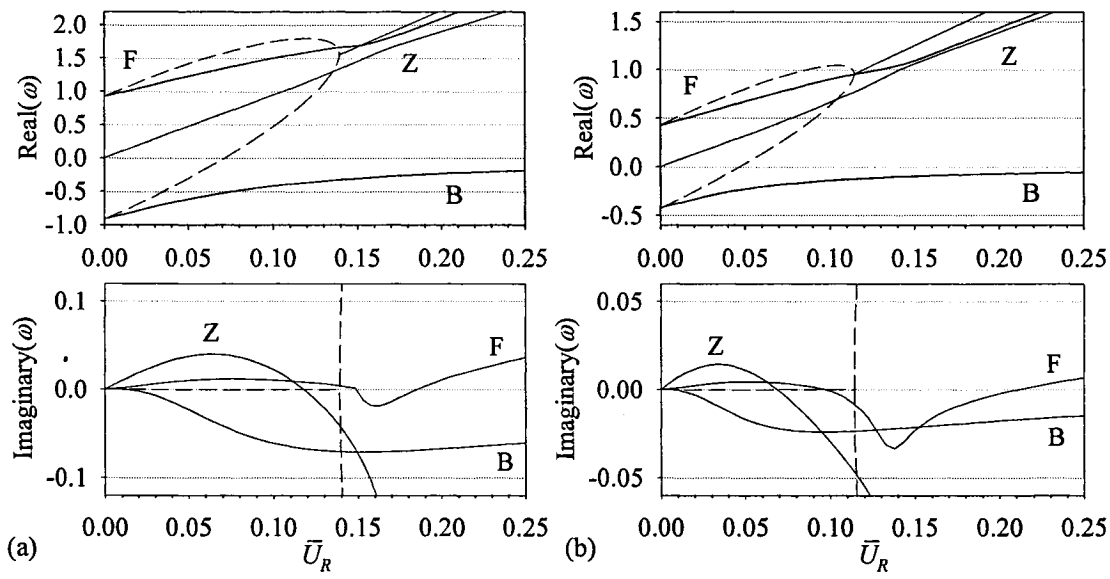

Fig. 15. Comparison of the frequency evolution of a vibrating non-rotating tube conveying turbulent flow obtained with the classical no-slip model at Re=10^5 (——), and with the inviscid model (·····), for dimensionless wavenumbers (a) k=15, n=8; (b) k=10, n=0. The letters F and B indicate the forward and backward travelling waves and the letter Z indicates the travelling wave emanating from the origin.

6.1.2. Slip model

The equations of the slip model tend towards those of the inviscid theory as the Reynolds number is increased; we can therefore assume that the results and predictions with this model will do the same as the Reynolds number is increased. In the slip model, viscosity allows for the transmission of a little shear from the flow to the wall (recall that this is not a *free*-slip model), but its major role is to provide dissipation to the system. In Fig. 16, the frequency evolutions obtained with the slip model are compared with those obtained with the inviscid theory. The four oscillatory modes studied are the same four as in Fig. 12 for the classical no-slip model. The behaviour of the system obeying the slip model is very close to the inviscid one. Not only are the predicted critical reduced flow velocities close, the complex frequencies are also very similar. One difference which is expected is that when the inviscid system loses stability through coupled-mode flutter, in the system obeying the slip model it is the forward travelling wave that flutters. Also, one could have thought that the addition of dissipation in the system would delay the onset of instability, but for all four cases of Fig. 16, the critical flow velocity is lower for the slip model than for the inviscid one.

As mentioned earlier, the main effect viscosity has in the slip model is to provide dissipation. In order to understand the repercussions of this on the dynamics of the system, we compare the frequency evolution of mode k=15, n=8 obtained at a Reynolds number of 10^3 in Fig. 16 (a) and at Reynolds numbers 10, 10^2, 10^4 and 10^5 in Fig. 17. It can be seen that for low Reynolds numbers $10 \leq \mathrm{Re} \leq 10^3$, viscosity has a strong effect on the real frequencies while, as the Reynolds number is increased past 10^3, the frequency curves seem to converge towards the inviscid theory frequency curves. The imaginary frequencies of the system decrease steeply as the Reynolds number increases. The surprising thing from Fig. 17, is that the predicted critical reduced flow velocity of the system does not vary with the Reynolds number. The slip model predicts that the forward travelling wave starts fluttering at $\bar{U}_R = 0.12$ for the entire range of studied Reynolds numbers $10 \leq \mathrm{Re} \leq 10^5$ (note that this is so even for Fig. 17 (d), though not clearly visible). One would usually expect that a change in the damping of a system would not

influence the occurrence of a static instability, i.e. a divergence, but that it would influence the onset of a dynamic instability such as the flutter encountered here.

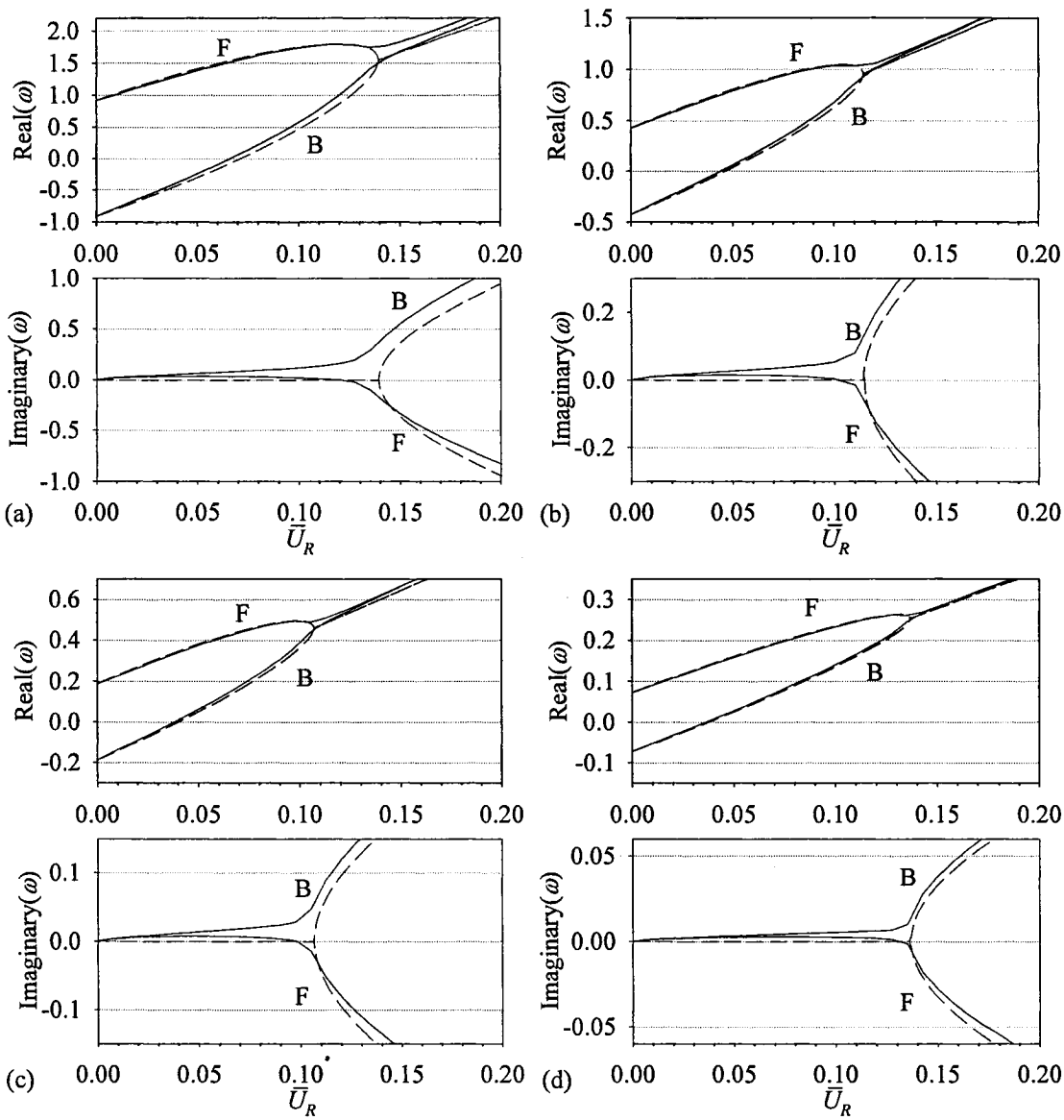

Fig. 16. Comparison of the frequency evolution of a vibrating non-rotating tube conveying fluid obtained with the slip model at Re=10^3 (——), and with the inviscid model (- - - - - -), for dimensionless wavenumbers (a) k=15, n=8; (b) k=10, n=0; (c) k=5, n=6; (d) k=2, n=3. The letters F and B indicate the forward and backward travelling waves.

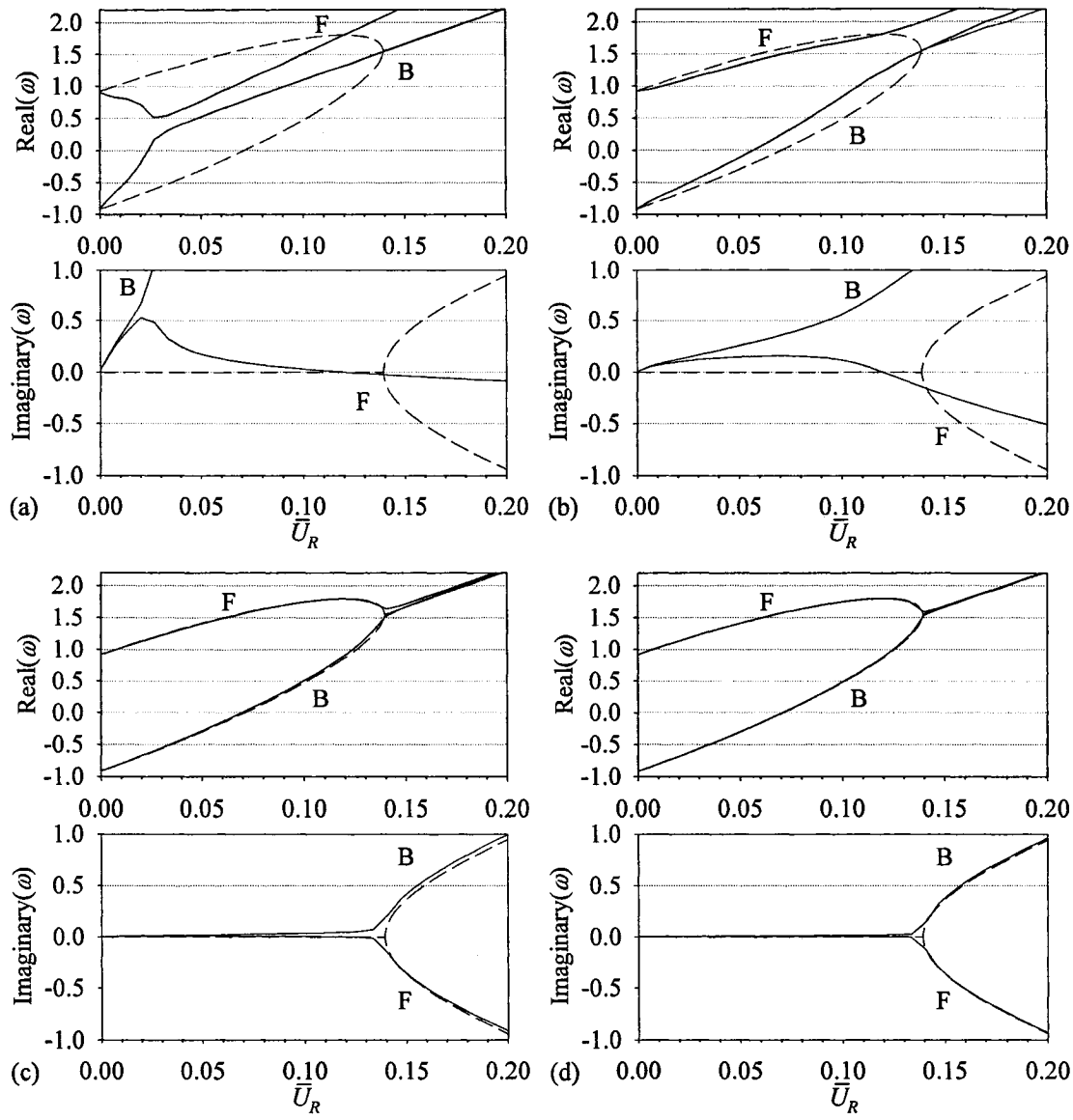

Fig. 17. Effect of the Reynolds number on the slip model prediction of the frequency evolution of a vibrating non-rotating tube conveying fluid for dimensionless wavenumbers k=15 and n=8 (——), for (a) Re=10; (b) Re=10^2; (c) Re=10^4; (d) Re=10^5. The letters F and B indicate the forward and backward travelling waves. The inviscid results are plotted for comparison (-------).

6.1.3. Average-velocity model

The average-velocity model presented in Section 3.8.3 with its numerical method of solution developed in Section 4.6.3 is based on the classical no-slip model, but in the perturbation velocity boundary condition the mean reduced velocity evaluated at the wall

has been replaced with the average mean reduced velocity. This can be interpreted as an effective velocity acting on the wall.

The four oscillatory modes studied in Fig. 12 for the classical no-slip model and in Fig. 16 for the slip model are again studied in Fig. 18, but this time the results are obtained with the average-velocity model. In Fig. 16 (a)-(d), for a laminar flow with $\mathrm{Re} = 10^3$, the average-velocity model predicts instability for the combinations of dimensionless wavenumbers k=15 with n=8, k=10 with n=0, k=5 with n=6, and k=2 with n=3 at $\bar{U}_R = 0.105$, $\bar{U}_R = 0.070$, $\bar{U}_R = 0.073$ and $\bar{U}_R = 0.165$ respectively. These predictions are in the same range as those of the inviscid model: $\bar{U}_R = 0.140$, $\bar{U}_R = 0.115$, $\bar{U}_R = 0.107$, $\bar{U}_R = 0.137$.

The neutral stability curves of the system are obtained using the average-velocity model; they are plotted in Fig. 19. Although the values of the critical reduced velocities differ, the neutral stability curves obtained with the average-velocity model display the same trends as those obtained with the inviscid theory in Fig. 7 of Chapter 5. At high axial wavenumber, for every circumferential wavenumber, the critical flow velocity increases as the axial wavenumber is increased further. At low axial wavenumber, except for the axisymmetric mode (n=0), the critical flow velocity of every circumferential mode increases as the axial wavenumber is decreased. It is not obvious why the axisymmetric mode has a neutral stability curve different from the other circumferential wavenumbers. Also it is quite peculiar that it is always the axisymmetric mode that is the most unstable mode for any axial wavenumber. Recall that with the inviscid model, in Fig. 7, the most unstable circumferential wavenumber depends on the axial wavenumber.

They results obtained with the average velocity model are interesting in the sense that the onset of instability and complex frequencies are closer to the inviscid ones. Nevertheless, the "effective velocity" applied on the wall is completely arbitrary and it is therefore hard to consider these results as being any better than those obtained with the classical no-slip or the slip model.

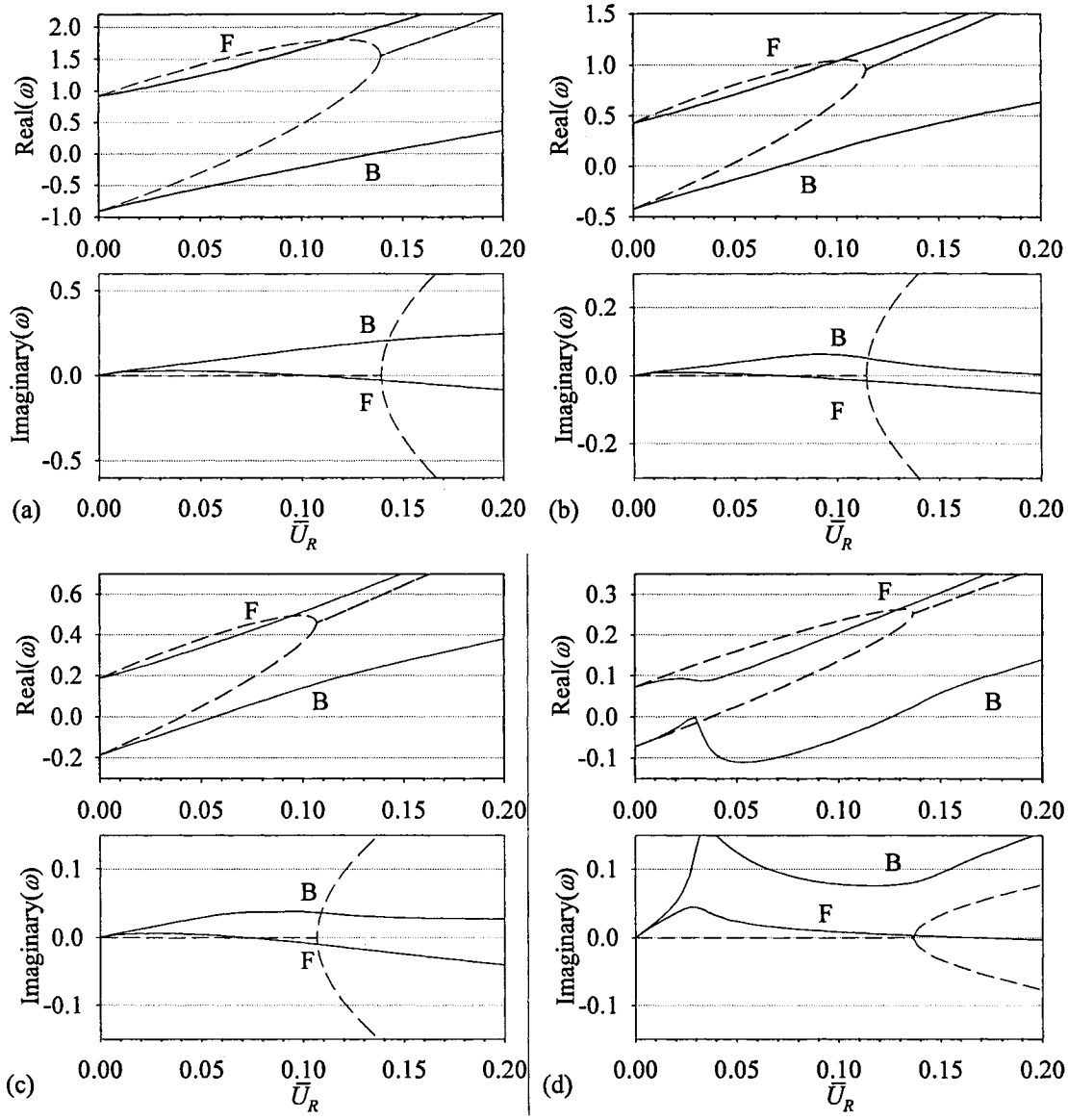

Fig. 18. Comparison of the frequency evolution of a vibrating non-rotating tube conveying laminar flow obtained with the average-velocity model at Re=10^3 (——), and with the inviscid model (- - - - - -), for dimensionless wavenumbers (a) k=15, n=8; (b) k=10, n=0; (c) k=5, n=6; (d) k=2, n=3. The letters F and B indicate the forward and backward travelling waves.

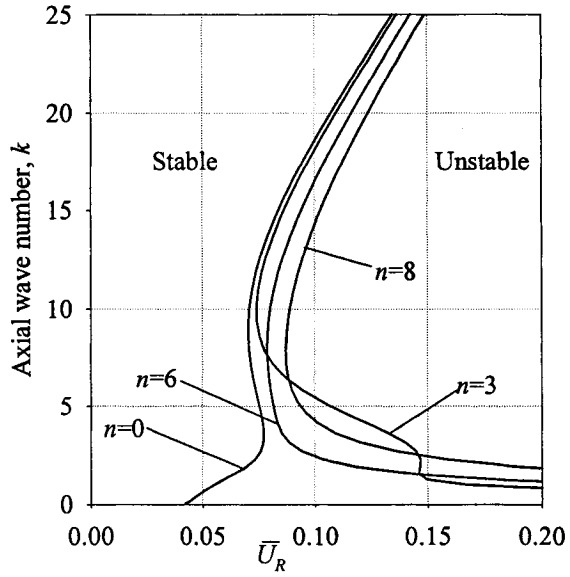

Fig. 19. Neutral stability curves of vibrating modes of non-rotating tube with flowing viscous fluid modelled with the average-velocity model at Re=10^3.

The average-velocity model is applied to the case of a cylindrical shell conveying a turbulent flow with a Reynolds number of 10^5. The frequency evolutions of the modes with wavenumbers k=15, n=8, and k=10, n=0 are plotted in Fig. 20. We see that the real part of the complex frequencies found with the average-velocity model matches well with the inviscid model for this high Reynolds number; but, as was the case when modelling turbulent flow with the classical no-slip model, the critical flow velocity of the system is far too low to be believable. The "effective velocity" applied at the wall being completely arbitrary, it is probable that it is simply too large. If only a fraction of the average mean velocity was applied at the wall, would the results make more sense? The delta model allows more flexibility in the level of correction and avoids the arbitrariness of the correction of the average-velocity model.

In El Chebair (1988) and El Chebair et al. (1990), satisfactory results are obtained with a model similar to the average-velocity model in the turbulent regime. It is not obvious why it worked there and not here but significant differences arise between the two models. In El Chebair, the turbulent profile simply consists in the empirical power law. The law of the wall is not used. Therefore, the slope of their profile is infinite at the wall but it does not affect their results because, in their application of the perturbation boundary conditions, the first-order difference between applying them at the deformed

position or the undeformed position was neglected; here it leads to the $w[\partial U_R/\partial r]_{\bar{r}=\bar{r}_0}$ term in eq. (3.63).

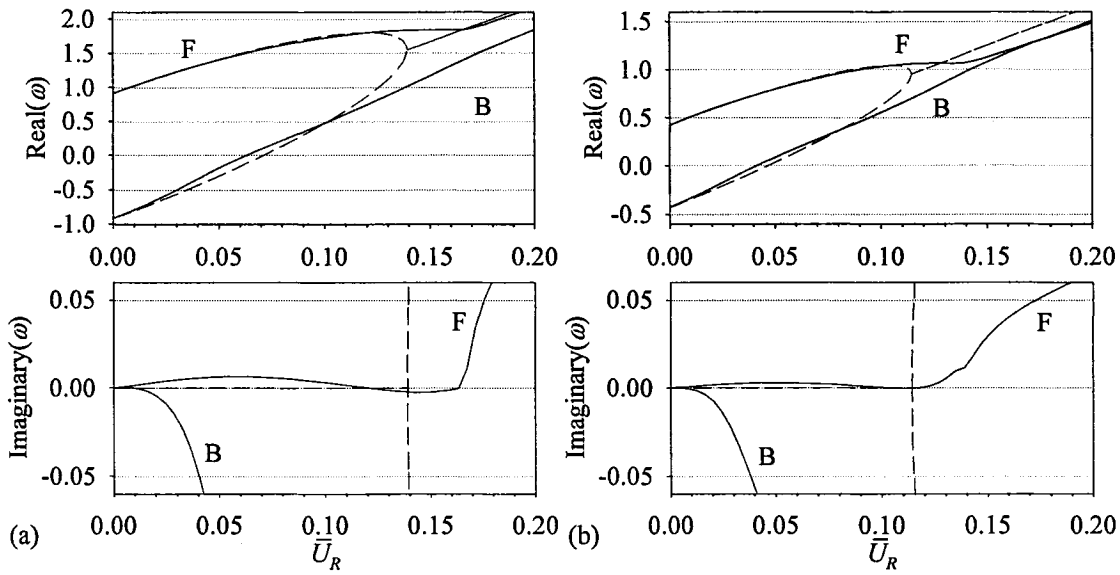

Fig. 20. Comparison of the frequency evolution of a vibrating non-rotating tube conveying turbulent flow obtained with average-velocity model at Re=10^5 (——), and with the inviscid model (-------), for dimensionless wavenumbers (a) k=15, n=8; (b) k=10, n=0. The letters F and B indicate the forward and backward travelling waves.

6.1.4. Delta model

The delta model is presented in Section 3.8.4. with its numerical method of solution developed in Section 4.6.4. Based on the original idea of Dowell (1971), the flow is solved over the domain $0 \le r \le (1-\delta)$, where δ corresponds to the deformation of the shell measured in percentage of the radius. This δ has for effect to restore the term which depends on the slope of the wall in the perturbation velocity boundary conditions. By varying the distance δ, the level of correction brought to the theory can be changed. The correction has a measure: it is equivalent to the deformation of the shell, which gives a physical meaning to the parameter δ, in contrast to the arbitrary "effective velocity" of the average-velocity model. This makes the model easier to accept.

The frequency evolution of the mode with wavenumbers k=10 and n=0 obtained with the delta model is shown in Fig. 21 for values of the parameter δ ranging from 0 to 50%. Of course a value of $\delta = 50\%$ is absurd (even $\delta = 10\%$ is extremely large); but the stability of the system is not very sensitive to the parameter δ and it has to reach these high values in order to have a significant effect. In Fig. 21 (e), the dynamics obtained with the delta model approaches that of the inviscid model; but at a value of 40%, the parameter δ cannot be judged to be physically meaningful. The parabolic profile seems to render the system insensitive to the δ parameter. As shown next, the delta model is very effective with a turbulent profile.

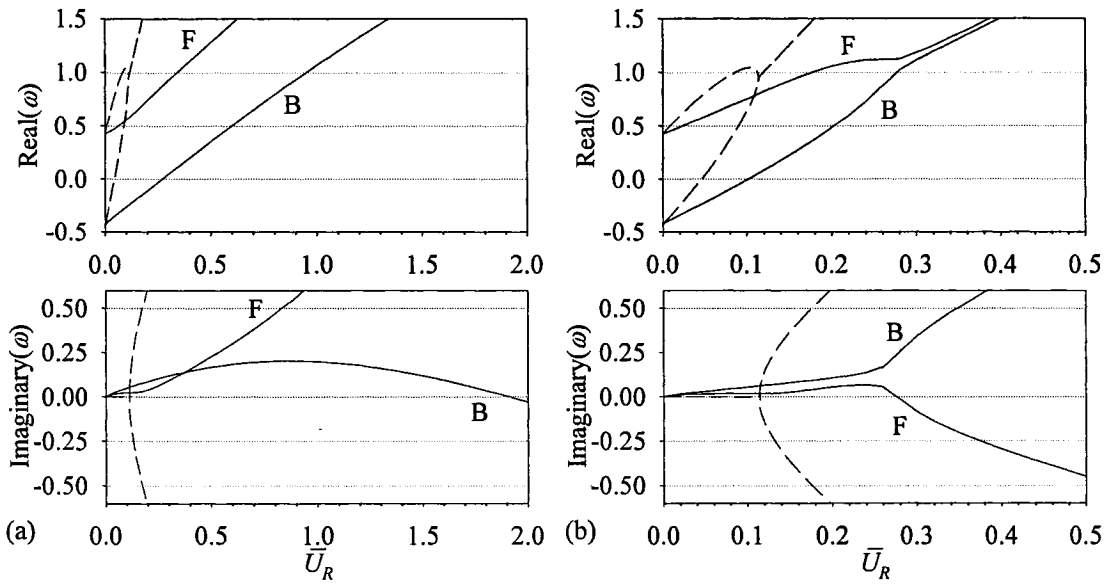

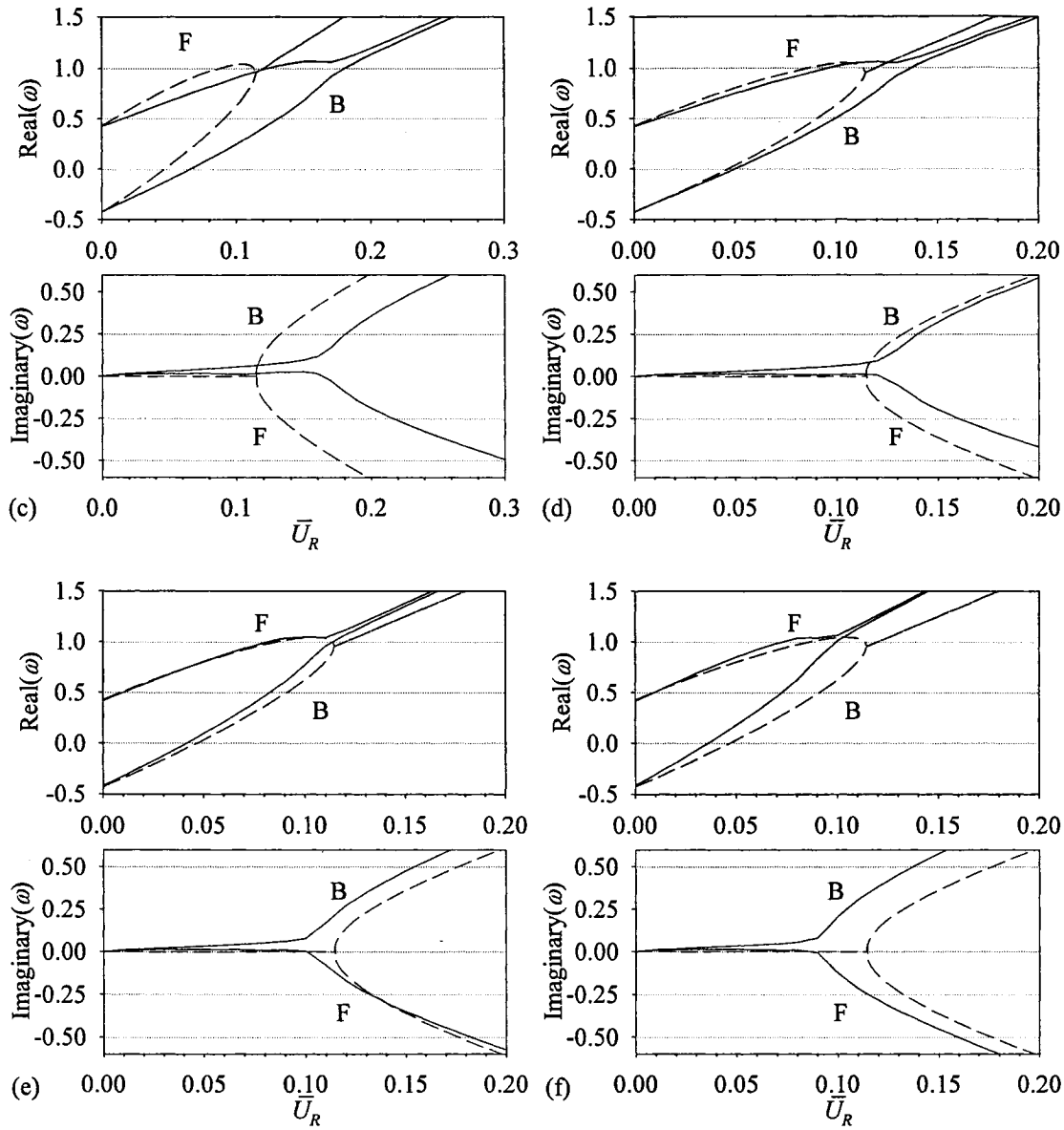

Fig. 21. Effect of the parameter δ on the frequency evolution of a vibrating non-rotating tube obtained with the delta model at Re=10^3 (——), for dimensionless wavenumbers k=10 and n=0, for (a) δ=0; (b) δ=10%; (c) δ=20%; (d) δ=30%; (e) δ=40%; (f) δ=50%. The letters F and B indicate the forward and backward travelling waves. The inviscid results are plotted for comparison (·····).

El Chebair et al. (1990) found that as the value of δ was increased, the onset of instability converged towards the value obtained with the average-velocity model. As the average-velocity model has not been successful at predicting the stability of the system for turbulent flow here (as explained in Section 6.1.3), instead we compare the results with the inviscid model. Based on experimentally measured deformations, El Chebair et al. picked values of δ between 1% and 2%.

The dynamics in the mode with wavenumbers k=15 and n=8, as predicted by the delta model for a turbulent flow with $\mathrm{Re} = 10^5$, is presented in Fig. 22 for values of the parameter δ ranging from 0 to 1%. In Fig. 22 (a), the dynamics obtained for $\delta = 0$ is, as expected, the same as the classical no-slip model in Fig. 15 (a). The very interesting result here is that, as δ is increased, the shape of the complex frequency curves of the system takes a similar form as in the inviscid model and the δ parameter does not have to reach astronomical values as was the case in the presence of a laminar profile. The critical reduced flow velocities for $\delta = 0,\ 0.1\%,\ 0.5\%$ and 1% are 0.048, 0.023, 0.122 and 0.135 respectively tends to approach the value predicted by the inviscid theory of 0.1395 as δ is increased. This is even more obvious in Fig. 23, where the critical reduced flow velocity of the mode with wavenumbers k=15, n=8 is plotted versus δ. It shows clearly that as δ is increased to about 1%, the critical flow velocity converges towards the prediction of the critical velocity of the inviscid theory. If the parameter δ is varied between half a percent to a percent the critical flow velocity does not change appreciably. This makes the correction of the delta model much less arbitrary than in the average-velocity model.

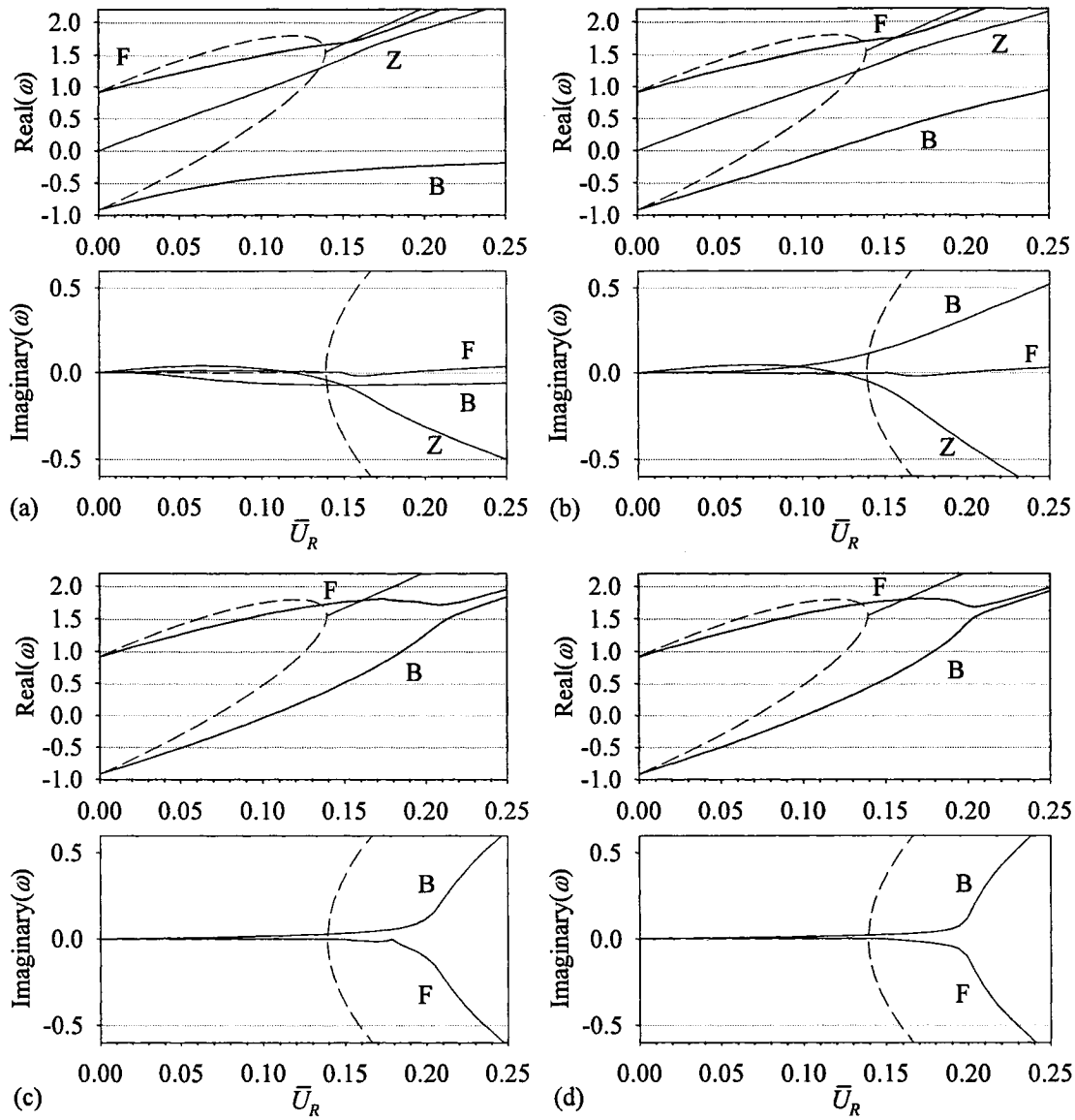

Fig. 22. Effect of the parameter δ on the frequency evolution of a vibrating non-rotating tube obtained with the delta model and a power-law/law of the wall velocity profile at Re=10^5 (——), for dimensionless wavenumbers k=15 and n=8, for (a) δ=0; (b) δ=0.1%; (c) δ=0.5%; (d) δ=1%. The letters F and B indicate the forward and backward travelling waves and the letter Z indicates the travelling wave emanating from the origin. The inviscid results are plotted for comparison (-------).

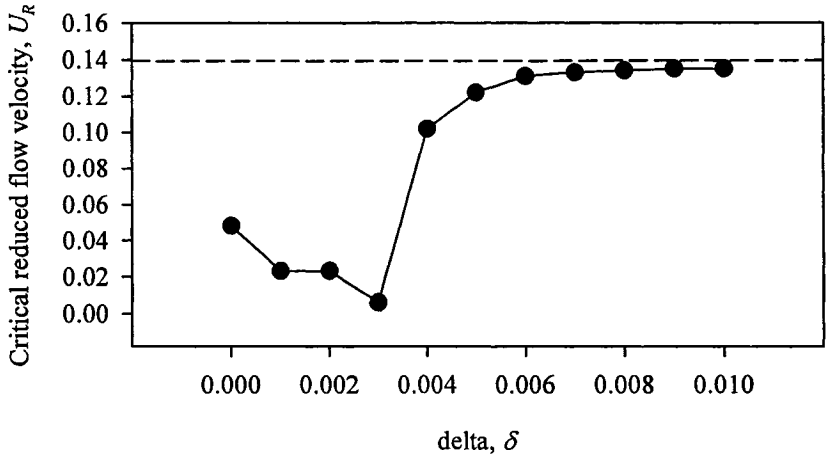

Fig. 23. Comparison of the prediction of the onset of instability of the delta model (—●—) for a power-law/law of the wall velocity profile at Re=10^5 and the inviscid theory (--------) for the dimensionless wavenumbers k=15 and n=8.

The profile in the delta model seems to have an important effect on the complex frequencies of the system. The curves of the $\delta = 1\%$ have the same shape as those obtained with the inviscid models, but the values are fairly different, even though the critical flow velocities match. On the other hand, the slip model with its "square" profile has complex frequencies very close to the inviscid ones for high enough Reynolds number (see Fig. 15 and Fig. 16). So, for equivalent average reduced flow velocity $\bar{U}_R$, the viscous flow has a faster centreline velocity than the inviscid flow as shown in Fig. 4 and this could certainly affect the values of the frequencies of the system.

Adopting a value of $\delta = 1\%$, the dynamics of the system can be obtained for different modes of oscillations. The frequency evolutions of the modes with the combinations of dimensionless wavenumbers k=15 with n=8, k=10 with n=0, k=5 with n=6, and k=2 with n=3 are obtained for a turbulent profile at $\mathrm{Re} = 10^5$ in Fig. 24 and for $\mathrm{Re} = 10^4$ in Fig. 25. At a Reynolds number of 10^5, all the predictions of instability are within 15% below the inviscid predictions. When the Reynolds number is reduced to 10^4, the predictions of the onset of instability of the three modes of Fig. 25 (a)-(c) do not change very much and still fall within 15% below the inviscid predictions, but the mode k=2, n=3 is well below at a critical reduced velocity of 0.079 versus 0.137 for the inviscid

theory. It turns out that if the parameter δ is increased further past 1% (not shown), the critical flow velocity of this mode will converge again towards the inviscid prediction.

An interesting particularity of the results obtained with the delta model for the turbulent regime is that in some cases, not only is there a forward and a backward travelling wave, but a Z-wave is present as well. The Z-wave emanates from the origin and the real part of its frequency increases proportionally to the mean flow velocity. In most of the cases where it is present, the real part of the Z-wave frequency traces a straight line proportional to the reduced flow velocity, but in some cases, such as in Fig. 25 (a)-(c), the straight line of the Z-frequency evolution bends abruptly as it gets close to the frequency of another travelling wave. Païdoussis (2003 Section 7.4.2) refers to this phenomenon as "mode exchange" via "mode veering". The two modes then exchange their properties: where it is usually the forward travelling wave which becomes unstable as in Fig. 26 (b)-(d), in Fig. 26 (a) a "mode exchange" occurs around $\bar{U}_R = 0.13$ and it is the Z-wave which subsequently becomes unstable.

The Z-wave was not found in every plot, but this is probably due to the technique employed to obtain the frequency evolution curves. It is plausible that the Z-wave is present in all cases modelled by the delta model with the turbulent profile or with classical no-slip model since it is equivalent to the delta model at $\delta = 0$. As discussed at the beginning of this chapter, to obtain the frequency curves, the frequencies are first found for a very small flow velocity and the flow velocity is then incremented. At this small velocity the Z-frequency is numerically nil. Add to this the fact that the Müller algorithm used to iteratively find the roots of the dispersion relation defined in Chapter 3 tends to converge much more easily on the forward and backward travelling wave frequencies than on the Z-wave. One must therefore know almost exactly where the Z-wave curve lies to find it. The Z-wave was actually discovered fortuitously. In the case of Fig. 25 (a), because of the "mode exchange", if too few points were used while incrementing the reduced flow velocity, the algorithm would tend to jump from one mode solution to another. If more points are used, one can really see the dynamics as plotted in Fig. 25 (a); namely that the two frequency curves bend abruptly and perform a "mode exchange". The reliability of the root-finding process has been a concern due to the lack of success in finding these Z-waves in all cases, but it seems that when they play a major

role in the stability of the system, i.e. when they become unstable, they tend to do it by first doing a "mode exchange" and hence influencing the forward travelling wave. One can then notice the reorientation or the deformation of the forward travelling wave which is a clue as to the presence of the Z-wave.

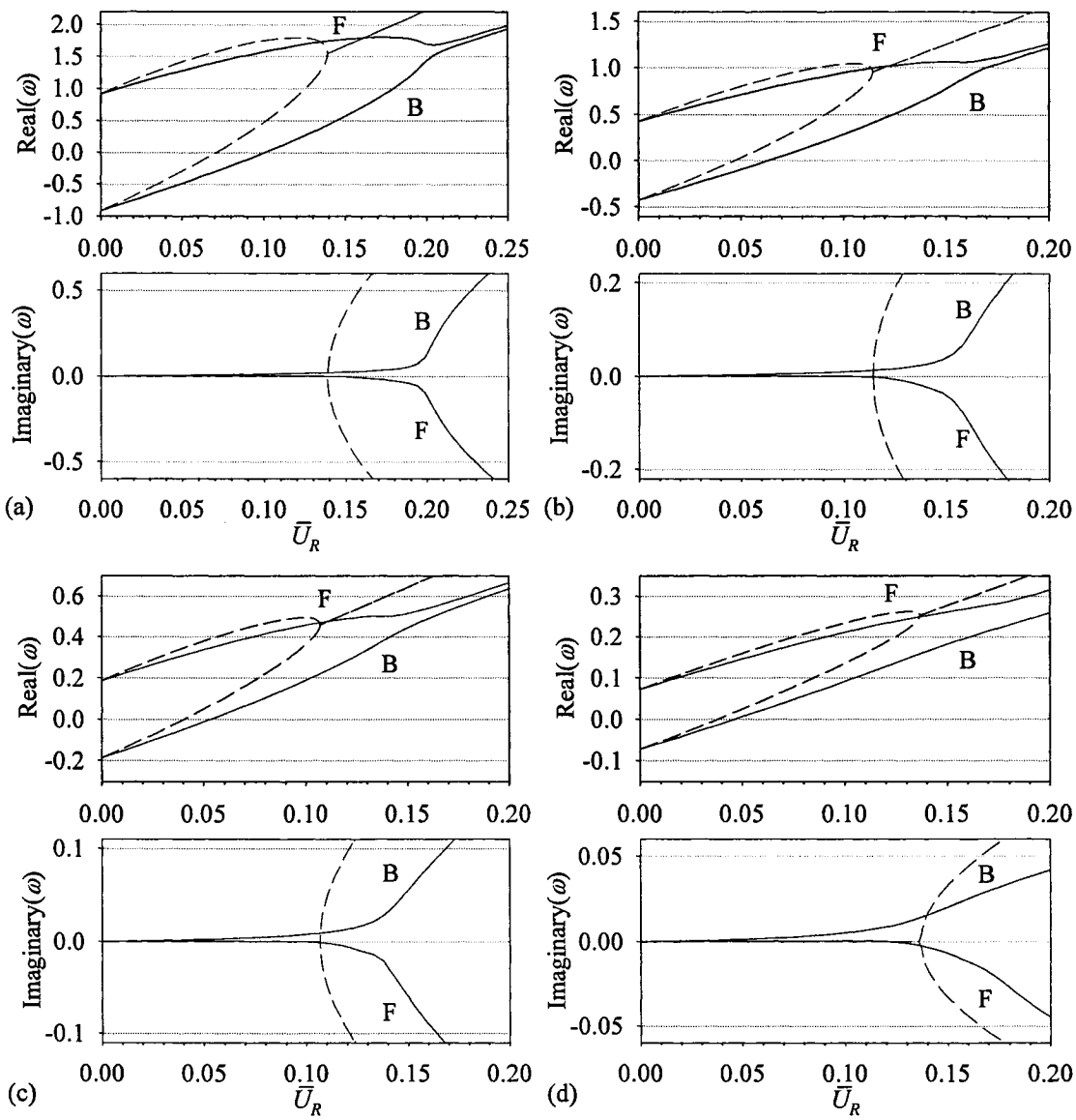

Fig. 24. Comparison of the frequency evolution of a vibrating non-rotating tube obtained with the delta model and a power-law/law of the wall velocity profile at Re=10^5 and δ=1% (——), and with the inviscid model (--------), for dimensionless wavenumbers (a) k=15, n=8; (b) k=10, n=0; (c) k=5, n=6; (d) k=2, n=3. The letters F and B indicate the forward and backward travelling waves.

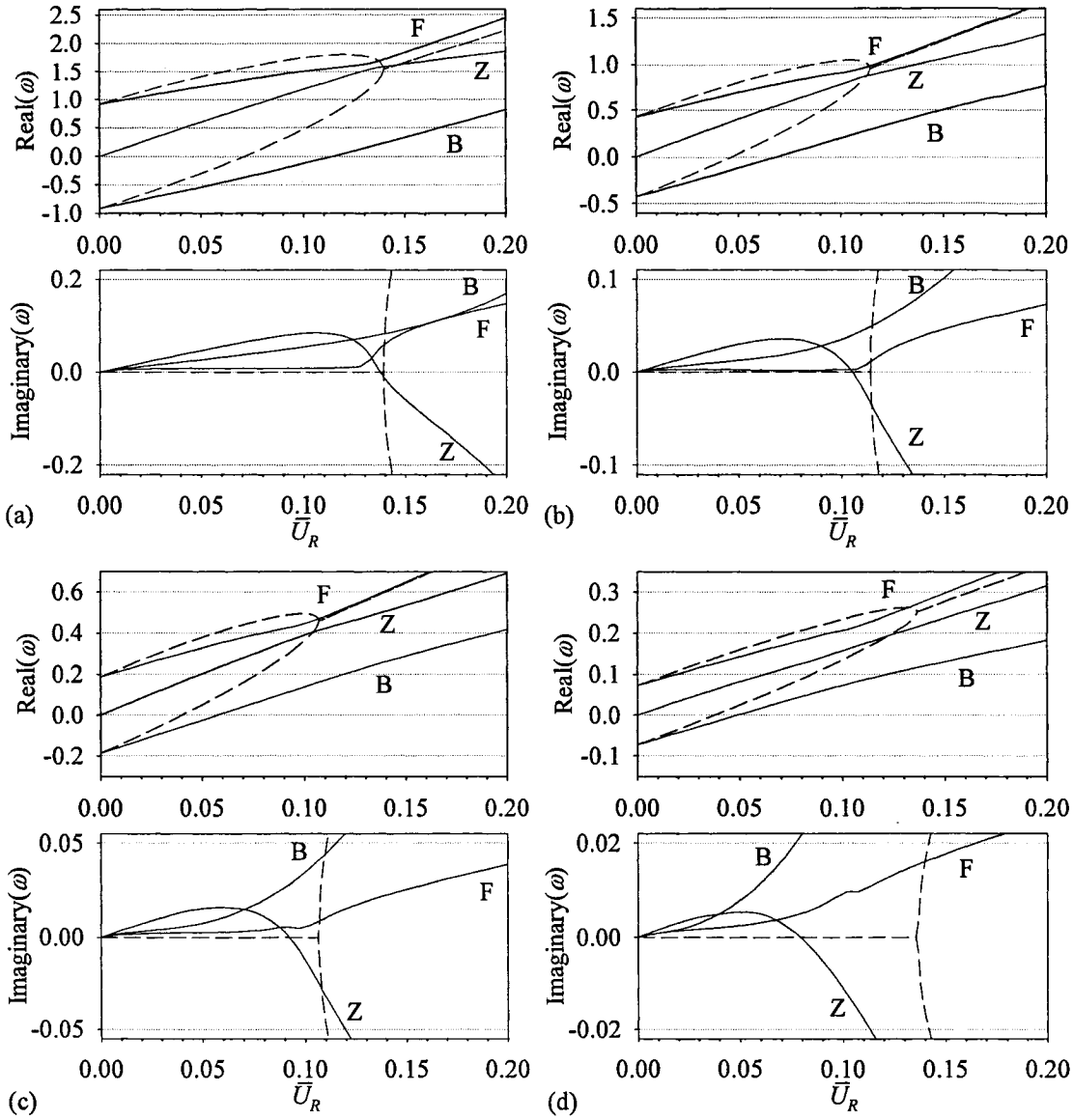

Fig. 25. Comparison of the frequency evolution of a vibrating non-rotating tube obtained with the delta model and a power-law/law of the wall velocity profile at Re=10^4 and δ=1% (——), and with the inviscid model (--------), for dimensionless wavenumbers (a) k=15, n=8; (b) k=10, n=0; (c) k=5, n=6; (d) k=2, n=3. The letters F and B indicate the forward and backward travelling waves and the letter Z indicates the travelling wave emanating from the origin.

In Fig. 26 is plotted the dynamics of the mode k=15, n=8 for values of the Reynolds number 10^4, 10^5, 10^6 and 10^7. As the Reynolds number is increased, the complex frequency curves become rounder and tend to match the shape of the inviscid model more and more. This is in agreement with engineering judgement, which leads us to believe that as the Reynolds number increases in a viscous theory, things tend towards

the inviscid theory. On the other hand, agreement between the inviscid and the delta model predictions of the onset of instability decreases as the Reynolds number is increased. For $\mathrm{Re}=10^4$, 10^5, 10^6 and 10^7, the delta model critical reduced flow velocities are 0.137, 0.135, 0.128 and 0.119 respectively while with the inviscid theory, the critical reduced flow velocity is 0.1395.

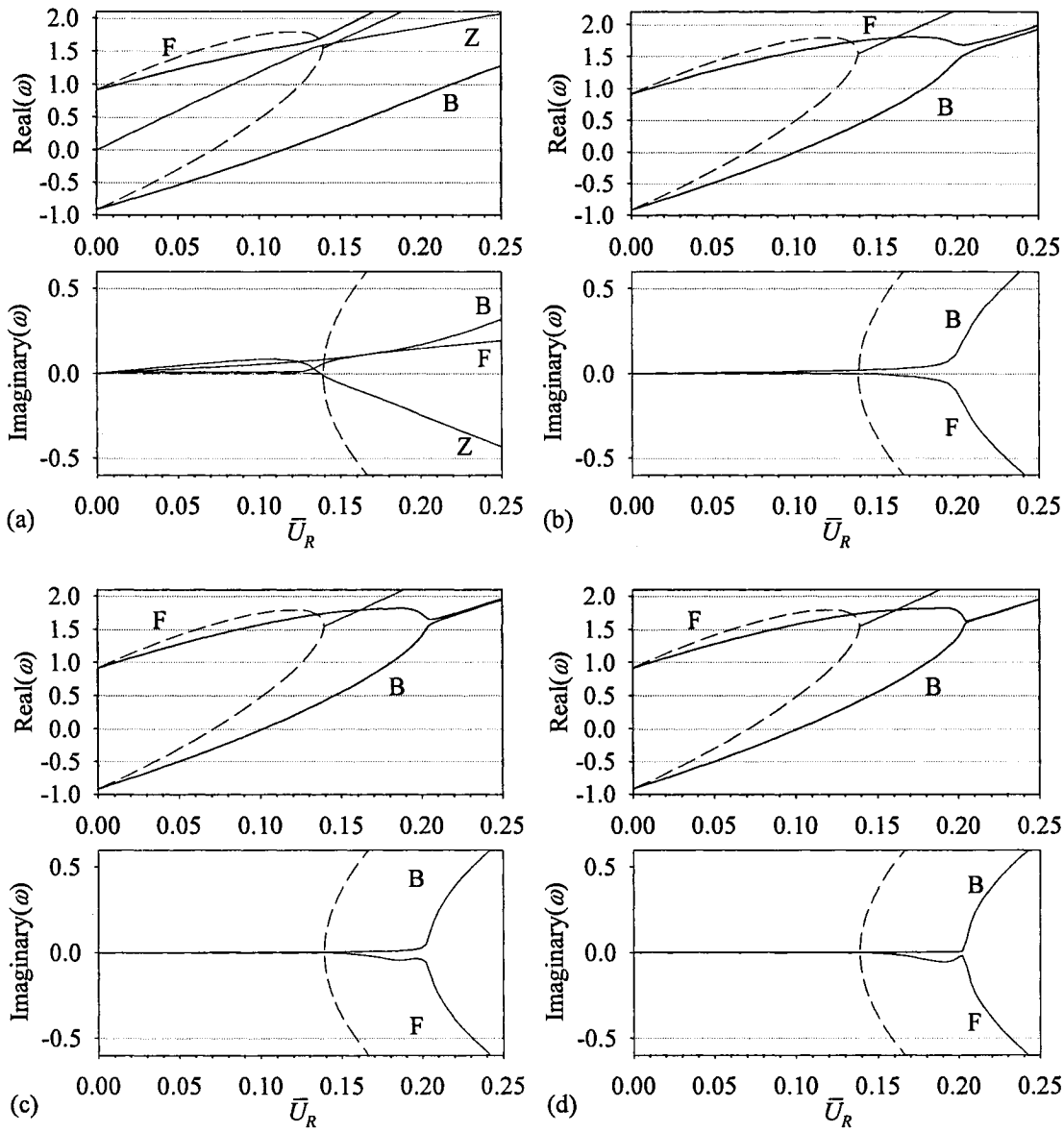

Fig. 26. Effect of the Reynolds number on the prediction of the frequency evolution of a vibrating non-rotating tube for dimensionless wavenumbers k=15 and n=8 obtained with the delta model with a power-law/law of the wall velocity profile and δ=1% (——), for (a) $\mathrm{Re}=10^4$; (b) $\mathrm{Re}=10^5$; (c) $\mathrm{Re}=10^6$; (d) $\mathrm{Re}=10^7$. The letters F and B indicate the forward and backward travelling waves and the letter Z indicates the travelling wave emanating from the origin. The inviscid results are plotted for comparison (-------).

6.2 Effect of rotation

As mentioned in the beginning of Chapter 6, if the Reynolds number is taken as a constant for an entire frequency evolution plot, then the viscosity, and therefore the damping, tends to zero as the reduced velocity tends to zero. It was found, while studying the effect of rotation in the inviscid model that the lines of singularities cover the entire range of reduced velocities. Therefore, it seems appropriate to consider the viscosity of the fluid to be constant and have the Reynolds number be proportional to the reduced velocity. Let us define the Stokes number

$$S_T \equiv \frac{2R'\rho'}{\mu'}\sqrt{\frac{E'}{\rho_s'\left(1-\nu^2\right)}} = \frac{\mathrm{Re}}{\bar{U}_R}. \tag{6.1}$$

In the simulations containing rotation, the Stokes number is kept constant. The physical properties of the system presented in Table 2 are that of a rubber tube containing water flow. From Munson et al. (2002), at room temperature, water has a viscosity $\mu' = 1.12\times10^{-6}\ \mathrm{N\cdot s/m^2}$. The Stokes number of the system with properties given in Table 2 can be calculated to be $S_T = 1\ 220\ 795$. Simulations are performed for this Stokes number and also for a Stokes number 100 times smaller; this would be representative of a system with a fluid with the same density as water but a hundred times more viscous, such as oil.

The first simulations with rotation are performed using the classical no-slip model in the laminar regime and are presented in Fig. 27. Without rotation in Fig. 27 (a), the model predicts no instability. The addition of rotation does not change this aspect of the results. The case presented in Fig. 27 (b) for $\Omega = 0.1$ is the same as the one studied with the inviscid theory in Fig. 8 of Chapter 5. With the classical no-slip model, the addition of rotation seems to stabilise the system as the lowest imaginary frequencies Fig. 27 (b) are higher than in (a). Also, the introduction of rotation causes more "mode exchanges".

In Fig. 27, the F- and B- waves are shown to interact through "mode exchange" with the M10- and M5- waves. It happens here because the stability of the system is studied for a large range of $\bar{U}_R$. This is done to show that the system stays stable even for very large values of the reduced velocity. In the previously studied cases, whether

rotating or not, if large enough reduced velocities are reached, the lowest frequencies (here labelled F- and B-waves) do interact with the higher frequencies. We did not show such large ranges of $\bar{U}_R$ for those cases because instability was already reached.

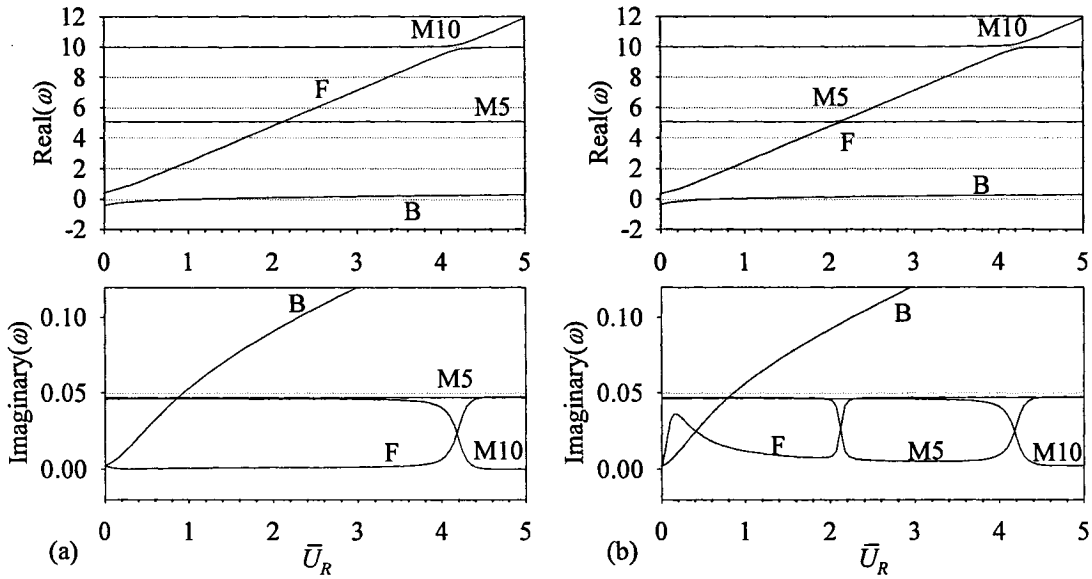

Fig. 27. Effect of rotation on the prediction of the frequency evolution of a vibrating tube for dimensionless wavenumbers k=10, n=0 obtained with the classical no-slip model with a parabolic velocity profile for S_T=1 220 795 (——), for (a) Ω=0; (b) Ω=0.1. The letters F and B indicate the forward and backward travelling waves, while M5 and M10 indicate the modes originating at real frequencies of about 5 and 10 respectively.

Using the delta model with a value of $\delta = 1\%$ in the turbulent regime, the effect of rotation on the mode with wavenumbers k=15, n=8 is plotted in Fig. 28 for $S_T = 1\ 220\ 795$ and in Fig. 29 for $S_T = 12\ 208$; on the mode with wavenumbers k=10, n=0 it is plotted in Fig. 30 for $S_T = 1\ 220\ 795$ and in Fig. 31 for $S_T = 12\ 208$. In all four cases, the small rate of rotation imposed on the system has a stabilising effect. In Fig. 28 and Fig. 30, for the cases with $S_T = 1\ 220\ 795$ the imaginary frequencies have a small dimple at $\bar{U}_R = 0.02$. The k=10, n=0 mode even becomes unstable for a very brief range of flow velocity, and then regains stability. This phenomenon is still present with the introduction of rotation but disappears from the more viscous cases.

The effect of rotation on the stability of the system is shown in Fig. 32. For the two modes studied and for high or low viscosity, the addition of a small rate of rotation

stabilises the system. It would seem though that if subjected to higher rates of rotation, the critical velocity of the system should decrease. Srinivasan and Lauterbach (1971) showed that, if spun fast enough, empty cylindrical shells become unstable. One would think that the same applies to fluid filled shells. If the shell-fluid system is spun fast enough, it will be unstable even without flow. So, before that critical rotation rate is reached, the critical flow rate should decrease.

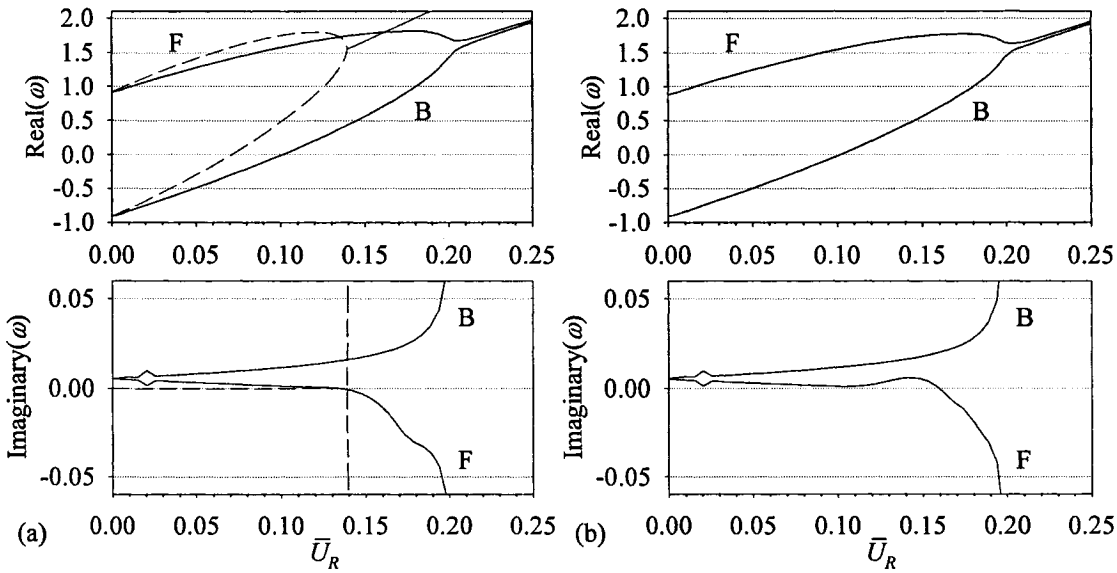

Fig. 28. Effect of rotation on the prediction of the frequency evolution of a vibrating tube for dimensionless wavenumbers k=15, n=8 obtained with the classical no-slip model with a parabolic velocity profile for S_T=1 220 795 (——), for (a) Ω=0; (b) Ω=0.05. The inviscid results for the case without rotation are plotted for comparison (-------). The letters F and B indicate the forward and backward travelling waves.

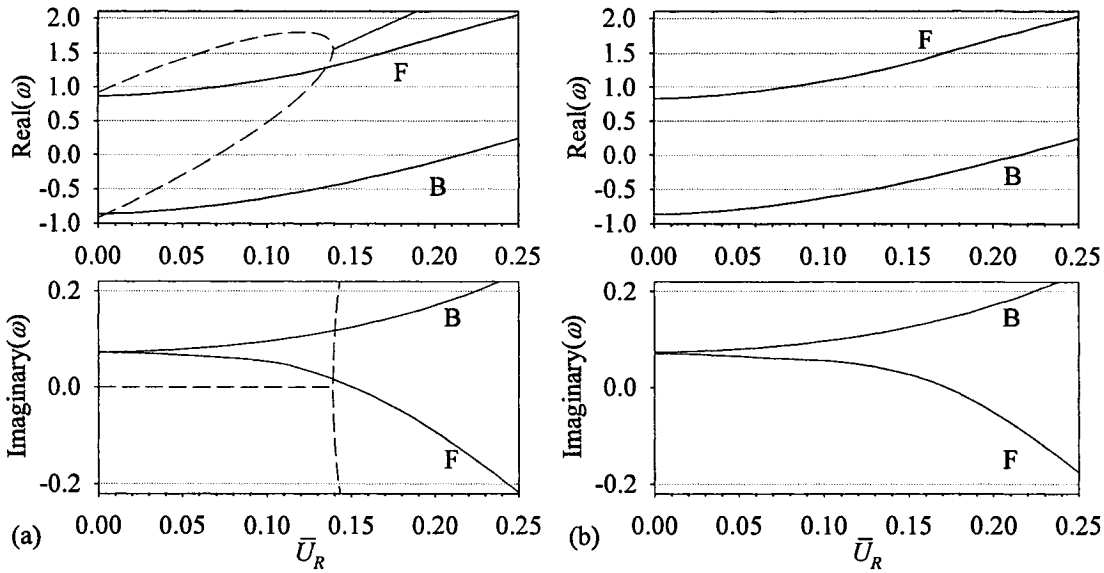

Fig. 29. Effect of rotation on the prediction of the frequency evolution of a vibrating tube for dimensionless wavenumbers k=15, n=8 obtained with the classical no-slip model with a parabolic velocity profile for S_T=12 208 (——), for (a) Ω=0; (b) Ω=0.05. The inviscid results for the case without rotation are plotted for comparison (-------). The letters F and B indicate the forward and backward travelling waves.

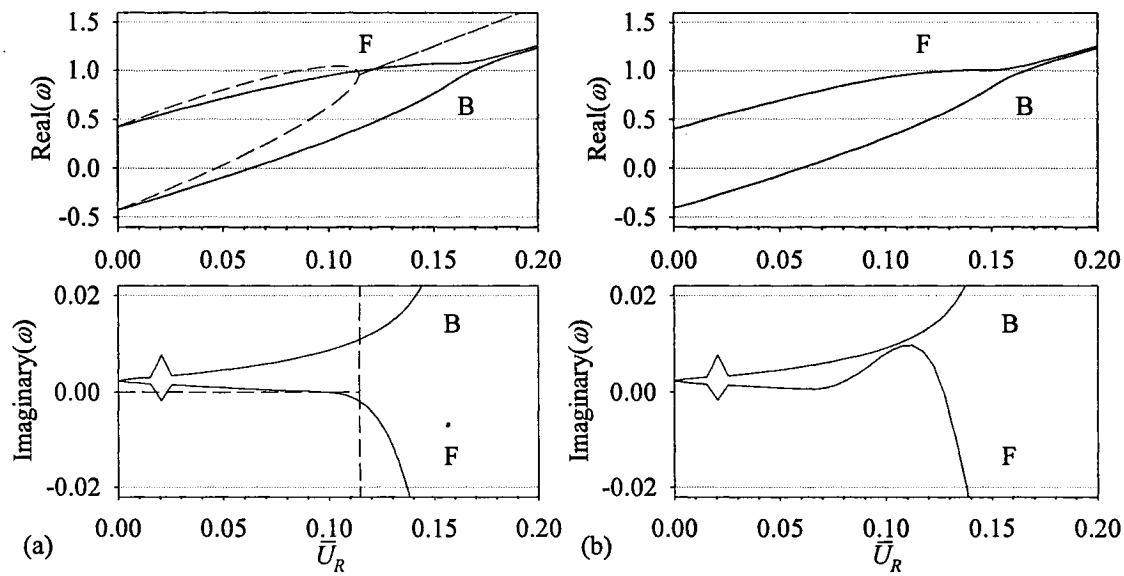

Fig. 30. Effect of rotation on the prediction of the frequency evolution of a vibrating tube for dimensionless wavenumbers k=10, n=0 obtained with the classical no-slip model with a parabolic velocity profile for S_T=1 220 795 (——), for (a) Ω=0; (b) Ω=0.05. The inviscid results for the case without rotation are plotted for comparison (-------). The letters F and B indicate the forward and backward travelling waves.

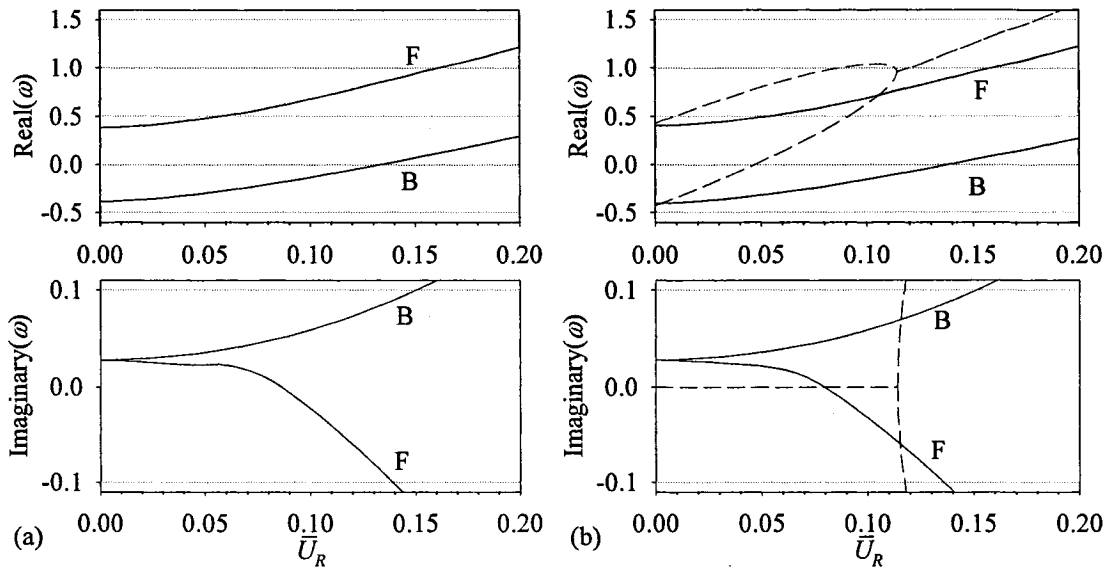

Fig. 31. Effect of rotation on the prediction of the frequency evolution of a vibrating tube for dimensionless wavenumbers k=10, n=0 obtained with the classical no-slip model with a parabolic velocity profile for S_T=12 208 (——), for (a) Ω=0; (b) Ω=0.05. The inviscid results for the case without rotation are plotted for comparison (-------). The letters F and B indicate the forward and backward travelling waves.

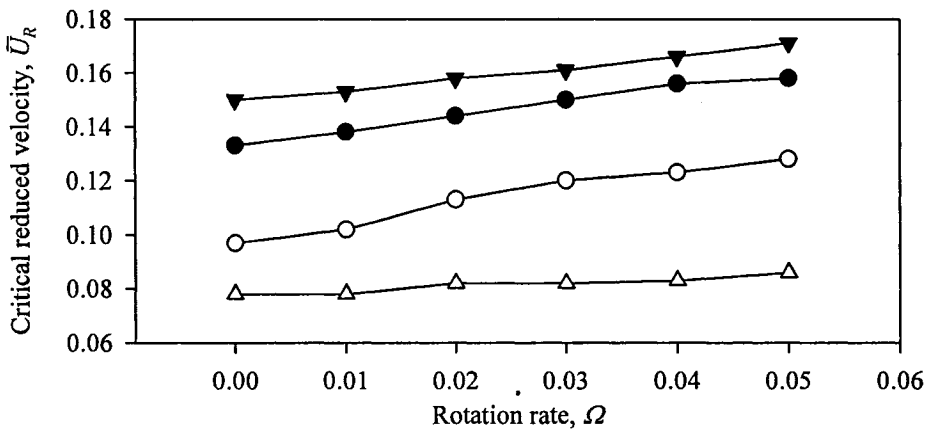

Fig. 32. Effect of rotation on the prediction of the onset of instability of the delta model for δ=1% for S_T=1 220 795, n=8, k=15 (—●—); S_T=12 208, n=8, k=15 (—▼—) ; S_T=1 220 795, n=0, k=10: (—○—) S_T=12 208, n=0, k=10 (—△—).

The results for higher rates of rotation are not presented because they were deemed not satisfactory. It seems that the "lines of no solution" discussed in Chapter 5 for the inviscid theory give rise to more frequencies in the viscous model in the same region of the parameter space, i.e. where $\Lambda^2 \geq 1$. In the viscous model, these are not

singularities, simply frequencies arising from the fluid. The problem is that the method employed for finding the roots of the dispersion relation was not appropriate to find these additional frequencies. The method employed was based on a Müller algorithm which would follow the frequencies found as the flow velocity was increased. But at high rates of rotation, when the region $\Lambda^2 \geq 1$ becomes large, the program would jump from one solution to the other and it would be very hard to obtain smooth curves. It must be emphasized that this issue is not due to singularities or inconsistencies in the model; it appears to be due solely to the root-finding method employed.

Since for any non-zero rate of rotation, there is a region in the parameter space where $\Lambda^2 \geq 1$, it is very probable that, even in the results presented here for small rates of rotation, some additional frequencies exist, but due to the root-finding method, they were not found. On the other hand, engineering judgement would lead us to believe that a frequency arising from the addition of a small rate of rotation should not influence the dynamics of the system dramatically.

Chapter 7

Conclusion

7.1. Concluding remarks

In this thesis the problem of the stability of a rotating cylindrical shell containing a co-rotating axial viscous flow is studied through the development of a theoretical fluid-structure interaction model. Learning from the flaws and breakdown of the inviscid model, it was believed that the added realism brought in by the introduction of viscosity in the theory would lead for a successful model. Adding viscosity in the model proved to be anything but trivial, and obtaining satisfactory results with the viscous theory has been in itself a challenging problem.

The equations of the inviscid model of Lai and Chow (1973) were rederived and the problem was studied further. The results that Lai and Chow obtained without rotation were reproduced, but it was impossible to obtain the same curves they have for the system subjected to rotation. Cortelezzi et al. (2004) had pointed out that it was impossible to reproduce the curves of Lai and Chow because of the presence of "islets where a solution is not feasible" in the parameter space due to the form of the pressure solution. It was shown in Chapter 5 that there were in fact an infinite number of lines of no solution and that a plausible explanation to the smooth curves exempt of singularities of Lai and Chow possibly is the very limited number of terms used in the evaluation of the Bessel functions expansions. Finally, a hypothetical physical explanation for the singularities in the inviscid model pressure solution was put forward in Chapter 5. Because of the often cited similarities between swirling flows and stratified flows, it is believed that a phenomenon similar to atmospheric flow blocking could explain the poles in the pressure solution of the rotating flow in the presence of the deforming wall.

Once the weaknesses of the inviscid theory were fully assessed, a new model based on viscous theory was developed. Assuming a travelling-wave perturbation scheme, the linear Donnell-Mushtari thin shell equations were coupled with the fluid

stresses obtained by solving the incompressible Navier-Stokes equation for a laminar or turbulent flow. A novel triple-perturbation approach had to be established to consider the interaction between the fluid and the structure. This triple-perturbation approach is in essence a superposition of three fluid fields caused by the three components of shell deformation for a given oscillation mode.

The complexity of the problem at the shell-fluid interface and the inclusion of viscosity rendered necessary the development of an original numerical method to solve the flow. Due to the limited number of boundary conditions at the shell-fluid interface, a staggered grid was used to discretise the fluid domain. To deal with the mathematical singularity in the fluid equations of motion at the centre of the flow, the pressure flux was introduced in the equations.

Similarly to the problems encountered by Dowell (1971) and El Chebair et al. (1990), it was found that the usual technique for linear aeroelasticity studies, consisting of applying the fluid boundary conditions at the undeformed position of the wall instead of the instantaneous deformed position, greatly alters the stability of the system. Since the mean flow velocity is zero at the wall (contrary to the inviscid model where the mean flow velocity is constant across the flow cross-section), the shell-position-dependent terms in the fluid boundary conditions disappear. This is believed to be the source of the unreasonable results obtained. To remedy this problem, corrections were applied in the form of three variants of the classical no-slip model: (i) the slip model, (ii) the average-velocity model, and (iii) the delta model. In the first model, a slip is permitted at the wall, which reinstates the position-related terms in the boundary conditions, but it also gets rid of the velocity profile. In the average-velocity model, the perturbation boundary conditions are modified to allow a non-zero mean velocity acting on the wall, while leaving the steady velocity profile unaffected. In the delta model, the boundary conditions are applied at an assumed deformed position just off the shell mean position.

The dynamics of the system subjected to purely axial flow with no rotation was successfully studied with the classical no-slip model for both laminar and turbulent flow conditions. Because no experimental or previous theoretical data was available, it was impossible to validate the results obtained in the laminar regime. On the other hand it was

found that the system was overly unstable in the turbulent regime which made necessary the application of correction models.

With the slip model, it was possible to model the system for a wide range of Reynolds number and achieve results which approached the inviscid theory results as the Reynolds number was increased. It was also found that the Reynolds number does not influence the onset of instability with this model.

The average-velocity model used in the laminar regime allowed obtaining predictions of instability in the same range as those of the inviscid theory. This may well be fortuitous. On the other hand, when used in the turbulent regime, the average-velocity model predicted that the system is very unstable. The model was deemed very arbitrary, hence motivating the use of the delta model.

It was found that in the laminar regime the system was insensitive to the deformation scale parameter of the delta model. In contrast, in the turbulent regime, for acceptably small values of the deformation scale parameter, the prediction of the onset of instability of the system tended towards that predicted by the inviscid model. As the Reynolds number was increased, the frequency curves produced with the delta model tended to become more similar to those obtained with the inviscid model. The delta model in the turbulent regime also predicted the presence of a third frequency emerging from the origin and growing proportional to the mean flow velocity. In certain cases, it plays a role in the stability of the system through "mode exchange".

The results obtained for small rates of rotation showed that, both in the laminar and in the turbulent regime, the system tends to be stabilised when subjected to a small rate of rotation. On the other hand, it seems reasonable to suppose that this tendency should be reversed for higher rates of rotation, but it was impossible to show this due to the limitations of the root-finding method employed. The important finding this thesis led to is that the addition of viscosity in the theory allows successfully modelling the system subjected to rotation. The flow solution no longer breaks down as was the case with the inviscid theory.

7.2. Future work

As well as answering some questions, many new ones were raised in this thesis. The future work that the present thesis could provide the basis for is presented in the following lines, starting with the most readily feasible projects.

The models developed here were not fully exploited. It is probable that better results for the rotating system and more information about the Z-waves could have been obtained if better root finding methods had been employed. Due to time constraints, it was impossible to test different methods in the framework of this project. When solving the inviscid flow, the zero-contour level method was employed. It was deemed to be too computationally intensive to use this technique with the viscous flow because, for the viscous models, the frequencies are all complex. The technique could still be used but, instead of solving the system for a range of real frequencies and a range of flow velocities, the system would now have to be solved for a range of real frequencies, a range of imaginary frequencies, and a range of flow velocities. This then increases the amount of computations by an order of magnitude. Add to this the fact that the viscous flow requires much more computations than the inviscid flow, and the amount of computation time has to be counted in months rather than minutes for a single graph of frequency evolution. The technique was attempted here for a very low resolution plot, but the results were not conclusive and are not included in the thesis. Better techniques are most probably available which would be more efficient yet would capture every frequency.

In order to be able to compare the viscous models with experiments, the theoretical model should be applied to a finite-length system with structural boundary conditions. This would also make it possible to eventually study the problem of a fixed thin pipe with an axially flowing fluid entering with a rotation component. The rotation would die out with distance along the length of the pipe, hence why a finite-length system is required for this problem.

The stability of the system was altered by the application of the boundary conditions at the undeformed position of the wall rather than at the instantaneous deformed position. This rendered necessary the use of models with corrections. It seems

that there is no elegant solution to this linear problem. Thus, a large-amplitude (non-linear) study would be required to apply the boundary conditions at the instantaneous position of the shell wall. The difficulties encountered here concerning the boundary conditions would also be encountered in the 2-D problem of viscous flow over a flat plate. If one were to tackle the problem of shear-flow-structure interaction in the hope of finding a more elegant solution to deal with the interface and the application of the fluid boundary conditions, it would be good to first attempt the geometrically simpler 2-D flow over a flat plate. The other motivation to develop a large-amplitude flow model would be to prove or disprove the hypothesis that the physical phenomenon of "flow blocking" is what makes the inviscid solution blow up when rotation is present.

The last interesting idea would be to add a turbulence model to the flow model to account for the Reynolds stresses in the fluid.

Appendix A

Shell-fluid interface linearization

An arbitrary shell element is originally located at

$$\vec{r}_0 = \vec{e}_r + z_0\vec{e}_z . \tag{8.1}$$

Once the shell deforms, it is located at

$$\vec{r}_1 = (1+w)\vec{e}_r + v\vec{e}_\theta + (z_0+u)\vec{e}_z . \tag{8.2}$$

Because this is a linear study, the velocity of an element located at a deformed position $\vec{r}_1$ must be imposed on the element originally located at $\vec{r}_0$ in computational space. To do that, Taylor expansions can be used to at least include the linear difference between what happens at $\vec{r}_0$ and $\vec{r}_1$ in the model.

A velocity evaluated at the instantaneous shell position can be approximated by means of a Taylor series expansion about the mean position of the shell:

$$\begin{aligned} V|_{\vec{r}_1} = V|_{\vec{r}_0} + w\left.\frac{\partial V}{\partial r}\right|_{\vec{r}_0} + v\left.\frac{1}{r}\frac{\partial V}{\partial \theta}\right|_{\vec{r}_0} + u\left.\frac{\partial V}{\partial z}\right|_{\vec{r}_0} \\ + O(w^2) + O(v^2) + O(u^2) + O(uw) + O(vw) + O(uv). \end{aligned} \tag{8.3}$$

As can be expected, if $V(r,\theta,z)$ is a perturbation quantity, its evaluation at the deformed or undeformed position of the shell only differs by second order quantities. To show it, let

$$V_a(r,\theta,z) = \hat{v}_a(r)w . \tag{8.4}$$

The evaluation of eq. (8.4) at the deformed position of the shell is

$$V_a|_{\vec{r}_1} \simeq \hat{v}_a(r)w|_{\vec{r}_0} + w\left.\frac{\partial}{\partial r}\left[\hat{v}_a(r)w\right]\right|_{\vec{r}_0} + v\left.\frac{1}{r}\frac{\partial}{\partial \theta}\left[\hat{v}_a(r)w\right]\right|_{\vec{r}_0} + u\left.\frac{\partial}{\partial z}\left[\hat{v}_a(r)w\right]\right|_{\vec{r}_0} ; \tag{8.5}$$

recalling that $w = \bar{w}e^{i(\omega t - kz - n\theta)}$ and with some manipulation eq. (8.5) becomes

$$V_a|_{\vec{r}_1} \simeq \hat{v}_a(r)w|_{\vec{r}_0} + \left[\frac{\partial \hat{v}_a(r)}{\partial r}(w^2) - in\frac{\hat{v}_a(r)}{r}(vw) - ik\hat{v}_a(r)(uw)\right]_{\vec{r}_0} . \tag{8.6}$$

Since *u, v, w* are perturbation quantities, we see from eq. (8.6) that the difference between evaluating a perturbation velocity at the instantaneous deformed position of the shell or at its mean position is of second order.

On the other hand, if in eq. (8.3), we substitute a velocity that has a zeroth order term, evaluating the equation at the instantaneous position of the shell leads to a significant change versus evaluating it at the mean position of the shell. Let the velocity have a zeroth order term:

$$V_b(r,\theta,z) = U_b(r) + \hat{v}_b(r)w. \tag{8.7}$$

We evaluate this velocity of eq. (8.7) at the instantaneous position of the shell using a Taylor expansion as in eq. (8.3) :

$$\begin{aligned} V_b|_{\vec{r}_1} = &\left[U_b(r) + \hat{v}_b(r)w\right]_{\vec{r}_0} + w\frac{\partial}{\partial r}\left[U_b(r) + \hat{v}_b(r)w\right]\Big|_{\vec{r}_0} \\ &+ v\frac{1}{r}\frac{\partial}{\partial\theta}\left[\hat{v}_b(r)w\right]\Big|_{\vec{r}_0} + u\frac{\partial}{\partial z}\left[\hat{v}_b(r)w\right]\Big|_{\vec{r}_0}. \end{aligned} \tag{8.8}$$

Once again, recalling that $w = \bar{w}e^{i(\omega t - kz - n\theta)}$, eq. (8.8) can be manipulated to

$$\begin{aligned} V_b|_{\vec{r}_1} = &\left[U_b(r) + \hat{v}_b(r)w\right]_{\vec{r}_0} + \left[w\frac{\partial U_b(r)}{\partial r}\right]_{\vec{r}_0} \\ &+ \left[\frac{\partial \hat{v}_b(r)}{\partial r}\left(w^2\right) - in\frac{\hat{v}_b(r)}{r}(vw) - ik\hat{v}_b(r)(uw)\right]_{\vec{r}_0}. \end{aligned} \tag{8.9}$$

The terms in the third square bracket are of second order and can be neglected; but, unlike eq. (8.6), the evaluation at the instantaneous position of the shell introduces an extra term in eq. (8.9), namely the term in the second square bracket.

To summarise, evaluation of a perturbation quantity at the mean position of the shell or at its instantaneous position differs by negligible second-order terms, while the evaluation of a zeroth-order term at the mean position of the shell or at its instantaneous position differs by a significant first-order term.

Appendix B

The linear Euler equation

In the derivation of the inviscid fluid model of Chapter 2, the perturbation scheme is applied directly through the introduction of the travelling wave solution of eqs. (2.49). For a better understanding, one might want to have a careful look at the linearization of eqs. (2.43) and (2.44). Let us assume a perturbation scheme of the following form:

$$\begin{aligned} V_r &= \tilde{v}_r(r,\theta,z,t), \\ V_\theta &= \tilde{v}_\theta(r,\theta,z,t), \\ V_z &= \bar{U}_R + \tilde{v}_z(r,\theta,z,t), \\ P &= P_0(r) + \tilde{p}(r,\theta,z,t), \end{aligned} \tag{9.1}$$

where the perturbation quantities are denoted by a tilde $(\sim)$. Upon introducing eqs. (9.1) into eqs. (2.43) and (2.44), one obtains

$$\begin{aligned} &\frac{\partial \tilde{v}_r}{\partial t} - 2\Omega\tilde{v}_\theta + \tilde{v}_r\frac{\partial \tilde{v}_r}{\partial r} + \frac{\tilde{v}_\theta}{r}\frac{\partial \tilde{v}_r}{\partial \theta} - \frac{\tilde{v}_\theta^2}{r} + (\bar{U}_R + \tilde{v}_z)\frac{\partial \tilde{v}_r}{\partial z} - \Omega^2 r = -\frac{\partial P_0}{\partial r} - \frac{\partial \tilde{p}}{\partial r}, \\ &\frac{\partial \tilde{v}_\theta}{\partial t} + 2\Omega\tilde{v}_r + \tilde{v}_r\frac{\partial \tilde{v}_\theta}{\partial r} + \frac{\tilde{v}_\theta}{r}\frac{\partial \tilde{v}_\theta}{\partial \theta} + \frac{\tilde{v}_r\tilde{v}_\theta}{r} + (\bar{U}_R + \tilde{v}_z)\frac{\partial \tilde{v}_\theta}{\partial z} = -\frac{1}{r}\frac{\partial \tilde{p}}{\partial \theta}, \\ &\frac{\partial \tilde{v}_z}{\partial t} + \tilde{v}_r\frac{\partial \tilde{v}_z}{\partial r} + \frac{\tilde{v}_\theta}{r}\frac{\partial \tilde{v}_z}{\partial \theta} + (\bar{U}_R + \tilde{v}_z)\frac{\partial \tilde{v}_z}{\partial z} = -\frac{\partial \tilde{p}}{\partial z}, \end{aligned} \tag{9.2}$$

and

$$\frac{1}{r}\frac{\partial}{\partial r}(r\tilde{v}_r) + \frac{1}{r}\frac{\partial \tilde{v}_\theta}{\partial \theta} + \frac{\partial \tilde{v}_z}{\partial z} = 0. \tag{9.3}$$

If we keep only the leading-order terms in eqs. (9.2) we obtain

$$-\Omega^2 r = -\frac{\partial P_0}{\partial r}. \tag{9.4}$$

If we keep only the first-order terms in eqs. (9.2) and (9.3), we obtain

$$
\begin{aligned}
&\frac{\partial \tilde{v}_r}{\partial t} - 2\Omega\tilde{v}_\theta + \bar{U}_R \frac{\partial \tilde{v}_r}{\partial z} = -\frac{\partial \tilde{p}}{\partial r}, \\
&\frac{\partial \tilde{v}_\theta}{\partial t} + 2\Omega\tilde{v}_r + \bar{U}_R \frac{\partial \tilde{v}_\theta}{\partial z} = -\frac{1}{r}\frac{\partial \tilde{p}}{\partial \theta}, \\
&\frac{\partial \tilde{v}_z}{\partial t} + \bar{U}_R \frac{\partial \tilde{v}_z}{\partial z} = -\frac{\partial \tilde{p}}{\partial z}, \\
&\frac{\partial \tilde{v}_r}{\partial r} + \frac{\tilde{v}_r}{r} + \frac{1}{r}\frac{\partial \tilde{v}_\theta}{\partial \theta} + \frac{\partial \tilde{v}_z}{\partial z} = 0.
\end{aligned}
\tag{9.5}
$$

Assuming that the perturbation quantities of eqs. (9.5) take the form of travelling waves,

$$
\begin{aligned}
\tilde{p} &= p(r)\exp(-ikz - in\theta + i\omega t) &&= p(r)e^{i\alpha}, \\
\tilde{v}_r &= v_r(r)\exp(-ikz - in\theta + i\omega t) &&= v_r(r)e^{i\alpha}, \\
\tilde{v}_\theta &= v_\theta(r)\exp(-ikz - in\theta + i\omega t) &&= v_\theta(r)e^{i\alpha}, \\
\tilde{v}_z &= v_z(r)\exp(-ikz - in\theta + i\omega t) &&= v_z(r)e^{i\alpha},
\end{aligned}
\tag{9.6}
$$

the equations of motion (2.55)-(2.58) are obtained.

Appendix C

The linear Navier-Stokes equation

In the derivation of the viscous fluid model of Chapter 3, the perturbation scheme is applied directly through the introduction of the travelling wave solution of eq.(3.22). For a better understanding, one might want to have a careful look at the linearization of eqs. (3.14)-(3.17). Let us assume a perturbation scheme of the following form:

$$\begin{aligned} V_r &= \tilde{v}_r(r,\theta,z,t), \\ V_\theta &= \tilde{v}_\theta(r,\theta,z,t), \\ V_z &= U_R(r)+\tilde{v}_z(r,\theta,z,t), \\ P &= P_0(r,z)+\tilde{p}(r,\theta,z,t), \end{aligned} \tag{10.1}$$

where the perturbation quantities are denoted by a tilde $(\sim)$. Upon introducing eqs. (10.1) into eqs. (3.14)-(3.17), one obtains

$$\begin{aligned} &\frac{\partial \tilde{v}_r}{\partial t}-2\Omega\tilde{v}_\theta+\tilde{v}_r\frac{\partial \tilde{v}_r}{\partial r}+\frac{\tilde{v}_\theta}{r}\frac{\partial \tilde{v}_r}{\partial \theta}-\frac{\tilde{v}_\theta^2}{r}+\left(U_R(r)+\tilde{v}_z\right)\frac{\partial \tilde{v}_r}{\partial z}-\Omega^2 r \\ &=-\frac{\partial P_0}{\partial r}-\frac{\partial \tilde{p}}{\partial r}+\frac{2\bar{U}_R}{\mathrm{Re}}\left[\frac{\partial}{\partial r}\left(\frac{1}{r}\frac{\partial}{\partial r}(r\tilde{v}_r)\right)+\frac{1}{r^2}\frac{\partial^2 \tilde{v}_r}{\partial \theta^2}+\frac{\partial^2 \tilde{v}_r}{\partial z^2}-\frac{2}{r^2}\frac{\partial \tilde{v}_\theta}{\partial \theta}\right], \end{aligned} \tag{10.2}$$

$$\begin{aligned} &\frac{\partial \tilde{v}_\theta}{\partial t}+2\Omega\tilde{v}_r+\tilde{v}_r\frac{\partial \tilde{v}_\theta}{\partial r}+\frac{\tilde{v}_\theta}{r}\frac{\partial \tilde{v}_\theta}{\partial \theta}+\frac{\tilde{v}_r\tilde{v}_\theta}{r}+\left(U_R(r)+\tilde{v}_z\right)\frac{\partial \tilde{v}_\theta}{\partial z} \\ &=-\frac{1}{r}\frac{\partial \tilde{p}}{\partial \theta}+\frac{2\bar{U}_R}{\mathrm{Re}}\left[\frac{\partial}{\partial r}\left(\frac{1}{r}\frac{\partial}{\partial r}(r\tilde{v}_\theta)\right)+\frac{1}{r^2}\frac{\partial^2 \tilde{v}_\theta}{\partial \theta^2}+\frac{\partial^2 \tilde{v}_\theta}{\partial z^2}+\frac{2}{r^2}\frac{\partial \tilde{v}_r}{\partial \theta}\right], \end{aligned} \tag{10.3}$$

$$\begin{aligned} &\frac{\partial \tilde{v}_z}{\partial t}+\tilde{v}_r\left(\frac{\partial U_R(r)}{\partial r}+\frac{\partial \tilde{v}_z}{\partial r}\right)+\frac{\tilde{v}_\theta}{r}\frac{\partial \tilde{v}_z}{\partial \theta}+\left(U_R(r)+\tilde{v}_z\right)\frac{\partial \tilde{v}_z}{\partial z} \\ &=-\frac{\partial P_0}{\partial z}-\frac{\partial \tilde{p}}{\partial z}+\frac{2\bar{U}_R}{\mathrm{Re}}\left[\frac{1}{r}\frac{\partial}{\partial r}\left(r\frac{\partial U_R(r)}{\partial r}+r\frac{\partial \tilde{v}_z}{\partial r}\right)+\frac{1}{r^2}\frac{\partial^2 \tilde{v}_z}{\partial \theta^2}+\frac{\partial^2 \tilde{v}_z}{\partial z^2}\right], \end{aligned} \tag{10.4}$$

and

$$\frac{1}{r}\frac{\partial}{\partial r}(r\tilde{v}_r)+\frac{1}{r}\frac{\partial \tilde{v}_\theta}{\partial \theta}+\frac{\partial \tilde{v}_z}{\partial z}=0. \tag{10.5}$$

If we keep only the leading-order terms in eqs. (10.2) and (10.4), we obtain

$$-\Omega^2 r = -\frac{\partial P_0}{\partial r}, \tag{10.6}$$

$$0 = -\frac{\partial P_0}{\partial z} + \frac{2\bar{U}_R}{\mathrm{R_e}} \frac{1}{r} \frac{\partial}{\partial r}\left(r \frac{\partial U_R(r)}{\partial r} \right). \tag{10.7}$$

If we keep only the first-order terms in eqs. (10.2)-(10.5), we obtain

$$\begin{aligned} &\frac{\partial \tilde{v}_r}{\partial t} - 2\Omega \tilde{v}_\theta + U_R(r) \frac{\partial \tilde{v}_r}{\partial z} \\ &= -\frac{\partial \tilde{p}}{\partial r} + \frac{2\bar{U}_R}{\mathrm{Re}} \left[\frac{\partial}{\partial r}\left(\frac{1}{r} \frac{\partial}{\partial r}(r\tilde{v}_r) \right) + \frac{1}{r^2} \frac{\partial^2 \tilde{v}_r}{\partial \theta^2} + \frac{\partial^2 \tilde{v}_r}{\partial z^2} - \frac{2}{r^2} \frac{\partial \tilde{v}_\theta}{\partial \theta} \right], \end{aligned} \tag{10.8}$$

$$\begin{aligned} &\frac{\partial \tilde{v}_\theta}{\partial t} + 2\Omega \tilde{v}_r + U_R(r) \frac{\partial \tilde{v}_\theta}{\partial z} \\ &= -\frac{1}{r} \frac{\partial \tilde{p}}{\partial \theta} + \frac{2\bar{U}_R}{\mathrm{Re}} \left[\frac{\partial}{\partial r}\left(\frac{1}{r} \frac{\partial}{\partial r}(r\tilde{v}_\theta) \right) + \frac{1}{r^2} \frac{\partial^2 \tilde{v}_\theta}{\partial \theta^2} + \frac{\partial^2 \tilde{v}_\theta}{\partial z^2} + \frac{2}{r^2} \frac{\partial \tilde{v}_r}{\partial \theta} \right], \end{aligned} \tag{10.9}$$

$$\begin{aligned} &\frac{\partial \tilde{v}_z}{\partial t} + \tilde{v}_r \frac{\partial U_R(r)}{\partial r} + U_R(r) \frac{\partial \tilde{v}_z}{\partial z} \\ &= -\frac{\partial \tilde{p}}{\partial z} + \frac{2\bar{U}_R}{\mathrm{Re}} \left[\frac{1}{r} \frac{\partial}{\partial r}\left(r \frac{\partial \tilde{v}_z}{\partial r} \right) + \frac{1}{r^2} \frac{\partial^2 \tilde{v}_z}{\partial \theta^2} + \frac{\partial^2 \tilde{v}_z}{\partial z^2} \right], \end{aligned} \tag{10.10}$$

$$\frac{\partial \tilde{v}_r}{\partial r} + \frac{\tilde{v}_r}{r} + \frac{1}{r} \frac{\partial \tilde{v}_\theta}{\partial \theta} + \frac{\partial \tilde{v}_z}{\partial z} = 0. \tag{10.11}$$

Assuming that the perturbation quantities of eqs. (10.8)-(10.11) take the form of a triple perturbation travelling wave proportional to the three shell wall deformations:

$$\begin{aligned} \tilde{v}_z &= \left[\hat{v}_{z,u}(r)\bar{u} + \hat{v}_{z,v}(r)\bar{v} + \hat{v}_{z,w}(r)\bar{w} \right] \exp(-ikz - in\theta + i\omega t), \\ \tilde{v}_\theta &= \left[\hat{v}_{\theta,u}(r)\bar{u} + \hat{v}_{\theta,v}(r)\bar{v} + \hat{v}_{\theta,w}(r)\bar{w} \right] \exp(-ikz - in\theta + i\omega t), \\ \tilde{v}_r &= \left[\hat{v}_{r,u}(r)\bar{u} + \hat{v}_{r,v}(r)\bar{v} + \hat{v}_{r,w}(r)\bar{w} \right] \exp(-ikz - in\theta + i\omega t), \end{aligned} \tag{10.12}$$

the following four equations are obtained:

$$
\begin{aligned}
&\left(i\omega - ikU_R(r)\right)\left\{\hat{v}_{r,w}\overline{w} + \hat{v}_{r,v}\overline{v} + \hat{v}_{r,u}\overline{u}\right\} - 2\Omega\left\{\hat{v}_{\theta,w}\overline{w} + \hat{v}_{\theta,v}\overline{v} + \hat{v}_{\theta,u}\overline{u}\right\} \\
&= -\left\{\frac{\partial \hat{p}_w}{\partial r}\overline{w} + \frac{\partial \hat{p}_v}{\partial r}\overline{v} + \frac{\partial \hat{p}_u}{\partial r}\overline{u}\right\} \\
&+ \frac{2\overline{U}_R}{\mathrm{Re}}\left[\left\{\frac{\partial^2 \hat{v}_{r,w}}{\partial r^2}\overline{w} + \frac{\partial^2 \hat{v}_{r,v}}{\partial r^2}\overline{v} + \frac{\partial^2 \hat{v}_{r,u}}{\partial r^2}\overline{u}\right\}\right. \\
&+ \left\{\frac{1}{r}\frac{\partial \hat{v}_{r,w}}{\partial r}\overline{w} + \frac{1}{r}\frac{\partial \hat{v}_{r,v}}{\partial r}\overline{v} + \frac{1}{r}\frac{\partial \hat{v}_{r,u}}{\partial r}\overline{u}\right\} \\
&- \left(\frac{1+n^2}{r^2} + k^2\right)\left\{\hat{v}_{r,w}\overline{w} + \hat{v}_{r,v}\overline{v} + \hat{v}_{r,u}\overline{u}\right\} \\
&\left. + \frac{2in}{r^2}\left\{\hat{v}_{\theta,w}\overline{w} + \hat{v}_{\theta,v}\overline{v} + \hat{v}_{\theta,u}\overline{u}\right\}\right],
\end{aligned}
\tag{10.13}
$$

$$
\begin{aligned}
&\left(i\omega - ikU_R(r)\right)\left\{\hat{v}_{\theta,w}\overline{w} + \hat{v}_{\theta,v}\overline{v} + \hat{v}_{\theta,u}\overline{u}\right\} + 2\Omega\left\{\hat{v}_{r,w}\overline{w} + \hat{v}_{r,v}\overline{v} + \hat{v}_{r,u}\overline{u}\right\} \\
&= \frac{in}{r}\left\{\hat{p}_w\overline{w} + \hat{p}_v\overline{v} + \hat{p}_u\overline{u}\right\} \\
&+ \frac{2\overline{U}_R}{\mathrm{Re}}\left[\left\{\frac{\partial^2 \hat{v}_{\theta,w}}{\partial r^2}\overline{w} + \frac{\partial^2 \hat{v}_{\theta,v}}{\partial r^2}\overline{v} + \frac{\partial^2 \hat{v}_{\theta,u}}{\partial r^2}\overline{u}\right\}\right. \\
&+ \left\{\frac{1}{r}\frac{\partial \hat{v}_{\theta,w}}{\partial r}\overline{w} + \frac{1}{r}\frac{\partial \hat{v}_{\theta,v}}{\partial r}\overline{v} + \frac{1}{r}\frac{\partial \hat{v}_{\theta,u}}{\partial r}\overline{u}\right\} \\
&- \left(\frac{1+n^2}{r^2} + k^2\right)\left\{\hat{v}_{\theta,w}\overline{w} + \hat{v}_{\theta,v}\overline{v} + \hat{v}_{\theta,u}\overline{u}\right\} \\
&\left. - \frac{2in}{r^2}\left\{\hat{v}_{r,w}\overline{w} + \hat{v}_{r,v}\overline{v} + \hat{v}_{r,u}\overline{u}\right\}\right],
\end{aligned}
\tag{10.14}
$$

$$
\begin{aligned}
&\left(i\omega - ikU_R(r)\right)\left\{\hat{v}_{z,w}\overline{w} + \hat{v}_{z,v}\overline{v} + \hat{v}_{z,u}\overline{u}\right\} + \frac{\partial U_R(r)}{\partial r}\left\{\hat{v}_{r,w}\overline{w} + \hat{v}_{r,v}\overline{v} + \hat{v}_{r,u}\overline{u}\right\} \\
&= ik\left\{\hat{p}_w\overline{w} + \hat{p}_v\overline{v} + \hat{p}_u\overline{u}\right\} \\
&+ \frac{2\overline{U}_R}{\mathrm{Re}}\left[\left\{\frac{\partial^2 \hat{v}_{z,w}}{\partial r^2}\overline{w} + \frac{\partial^2 \hat{v}_{z,v}}{\partial r^2}\overline{v} + \frac{\partial^2 \hat{v}_{z,u}}{\partial r^2}\overline{u}\right\}\right. \\
&+ \left\{\frac{1}{r}\frac{\partial \hat{v}_{z,w}}{\partial r}\overline{w} + \frac{1}{r}\frac{\partial \hat{v}_{z,v}}{\partial r}\overline{v} + \frac{1}{r}\frac{\partial \hat{v}_{z,u}}{\partial r}\overline{u}\right\} \\
&\left. - \left(\frac{n^2}{r^2} + k^2\right)\left\{\hat{v}_{z,w}\overline{w} + \hat{v}_{z,v}\overline{v} + \hat{v}_{z,u}\overline{u}\right\}\right],
\end{aligned}
\tag{10.15}
$$

$$\left\{\frac{\partial \hat{v}_{r,w}}{\partial r}\overline{w}+\frac{\partial \hat{v}_{r,v}}{\partial r}\overline{v}+\frac{\partial \hat{v}_{r,u}}{\partial r}\overline{u}\right\}+\frac{1}{r}\left\{\hat{v}_{r,w}\overline{w}+\hat{v}_{r,v}\overline{v}+\hat{v}_{r,u}\overline{u}\right\}$$
$$-\frac{in}{r}\left\{\hat{v}_{\theta,w}\overline{w}+\hat{v}_{\theta,v}\overline{v}+\hat{v}_{\theta,u}\overline{u}\right\}-ik\left\{\hat{v}_{z,w}\overline{w}+\hat{v}_{z,v}\overline{v}+\hat{v}_{z,u}\overline{u}\right\}=0. \tag{10.16}$$

Since the perturbations $\overline{u}$, $\overline{v}$, $\overline{w}$ are linearly independent, eqs. (10.13)-(10.16) must be valid for any combination of the perturbations. These four equations can be broken into three sets of four equations of motion (3.54)-(3.57), representing three superimposed flow solutions.

Appendix D

Accuracy of the numerical scheme

In Chapter 4, the continuity equation (4.5) is given by

$$\frac{1}{r}\frac{\partial}{\partial r}(r\hat{v}_r) - in\frac{1}{r}\hat{v}_\theta - ik\hat{v}_z = 0, \tag{11.1}$$

and from eq. (4.9) is discretised on the staggered grid as

$$\frac{\hat{v}_{r,j+\frac{1}{2}} - \hat{v}_{r,j-\frac{1}{2}}}{\Delta r} + \frac{1}{r_j}\frac{\hat{v}_{r,j+\frac{1}{2}} + \hat{v}_{r,j-\frac{1}{2}}}{2} - in\frac{1}{r_j}\frac{\hat{v}_{\theta,j+\frac{1}{2}} + \hat{v}_{\theta,j-\frac{1}{2}}}{2} - ik\frac{\hat{v}_{z,j+\frac{1}{2}} + \hat{v}_{z,j-\frac{1}{2}}}{2} = 0. \tag{11.2}$$

Expressing a velocity influence function in a Taylor series expansion, one gets

$$\hat{v}_{j+\frac{1}{2}} = \hat{v}_j + \left(r_{j+\frac{1}{2}} - r_j\right)\left.\frac{\partial\hat{v}}{\partial r}\right|_{r=r_j} + \frac{\left(r_{j+\frac{1}{2}} - r_j\right)^2}{2!}\left.\frac{\partial^2\hat{v}}{\partial r^2}\right|_{r=r_j} + \ldots = \sum_{m=0}^{\infty}\frac{\left(r_{j+\frac{1}{2}} - r_j\right)^m}{m!}\left[\frac{\partial^m\hat{v}}{\partial r^m}\right]_{r=r_j}, \tag{11.3}$$

which is equivalent to

$$\hat{v}_{j+\frac{1}{2}} = \hat{v}_j + \frac{\Delta r}{2}\left.\frac{\partial\hat{v}}{\partial r}\right|_{r=r_j} + \sum_{m=2}^{\infty}\frac{\Delta r^m}{2^m m!}\left[\frac{\partial^m\hat{v}}{\partial r^m}\right]_{r=r_j}, \tag{11.4}$$

where as in Chapter 4, we let $r_{j+1} - r_j = \Delta r$ or $r_{j+\frac{1}{2}} - r_j = \frac{\Delta r}{2}$. Similarly,

$$\hat{v}_{j-\frac{1}{2}} = \hat{v}_j - \frac{\Delta r}{2}\left.\frac{\partial\hat{v}}{\partial r}\right|_{r=r_j} + \sum_{m=2}^{\infty}\frac{(-1)^m\Delta r^m}{2^m m!}\left[\frac{\partial^m\hat{v}}{\partial r^m}\right]_{r=r_j}. \tag{11.5}$$

We can rewrite the numerical approximation of the continuity eq. (11.2) and set it equal to its local truncation error:

$$\frac{\hat{v}_{r,j+\frac{1}{2}} - \hat{v}_{r,j-\frac{1}{2}}}{\Delta r} + \frac{1}{r_j}\frac{\hat{v}_{r,j+\frac{1}{2}} + \hat{v}_{r,j-\frac{1}{2}}}{2} - in\frac{1}{r_j}\frac{\hat{v}_{\theta,j+\frac{1}{2}} + \hat{v}_{\theta,j-\frac{1}{2}}}{2} - ik\frac{\hat{v}_{z,j+\frac{1}{2}} + \hat{v}_{z,j-\frac{1}{2}}}{2} = \xi_{c,j}. \tag{11.6}$$

We substitute the Taylor series expansion of eqs. (11.4) and (11.5) into eq. (11.6)

$$\left\{\left.\frac{\partial \hat{v}_r}{\partial r}\right|_{r=r_j}+\sum_{m=2}^{\infty}\frac{\Delta r^{m-1}}{2^m m!}\left[\frac{\partial^m \hat{v}_r}{\partial r^m}\right]_{r=r_j}-\sum_{m=2}^{\infty}\frac{(-1)^m \Delta r^{m-1}}{2^m m!}\left[\frac{\partial^m \hat{v}_r}{\partial r^m}\right]_{r=r_j}\right\}+$$

$$\frac{1}{r_j}\left\{\hat{v}_{r,j}+\sum_{m=2}^{\infty}\frac{\Delta r^m}{2^{m+1} m!}\left[\frac{\partial^m \hat{v}_r}{\partial r^m}\right]_{r=r_j}+\sum_{m=2}^{\infty}\frac{(-1)^m \Delta r^m}{2^{m+1} m!}\left[\frac{\partial^m \hat{v}_r}{\partial r^m}\right]_{r=r_j}\right\}-$$

$$in\frac{1}{r_j}\left\{\hat{v}_{\theta,j}+\sum_{m=2}^{\infty}\frac{\Delta r^m}{2^{m+1} m!}\left[\frac{\partial^m \hat{v}_\theta}{\partial r^m}\right]_{r=r_j}+\sum_{m=2}^{\infty}\frac{(-1)^m \Delta r^m}{2^{m+1} m!}\left[\frac{\partial^m \hat{v}_\theta}{\partial r^m}\right]_{r=r_j}\right\}-$$

$$ik\left\{\hat{v}_{z,j}+\sum_{m=2}^{\infty}\frac{\Delta r^m}{2^{m+1} m!}\left[\frac{\partial^m \hat{v}_z}{\partial r^m}\right]_{r=r_j}+\sum_{m=2}^{\infty}\frac{(-1)^m \Delta r^m}{2^{m+1} m!}\left[\frac{\partial^m \hat{v}_z}{\partial r^m}\right]_{r=r_j}\right\}=\xi_{c,j}. \qquad (11.7)$$

This can be rewritten as

$$\left[\frac{\partial \hat{v}_r}{\partial r}+\frac{\hat{v}_r}{r}-in\frac{\hat{v}_\theta}{r}-ik\hat{v}_z\right]_{r=r_j}+$$

$$\sum_{m=2}^{\infty}\left[\left\{1-(-1)^m\right\}\frac{\Delta r^{m-1}}{2^m m!}\frac{\partial^m \hat{v}_r}{\partial r^m}+\left\{1+(-1)^m\right\}\frac{1}{r_j}\frac{\Delta r^m}{2^{m+1} m!}\frac{\partial^m \hat{v}_r}{\partial r^m}\right.$$

$$\left.-in\frac{1}{r}\left\{1+(-1)^m\right\}\frac{\Delta r^m}{2^{m+1} m!}\frac{\partial^m \hat{v}_\theta}{\partial r^m}-ik\left\{1+(-1)^m\right\}\frac{\Delta r^m}{2^{m+1} m!}\frac{\partial^m \hat{v}_z}{\partial r^m}\right]_{r=r_j}=\xi_{c,j}. \qquad (11.8)$$

The first line of eq. (11.8), is the exact continuity eq. (11.1). The local truncation error is then

$$\xi_{c,j}=\sum_{m=2}^{\infty}\left[\left\{1-(-1)^m\right\}\frac{\Delta r^{m-1}}{2^m m!}\frac{\partial^m \hat{v}_r}{\partial r^m}+\left\{1+(-1)^m\right\}\frac{1}{r_j}\frac{\Delta r^m}{2^{m+1} m!}\frac{\partial^m \hat{v}_r}{\partial r^m}\right.$$

$$\left.-in\frac{1}{r}\left\{1+(-1)^m\right\}\frac{\Delta r^m}{2^{m+1} m!}\frac{\partial^m \hat{v}_\theta}{\partial r^m}-ik\left\{1+(-1)^m\right\}\frac{\Delta r^m}{2^{m+1} m!}\frac{\partial^m \hat{v}_z}{\partial r^m}\right]_{r=r_j}. \qquad (11.9)$$

Taking the first non-zero terms of the error out of the series summation, we get

$$\xi_{c,j}=\Delta r^2\left[\frac{1}{24}\frac{\partial^3 \hat{v}_r}{\partial r^3}+\frac{1}{8r_j}\frac{\partial^2 \hat{v}_r}{\partial r^2}-in\frac{1}{8r}\frac{\partial^2 \hat{v}_\theta}{\partial r^2}-ik\frac{1}{8}\frac{\partial^2 \hat{v}_z}{\partial r^2}\right]_{r=r_j}+$$

$$\sum_{m=4}^{\infty}\left[\left\{1-(-1)^m\right\}\frac{\Delta r^{m-1}}{2^m m!}\frac{\partial^m \hat{v}_r}{\partial r^m}\right]_{r=r_j}+\sum_{m=3}^{\infty}\left[\left\{1+(-1)^m\right\}\frac{1}{r_j}\frac{\Delta r^m}{2^{m+1} m!}\frac{\partial^m \hat{v}_r}{\partial r^m},\right.$$

$$\left.-in\frac{1}{r}\left\{1+(-1)^m\right\}\frac{\Delta r^m}{2^{m+1} m!}\frac{\partial^m \hat{v}_\theta}{\partial r^m}-ik\left\{1+(-1)^m\right\}\frac{\Delta r^m}{2^{m+1} m!}\frac{\partial^m \hat{v}_z}{\partial r^m}\right]_{r=r_j} \qquad (11.10)$$

where the right-hand side of the first line is the leading-order error term. We can therefore say that the leading error term is proportional to the second power of Δr.

Similarly for the r- θ- and z-momentum equations (4.10)-(4.12), their respective local truncation errors are found:

$$\xi_{r,j-\frac{1}{2}} = \Delta r^2 \left[\left(\frac{1}{r} - \frac{1}{2r^2} \right) \frac{1}{24} \frac{\partial^3 q}{\partial r^3} - \frac{2\bar{U}_R}{\mathrm{Re}} \left(\frac{1}{6r} \frac{\partial^3 \hat{v}_r}{\partial r^3} - \frac{1}{12} \frac{\partial^4 \hat{v}_r}{\partial r^4} \right) \right]_{r=r_{j-\frac{1}{2}}} +$$

$$\left[\sum_{m=4}^{\infty} \left\{ \left[\frac{1}{r} - \frac{1}{2r^2} \right] \left\{ 1-(-1)^m \right\} \frac{\Delta r^{m-1}}{2^m m!} \frac{\partial^m q}{\partial r^m} - \frac{2\bar{U}_R}{\mathrm{Re}} \left[\frac{1}{2r} \left\{ 1-(-1)^m \right\} \frac{\Delta r^{m-1}}{m!} \frac{\partial^m \hat{v}_r}{\partial r^m} \right] \right\} \right.$$

$$\left. - \frac{2\bar{U}_R}{\mathrm{Re}} \sum_{m=5}^{\infty} \left\{ 1+(-1)^m \right\} \frac{\Delta r^{m-2}}{m!} \frac{\partial^m \hat{v}_r}{\partial r^m} \right]_{r=r_{j-\frac{1}{2}}}, \tag{11.11}$$

$$\xi_{\theta,j-\frac{1}{2}} = \Delta r^2 \left[-in \frac{1}{8r^2} \frac{\partial^2 q}{\partial r^2} - \frac{2\bar{U}_R}{\mathrm{Re}} \frac{1}{6r} \frac{\partial^3 \hat{v}_\theta}{\partial r^3} - \frac{2\bar{U}_R}{\mathrm{Re}} \frac{1}{12} \frac{\partial^4 \hat{v}_\theta}{\partial r^4} \right]_{r=r_{j-\frac{1}{2}}} +$$

$$\left[-in \frac{1}{2r^2} \sum_{m=3}^{\infty} \left\{ 1+(-1)^m \right\} \frac{\Delta r^m}{2^m m!} \frac{\partial^m q}{\partial r^m} - \frac{2\bar{U}_R}{\mathrm{Re}} \frac{1}{2r} \sum_{m=4}^{\infty} \left\{ 1-(-1)^m \right\} \frac{\Delta r^{m-1}}{m!} \frac{\partial^m \hat{v}_\theta}{\partial r^m} \right.$$

$$\left. - \frac{2\bar{U}_R}{\mathrm{Re}} \sum_{m=5}^{\infty} \left\{ 1+(-1)^m \right\} \frac{\Delta r^{m-2}}{m!} \frac{\partial^m \hat{v}_\theta}{\partial r^m} \right]_{r=r_{j-\frac{1}{2}}}, \tag{11.12}$$

$$\xi_{z,j-\frac{1}{2}} = \Delta r^2 \left[-\frac{ik}{8r} \frac{\partial^2 q}{\partial r^2} - \frac{\bar{U}_R}{6\mathrm{Re}} \frac{\partial^4 \hat{v}_z}{\partial r^4} - \frac{\bar{U}_R}{\mathrm{Re}} \frac{1}{3r} \frac{\partial^3 \hat{v}_z}{\partial r^3} \right]_{r=r_{j-\frac{1}{2}}} +$$

$$\left[-\frac{ik}{2r} \sum_{m=4}^{\infty} \left\{ 1+(-1)^m \right\} \frac{\Delta r^m}{2^m m!} \frac{\partial^m q}{\partial r^m} - \frac{2\bar{U}_R}{\mathrm{Re}} \sum_{m=6}^{\infty} \left\{ 1+(-1)^m \right\} \frac{\Delta r^{m-2}}{m!} \frac{\partial^m \hat{v}_z}{\partial r^m} \right.$$

$$\left. - \frac{2\bar{U}_R}{\mathrm{Re}} \frac{1}{2r} \sum_{m=5}^{\infty} \left\{ 1-(-1)^m \right\} \frac{\Delta r^{m-1}}{m!} \frac{\partial^m \hat{v}_z}{\partial r^m} \right]_{r=r_{j-\frac{1}{2}}}. \tag{11.13}$$

In eqs. (11.11)-(11.13), the first term on the right-hand side is the leading order error term. Since the leading error terms in all equations of the numerical scheme are all proportional to the second power of Δr, the scheme can be said second-order accurate.

Appendix E

Matlab Code for the Delta Model

```
%%%%%%%%%%%%%%%%%%%%%%%%%%%%%%%%%%%%%%%%%%%%%%%%%%%%%%%%%%%%%%%%%%%%%%%%%%%%
% RUNTONIGHT.M : TOP LEVEL PROGRAM FROM WHICH THE SIMULATIONS ARE RUN
%%%%%%%%%%%%%%%%%%%%%%%%%%%%%%%%%%%%%%%%%%%%%%%%%%%%%%%%%%%%%%%%%%%%%%%%%%%%

Umin=0.00001;       %Minimal velocity of the omega VS UR plot
Umax=0.25001;       %Maximal velocity of the omega VS UR plot
Npoints=200;        %Number of points on the omega VS UR plot
tol=1E-3;           %Relative tolerance on each complex part of the
        %frequency for the Muller algorithm in the
%dispertion relation
Omega=0;            %Rotation rate
nu=0.49;            %Poisson's ratio
Gamma=1.0536/1.0;   %Density ratio
chi=.038/1.9;       %Thickness to radius ratio of the shell (Called h in
%the thesis)
N=400;              %Number of pressure points in the discretisation of
%the flow domain. Usually between 400-2000.

%Loop for various values of the Reynolds number
for nv=5:-1:5
    RE=1*10^(nv)
    %Loop for various values of the delta parameter in the delta model
    for delta=0:0.001:0

        clear freq
        freq(1)=0.5;    %Guess of the frequency at UR=Umin
        freq(2)=-0.5;   %Guess of the frequency at UR=Umin
        k=10;           %Axial wavenumber
        n=0;            %Circumferential wavenumber
        curverey        %Calls the program CURVEREY.M

        clear freq
        freq(1)=0.2;    %Guess of the frequency at UR=Umin
        freq(2)=-0.2;   %Guess of the frequency at UR=Umin
        k=5;            %Axial wavenumber
        n=6;            %Circumferential wavenumber
        curverey        %Calls the program CURVEREY.M

    end
end

return
```

```
%%%%%%%%%%%%%%%%%%%%%%%%%%%%%%%%%%%%%%%%%%%%%%%%%%%%%%%%%%%%%%%%%%%%%%%%%%%%
% CURVEREY.M : PROGRAM WHICH FOLLOWS FREQUENCY CURVES FOR INCREMENTING
% VALUES OF UR
%%%%%%%%%%%%%%%%%%%%%%%%%%%%%%%%%%%%%%%%%%%%%%%%%%%%%%%%%%%%%%%%%%%%%%%%%%%%

h=(Umax-Umin)/(Npoints-1);  %UR step
clear results

%Loop for the different frequencies to be followed by the program
[garbage,nz]=size(freq);
for nf=1:nz
    oi=freq(nf)  %Frequencies for vanishingly small UR
    U=Umin;

    %Loop for the incrementing UR on the omega VS UR plot
    for iu=0:(Npoints-1)
```

```
        U=Umin+h*iu %Incrementing UR
        %Returns the converge complex frequency for the given parameters
        omega=mullervisc(nu,n,Omega,k,Gamma,chi,U,RE,N,tol,oi,oi*.99,oi*.98,delt⇒ a)
        %Put the results in a matrix
        results(iu+1,nf*3-2)=U;
        results(iu+1,nf*3-1)=real(omega);
        results(iu+1,nf*3-0)=imag(omega);

        %Use linear extrapolation to guess the complex frequency at the      %next UR step
        if iu>0
            oi=2*omega-omegao;
        else
            oi=omega;
        end
        omegao=omega;
    end;
end;

%Save the results on a CSV file
str1='PowLaw-3per-Omega=';
str2=num2str(Omega);
str3='-N';
str4=num2str(N);
str5='-RE=1E=';
str6=num2str(nv);
str7='-n=';
str8=num2str(n);
str9='-k=';
str10=num2str(k);
str11='-delta=';
str12=num2str(delta);
strend='part1.csv';
filename=strcat(str1,str2,str3,str4,str5,str6,str7,str8,str9,str10,str11⇒ ,str12,strend);
csvwrite(filename,results,0,0);
return
```

```
%%%%%%%%%%%%%%%%%%%%%%%%%%%%%%%%%%%%%%%%%%%%%%%%%%%%%%%%%%%%%%%%%%%%%%%%%%%%
% MULLERVISC.M : MULLER ROOT-FINDING ALGORITHM FINDING A COMPLEX FREQUENCY BASED ON THE
% PROVIDED GUESS TO SATISFY THE DISPERSION RELATION
%%%%%%%%%%%%%%%%%%%%%%%%%%%%%%%%%%%%%%%%%%%%%%%%%%%%%%%%%%%%%%%%%%%%%%%%%%%%
function omega = mullervisc(nu,n,Omega,k,Gamma,chi,U,RE,N,tol,oi,oi1,oi2,delta)

%oi, oi1 and oi3 are the three guesses for the complex frequency

%Evaluation of the determinant of the L-Matrix for two different guesses
%of the complex frequency. This value should converge to zero as the
%guess of omega gets closer to the solution.
fi2=omegavisc(nu,n,Omega,k,Gamma,chi,U,RE,N,oi2,delta);
fi1=omegavisc(nu,n,Omega,k,Gamma,chi,U,RE,N,oi1,delta);

er=10*tol;  %Initialise the error

while er>tol
    %Muller algorithm
    fi=omegavisc(nu,n,Omega,k,Gamma,chi,U,RE,N,oi,delta); %Evaluation of
                                                    %the determinant of the L-Matrix
    a0=fi;
    aa=(fi1-fi)/(oi1-oi);
    a2=((fi2-fi1)/(oi2-oi1)-aa)/(oi2-oi);
    a1=aa+(oi-oi1)*a2;

    %From Muller, I obtain two possibilities of omega. I keep the one
    %closest to my guesses.
    oip1=oi+2*a0/(-a1+sqrt(a1^2-4*a0*a2));
    oip2=oi+2*a0/(-a1-sqrt(a1^2-4*a0*a2));

    oi2=oi1;
    fi2=fi1;
    oi1=oi;
    fi1=fi;
```

```
    %The convergence criterion is based on the relative error of
    %imaginary and real parts of the frequency independently. Even if
    %one part is converged, it keeps iterating until the other part
    %converges.
    erreal1=abs(real((oi-oip1)/oi));
    erimag1=abs(imag((oi-oip1)/oi));
    er1=max(erreal1,erimag1);
    erreal2=abs(real((oi-oip2)/oi));
    erimag2=abs(imag((oi-oip2)/oi));
    er2=max(erreal2,erimag2);
    if er1>er2
        oi=oip2;
        er=er2;
    else
        oi=oip1;
        er=er1;
    end

end
omega=oi;
return
```

```
%%%%%%%%%%%%%%%%%%%%%%%%%%%%%%%%%%%%%%%%%%%%%%%%%%%%%%%%%%%%%%%%%%%%%%%%%%%%
% OMEGAVISC.M : FOR A GUESS OF THE COMPLEX FREQUENCY, THE OMEGAVISC FUNCTION RETURNS THE
% EVALUATION OF THE DETERMINANT OF THE EIGENVALUE PROBLEM MATRIX.
%%%%%%%%%%%%%%%%%%%%%%%%%%%%%%%%%%%%%%%%%%%%%%%%%%%%%%%%%%%%%%%%%%%%%%%%%%%%
function result = omegavisc(nu,n,Omega,k,Gamma,chi,U,RE,N,omega,delta)

%Avoid singular cases
if omega-k*U==0
    omega=0.99999999*omega;
end

Lambda=2*Omega/(omega-k*U);

%Find the fluid forces per unit deformation acting on the shell
clear GG
G=order2profilew(n,Omega,omega,k,Lambda,U,RE,N,delta)/chi/Gamma; %Fluid stresses caused by
                                %w-deformation of the shell
GG(3,3)=G(1);
GG(2,3)=G(2);
GG(1,3)=G(3);

G=order2profilev(n,Omega,omega,k,Lambda,U,RE,N,delta)/chi/Gamma; %Fluid stresses caused by
                                %v-deformation of the shell
GG(3,2)=G(1);
GG(2,2)=G(2);
GG(1,2)=G(3);

G=order2profileu(n,Omega,omega,k,Lambda,U,RE,N,delta)/chi/Gamma; %Fluid stresses caused by
                                %u-deformation of the shell
GG(3,1)=G(1);
GG(2,1)=G(2);
GG(1,1)=G(3);

%Determinant of the matrix of the eigenvalue problem is a polynomial of %degree 6 of omega
%This equation solves the force summation in the three directions
deg6=-1;
deg5=0;
deg4=(GG(2,2)+1/6*chi^2*k^2*n^2-1/2*k^2*nu+1/12*chi^2*n^4+1/12*chi^2*k^4+GG(1,1)+GG(3,3)
⇒       +1+3/2*n^2+2*Omega^2+3/2*k^2-1/2*n^2*nu);
deg3=(2*i*Omega*GG(3,2)-2*i*GG(2,3)*Omega+4*n*Omega);
deg2=(-GG(2,2)-GG(1,1)+Omega^2-1/2*n^2-3/2*k^2-1/8*k^6*chi^2+1/8*k^4*nu*chi^2*n^2
⇒       +1/8*k^2*nu*chi^2*n^4+1/6*Omega^2*chi^2*k^2*n^2-1/6*GG(2,2)*chi^2*k^2*n^2
⇒       +1/2*k^2*nu-k^2*n^2-3/2*k^2*Omega^2-1/8*n^6*chi^2-3/2*k^2*GG(3,3)-3/2*n^2*GG(3,3)
⇒       +Omega^2*GG(3,3)+GG(2,2)*Omega^2-GG(2,2)*GG(3,3)+GG(2,3)*GG(3,2)-1/2*k^4-1/2*n^4
⇒       -Omega^4+1/2*k*n*GG(1,2)+1/2*n^2*nu*GG(2,2)+1/2*GG(1,1)*k^2*nu+1/2*GG(2,1)*k*n
⇒       +1/2*k*n*nu*GG(1,2)+1/2*GG(2,1)*k*n*nu-k^2*GG(2,2)-1/2*n^2*GG(2,2)
```

```
⇒       -2*GG(1,1)*Omega^2-1/2*GG(1,1)*k^2-GG(1,1)*GG(2,2)+GG(2,1)*GG(1,2)
⇒       +1/2*n^2*nu+1/2*k^4*nu+n^2*k^2*nu+n^2*nu*Omega^2+1/2*n^4*nu+nu^2*k^2
⇒       +GG(3,1)*GG(1,3)-GG(1,1)*GG(3,3)-GG(1,1)*n^2-1/6*GG(1,1)*chi^2*k^2*n^2
⇒       +i*GG(3,1)*nu*k-i*nu*k*GG(1,3)+1/24*n^6*nu*chi^2+1/2*n^2*nu*GG(3,3)
⇒       -1/12*GG(1,1)*chi^2*n^4-1/12*GG(1,1)*chi^2*k^4-i*GG(2,3)*n
⇒       +1/2*k^2*nu*GG(3,3)+i*n*GG(3,2)-1/12*GG(2,2)*chi^2*n^4-1/12*GG(2,2)*chi^2*k^4
⇒       +1/12*Omega^2*chi^2*n^4+1/12*Omega^2*chi^2*k^4-1/2*k^2*nu*Omega^2
⇒       +1/24*k^6*nu*chi^2-3/8*k^2*chi^2*n^4-3/8*k^4*chi^2*n^2);
deg1=(-i*k*n*nu*GG(1,3)*Omega-i*n^2*Omega*GG(3,2)+2*nu*k*GG(1,2)*Omega
⇒       -i*n^2*nu*GG(2,3)*Omega+i*n^2*GG(2,3)*Omega+2*k^2*n*nu^2*Omega
⇒       +2*n^3*nu*Omega-*i*k^2*Omega*GG(3,2)+2*i*GG(1,1)*GG(2,3)*Omega
⇒       +2*GG(2,1)*nu*k*Omega+2*i*k^2*GG(2,3)*Omega+i*n^2*nu*Omega*GG(3,2)
⇒       +i*GG(3,1)*k*n*nu*Omega+i*GG(3,1)*k*n*Omega-4*k^2*n*Omega+2*k^2*n*nu*Omega
⇒       -2*n^3*Omega-2*i*GG(1,1)*Omega*GG(3,2)-i*k*n*GG(1,3)*Omega
⇒       +2*i*GG(3,1)*GG(1,2)*Omega-4*GG(1,1)*n*Omega-2*i*GG(2,1)*GG(1,3)*Omega);
deg0=-k^2*Omega^2-1/2*n^2*Omega^2+1/2*k^4+1/2*k^4*GG(3,3)
⇒       +1/12*n^4*nu*Omega^2*chi^2*k^2+1/24*n^2*nu*Omega^2*chi^2*k^4-1/2*k*n*GG(1,2)
⇒       -GG(2,1)*GG(1,2)*GG(3,3)-1/2*GG(3,1)*GG(1,3)*k^2-GG(3,1)*GG(1,3)*n^2
⇒       +GG(3,1)*GG(1,3)*Omega^2-GG(3,1)*GG(1,3)*GG(2,2)+k^2*n^2*GG(3,3)
⇒       -k^2*Omega^2*GG(3,3)-k^2*GG(2,2)*Omega^2+k^2*GG(2,2)*GG(3,3)-k^2*GG(2,3)*GG(3,2)
⇒       +1/12*k^6*GG(2,2)*chi^2-1/2*k^4*nu*GG(3,3)-1/2*n^2*Omega^2*GG(3,3)
⇒       -1/2*n^2*GG(2,2)*Omega^2+1/2*n^2*GG(2,2)*GG(3,3)-1/2*n^2*GG(2,3)*GG(3,2)
⇒       +1/24*n^6*GG(2,2)*chi^2-1/2*n^4*nu*GG(3,3)+1/12*GG(1,1)*n^6*chi^2
⇒       -GG(1,1)*Omega^2*GG(3,3)-GG(1,1)*GG(2,2)*Omega^2-GG(1,1)*n^2*Omega^2
⇒       +GG(3,1)*GG(1,2)*GG(2,3)+GG(2,1)*GG(1,2)*Omega^2-1/2*GG(1,1)*k^2*Omega^2
⇒       +1/24*GG(1,1)*k^6*chi^2-GG(1,1)*GG(2,3)*GG(3,2)+1/2*GG(1,1)*k^2*GG(3,3)
⇒       +GG(2,1)*GG(1,3)*GG(3,2)+GG(1,1)*n^2*GG(3,3)-1/2*n^2*nu*GG(2,2)-1/2*GG(1,1)*k^2*nu
⇒       +GG(1,1)*GG(2,2)*GG(3,3)-1/2*GG(2,1)*k*n-nu^2*k^2*GG(2,2)+1/2*k*n*nu*GG(1,2)
⇒       -1/12*GG(2,1)*GG(1,2)*chi^2*k^4-1/12*GG(2,1)*GG(1,2)*chi^2*n^4-
⇒       1/2*GG(2,1)*k*n*GG(3,3)+1/2*GG(2,1)*k*n*Omega^2-1/24*GG(2,1)*k*n^5*chi^2
⇒       -1/12*GG(2,1)*k^3*n^3*chi^2-1/24*GG(2,1)*k^5*n*chi^2+1/2*GG(2,1)*k*n*nu
⇒       +1/2*GG(3,1)*k*n*GG(2,3)+i*GG(3,1)*GG(1,2)*n+1/2*GG(3,1)*GG(1,3)*k^2*nu
⇒       +5/24*k^4*GG(2,2)*chi^2*n^2+1/6*k^2*GG(2,2)*chi^2*n^4+i*k^2*GG(2,3)*n
⇒       -n^2*k^2*nu*GG(3,3)+1/2*n^2*nu*Omega^2*GG(3,3)+1/2*n^2*nu*GG(2,2)*Omega^2
⇒       -1/2*n^2*nu*GG(2,2)*GG(3,3)+1/2*n^2*nu*GG(2,3)*GG(3,2)-1/24*n^6*nu*GG(2,2)*chi^2
⇒       +1/12*GG(1,1)*GG(2,2)*chi^2*k^4+1/12*GG(1,1)*GG(2,2)*chi^2*n^4
⇒       +i*GG(1,1)*GG(2,3)*n-1/12*GG(1,1)*Omega^2*chi^2*n^4-1/12*GG(1,1)*Omega^2*chi^2*k^4
⇒       +1/2*GG(1,1)*k^2*nu*Omega^2-1/24*GG(1,1)*k^6*nu*chi^2+5/24*GG(1,1)*k^2*chi^2*n^4
⇒       +1/6*GG(1,1)*k^4*chi^2*n^2-1/2*GG(1,1)*k^2*nu*GG(3,3)+1/2*k*n*GG(1,2)*Omega^2
⇒       -1/2*k*n*GG(1,2)*GG(3,3)+1/2*k*n*GG(1,3)*GG(3,2)-1/12*k^3*n^3*GG(1,2)*chi^2
⇒       -1/24*k^5*n*GG(1,2)*chi^2-1/24*k*n^5*GG(1,2)*chi^2-i*GG(2,1)*GG(1,3)*n
⇒       +1/2*i*nu*k^3*GG(1,3)-1/2*i*nu^2*k^3*GG(1,3)+1/2*i*GG(3,1)*k*n^2
⇒       -1/2*i*GG(3,1)*nu*k^3+1/2*i*GG(3,1)*nu^2*k^3-i*k^2*n*GG(3,2)-1/2*i*n^3*nu*GG(2,3)
⇒       +1/2*i*n^3*nu*GG(3,2)-i*GG(1,1)*n*GG(3,2)-1/2*i*k*n^2*GG(1,3)
⇒       +k^2*GG(2,2)+1/2*n^4*GG(3,3)+1/2*n^2*GG(2,2)-GG(1,1)*Omega^2
⇒       +1/2*GG(1,1)*k^2+GG(1,1)*GG(2,2)+GG(1,1)*Omega^4-GG(2,1)*GG(1,2)+1/2*nu^3*k^4
⇒       -1/2*nu^2*k^4+1/24*k^8*chi^2-1/2*k^4*nu-1/2*k^4*Omega^2+k^2*Omega^4+1/24*n^8*chi^2
⇒       -1/2*n^4*Omega^2+1/2*n^2*Omega^4-1/6*k^6*nu*chi^2*n^2-1/4*k^4*nu*chi^2*n^4
⇒       -5/24*k^4*Omega^2*chi^2*n^2-1/6*k^2*Omega^2*chi^2*n^4-1/6*n^6*k^2*nu*chi^2
⇒       +n^2*k^2*nu*Omega^2+1/24*n^6*nu*Omega^2*chi^2+1/6*k^2*n^6*chi^2-k^2*n^2*Omega^2
⇒       -1/12*k^6*Omega^2*chi^2+1/2*k^4*nu*Omega^2-1/24*k^8*nu*chi^2+
⇒       1/4*k^4*chi^2*n^4+1/6*k^6*chi^2*n^2-1/24*n^6*Omega^2*chi^2+1/2*n^2*nu*Omega^2
⇒       -1/24*n^8*nu*chi^2+1/2*n^4*nu*Omega^2-1/2*n^2*nu*Omega^4
⇒       -1/12*GG(1,1)*k^4*nu*chi^2*n^2+1/2*GG(3,1)*k*n*nu*GG(2,3)
⇒       +1/2*k*n*nu*GG(1,2)*Omega^2-1/2*k*n*nu*GG(1,2)*GG(3,3)
⇒       -1/12*n^4*nu*GG(2,2)*chi^2*k^2-1/24*n^2*nu*GG(2,2)*chi^2*k^4
⇒       -1/6*GG(1,1)*Omega^2*chi^2*k^2*n^2+1/6*GG(1,1)*GG(2,2)*chi^2*k^2*n^2
⇒       +1/2*k*n*nu*GG(1,3)*GG(3,2)-1/12*k^3*n^3*nu*GG(1,2)*chi^2
⇒       -1/24*k^5*n*nu*GG(1,2)*chi^2-1/24*k*n^5*nu*GG(1,2)*chi^2
⇒       -1/24*GG(2,1)*k^5*n*nu*chi^2-1/12*GG(2,1)*k^3*n^3*nu*chi^2
⇒       -1/24*GG(2,1)*k*n^5*nu*chi^2+1/2*GG(2,1)*k*n*nu*Omega^2-1/2*GG(2,1)*k*n*nu*GG(3,3)
⇒       -1/6*GG(2,1)*GG(1,2)*chi^2*k^2*n^2+i*GG(2,1)*nu*k*GG(3,2)
```

```
⇒       +i*nu*k*GG(1,3)*GG(2,2)+i*GG(3,1)*nu*k*Omega^2-1/24*GG(1,1)*k^2*nu*chi^2*n^4
⇒       +1/2*i*k^2*n*nu*GG(3,2)-1/2*i*nu*k^2*n*GG(2,3)+1/2*i*k^2*n*nu^2*GG(3,2)
⇒       +1/2*i*k*n^2*nu*GG(1,3)-1/2*i*nu^2*k^2*n*GG(2,3)-i*nu*k*GG(1,2)*GG(2,3)
⇒       -i*nu*k*GG(1,3)*Omega^2-i*GG(3,1)*nu*k*GG(2,2)+nu^2*k^2*Omega^2-1/2*i*n^3*GG(3,2)
⇒       -1/2*i*GG(3,1)*k*n^2*nu+1/2*i*n^3*GG(2,3);

%Evaluate the determinant for the current value of omega
eq=[deg6 deg5 deg4 deg3 deg2 deg1 deg0];
result=polyval(eq,omega);
return
```

```
%%%%%%%%%%%%%%%%%%%%%%%%%%%%%%%%%%%%%%%%%%%%%%%%%%%%%%%%%%%%%%%%%%%%%%%%%%%%
% ORDER2PROFILEU.M : FUNCTION RETURNING THE FLUID FORCES PER UNIT OF u-PERTURBATION
%%%%%%%%%%%%%%%%%%%%%%%%%%%%%%%%%%%%%%%%%%%%%%%%%%%%%%%%%%%%%%%%%%%%%%%%%%%%
function stressout = order2profileu(n,Omega,omega,k,Lambda,UR,RE,N,delta)

h=(1-delta)/(N+1/2);            %Distance between two pressure points
clear a;                        %[a]{x}={b}
clear b;
clear x;
a=sparse(4*(N),4*N);
b=sparse(4*N,1);

%Compute the velocity profile and its derivative over the section
ru=0:1/(2*N-1):1;
U=profile(UR,RE,2*N-1,delta);   %Compute the velocity profile

%Boundary Conditions
r=0;
b(1)=0;

%Velocity influence functions at the wall
r=1-delta;
vrw=0;
vtw=0;
vsw=i*omega-i*k*interp1(ru,U(1,:),r,'linear');

%Boundary conditions
r=1-h-delta;
rc=r+h/2;
b(4*N-3)=-2*UR/RE*(1/h^2+1/2/r/h)*vrw;
b(4*N-2)=0;
b(4*N-1)=-2*UR/RE*(1/h^2+1/2/r/h)*vsw;
b(4*N-0)=-(1/2/rc+1/h)*vrw+i*k/2*vsw;

%Special first node next to the centre of the flow
r=h/2;
rc=h;
%Aa
a(1,1)=-i*omega+i*k*interp1(ru,U(1,:),r,'linear')-2*UR/RE*(3/2/r/h+(1+n^2)/r^2+k^2-2/h^2);
a(1,2)=2*Omega+i*n*2*UR/RE*2/r^2;
a(1,3)=0;
a(2,1)=-a(1,2);
a(2,2)=a(1,1);
a(2,3)=0;
a(3,1)=-interp1(ru,U(2,:),r,'linear');
a(3,2)=0;
a(3,3)=a(1,1)+2*UR/RE/r^2;
a(4,1)=1/2/rc-1/h;
a(4,2)=-i*n/2/rc;
a(4,3)=-i*k/2;
%P1
a(1,4)=1/2/r^2-1/r/h;
a(2,4)=i*n/2/r^2;
a(3,4)=i*k/2/r;
a(4,4)=0;
%Ab
a(1,5)=2*UR/RE*(2/r/h-5/h^2);
a(1,6)=0;
```

```
a(1,7)=0;
a(2,5)=0;
a(2,6)=a(1,5);
a(2,7)=0;
a(3,5)=0;
a(3,6)=0;
a(3,7)=a(1,5);
a(4,5)=(1/2/rc+1/h);
a(4,6)=-i*n/2/rc;
a(4,7)=-i*k/2;
%Ac
a(1,9) =2*UR/RE*(-1/2/r/h+4/h^2);
a(1,10)=0;
a(1,11)=0;
a(2,9) =0;
a(2,10)=a(1,9);
a(2,11)=0;
a(3,9) =0;
a(3,10)=0;
a(3,11)=a(1,9);
a(4,9) =0;
a(4,10)=0;
a(4,11)=0;
%Ad
a(1,13)=-2*UR/RE/h^2;
a(1,14)=0;
a(1,15)=0;
a(2,13)=0;
a(2,14)=a(1,13);
a(2,15)=0;
a(3,13)=0;
a(3,14)=0;
a(3,15)=a(1,13);
a(4,13)=0;
a(4,14)=0;
a(4,15)=0;


%Loop for all the nodes in the domain
for j=2:N

    r=0.00+(j-1/2)*h;
    rc=r+h/2;

    if j>1
    %A3
    a(4*j-3,4*j-7)=2*UR/RE*(1/h^2-1/2/r/h);
    a(4*j-3,4*j-6)=0;
    a(4*j-3,4*j-5)=0;
    a(4*j-2,4*j-7)=0;
    a(4*j-2,4*j-6)=a(4*j-3,4*j-7);
    a(4*j-2,4*j-5)=0;
    a(4*j-1,4*j-7)=0;
    a(4*j-1,4*j-6)=0;
    a(4*j-1,4*j-5)=a(4*j-3,4*j-7);
    a(4*j-0,4*j-7)=0;
    a(4*j-0,4*j-6)=0;
    a(4*j-0,4*j-5)=0;

    %P2
    a(4*j-3,4*j-4)=1/2/r^2+1/r/h;
    a(4*j-2,4*j-4)=i*n/2/r^2;
    a(4*j-1,4*j-4)=i*k/2/r;
    a(4*j-0,4*j-4)=0;
    end

    %A1
    a(4*j-3,4*j-3)=-i*omega+i*k*interp1(ru,U(1,:),r,'linear')
⇒       -2*UR/RE*((1+n^2)/r^2+k^2+2/h^2);
    a(4*j-3,4*j-2)=2*Omega+i*n*2*UR/RE*2/r^2;
    a(4*j-3,4*j-1)=0;
```

```
    a(4*j-2,4*j-3)=-a(4*j-3,4*j-2);
    a(4*j-2,4*j-2)=a(4*j-3,4*j-3);
    a(4*j-2,4*j-1)=0;
    a(4*j-1,4*j-3)=-interp1(ru,U(2,:),r,'linear');
    a(4*j-1,4*j-2)=0;
    a(4*j-1,4*j-1)=a(4*j-3,4*j-3)+2*UR/RE/r^2;
    a(4*j-0,4*j-3)=1/2/rc-1/h;
    a(4*j-0,4*j-2)=-i*n/2/rc;
    a(4*j-0,4*j-1)=-i*k/2;

    %P1
    a(4*j-3,4*j+0)=1/2/r^2-1/r/h;
    a(4*j-2,4*j+0)=i*n/2/r^2;
    a(4*j-1,4*j+0)=i*k/2/r;
    a(4*j-0,4*j+0)=0;

    if j<N
    %A2
    a(4*j-3,4*j+1)=2*UR/RE*(1/h^2+1/2/h/r);
    a(4*j-3,4*j+2)=0;
    a(4*j-3,4*j+3)=0;
    a(4*j-2,4*j+1)=0;
    a(4*j-2,4*j+2)=a(4*j-3,4*j+1);
    a(4*j-2,4*j+3)=0;
    a(4*j-1,4*j+1)=0;
    a(4*j-1,4*j+2)=0;
    a(4*j-1,4*j+3)=a(4*j-3,4*j+1);
    a(4*j-0,4*j+1)=1/2/rc+1/h;
    a(4*j-0,4*j+2)=-i*n/2/rc;
    a(4*j-0,4*j+3)=-i*k/2;
    end
end;

%conditionnumb=condest(a)
x=a\b;

clear rr
clear rrp
clear vr
clear vt
clear vs
clear q

%Pressure and velocity influence function values found close to the wall
vr(N-2)=x(4*(N-2)-3);
vr(N-1)=x(4*(N-1)-3);
vr(N)=x(4*N-3);
rrp(N-1)=0.00+(N-1)*h;
rrp(N)=0.00+N*h;
q(N-2)=x(4*(N-2)-0);
q(N-1)=x(4*(N-1)-0);
q(N)=x(4*N-0);
%Evaluation of the pressure flux influence function on the wall
q(N+1)=(15*q(N)-10*q(N-1)+3*q(N-2))/8;
stressout=zeros(3,1);
%Pressure and velocity influence function values close to the wall
rw=1-delta;
piw=q(N+1)/rw;
vsw1=x(4*N-1);
vtw1=x(4*N-2);
vrw1=x(4*N-3);
vsw2=x(4*N-5);
vtw2=x(4*N-6);
vrw2=x(4*N-7);
%Velocity influence function derivatives close to the wall
dvtdr=(3*vtw-4*vtw1+vtw2)/2/h;
dvsdr=(3*vsw-4*vsw1+vsw2)/2/h;

%Viscous sublayer. This is only used to evaluate dpdz if the turbulent velocity profile is
used.
fi=sqrt(0.02);
```

```
for jj=1:25
    fi=(-2*log10(delta/7.4+2.51/RE/fi))^(-1);
end
fcolebrook=fi^2;
dpdz=-fcolebrook*UR^2/4;
%dpdz=-12*UR^2/RE;  %Evaluation of the mean quantity dpdz if the laminar velocity profile
is used.

%Fluid stresses per unit u-perturbation on the wall
stressout(1)=-piw+4*UR/RE*(i*n*vtw/rw+i*k*vsw-vrw/rw)-dpdz;
stressout(2)=2*UR/RE*(-vtw/rw+dvtdr-i*n/rw*vrw);
stressout(3)=2*UR/RE*(-i*k*vrw+dvsdr);
```

```
%%%%%%%%%%%%%%%%%%%%%%%%%%%%%%%%%%%%%%%%%%%%%%%%%%%%%%%%%%%%%%%%%%%%%%%%%%%%
% ORDER2PROFILEV.M : FUNCTION RETURNING THE FLUID FORCES PER UNIT OF v-PERTURBATION
%%%%%%%%%%%%%%%%%%%%%%%%%%%%%%%%%%%%%%%%%%%%%%%%%%%%%%%%%%%%%%%%%%%%%%%%%%%%
function stressout = order2profilev(n,Omega,omega,k,Lambda,UR,RE,N,delta)

h=(1-delta)/(N+1/2);            %Distance between two pressure points
clear a;                        %[a]{x}={b}
clear b;
clear x;
a=sparse(4*(N),4*N);
b=sparse(4*N,1);

%Compute the velocity profile and its derivative over the section
ru=0:1/(2*N-1):1;
U=profile(UR,RE,2*N-1,delta);   %Compute the velocity profile

%Boundary Conditions
r=0;
b(1)=0;

%Velocity influence functions at the wall
r=1-delta;
vrw=0;
vtw=i*omega-i*k*interp1(ru,U(1,:),r,'linear');
vsw=0;

%Boundary conditions
r=1-h-delta;
rc=r+h/2;
b(4*N-3)=-2*UR/RE*(1/h^2+1/2/r/h)*vrw;
b(4*N-2)=0;
b(4*N-1)=-2*UR/RE*(1/h^2+1/2/r/h)*vsw;
b(4*N-0)=-(1/2/rc+1/h)*vrw+i*k/2*vsw;

%Special first node next to the centre of the flow
r=h/2;
rc=h;
%Aa
a(1,1)=-i*omega+i*k*interp1(ru,U(1,:),r,'linear')-2*UR/RE*(3/2/r/h+(1+n^2)/r^2+k^2-2/h^2);
a(1,2)=2*Omega+i*n*2*UR/RE*2/r^2;
a(1,3)=0;
a(2,1)=-a(1,2);
a(2,2)=a(1,1);
a(2,3)=0;
a(3,1)=-interp1(ru,U(2,:),r,'linear');
a(3,2)=0;
a(3,3)=a(1,1)+2*UR/RE/r^2;
a(4,1)=1/2/rc-1/h;
a(4,2)=-i*n/2/rc;
a(4,3)=-i*k/2;
%P1
a(1,4)=1/2/r^2-1/r/h;
a(2,4)=i*n/2/r^2;
a(3,4)=i*k/2/r;
a(4,4)=0;
%Ab
a(1,5)=2*UR/RE*(2/r/h-5/h^2);
```

```
a(1,6)=0;
a(1,7)=0;
a(2,5)=0;
a(2,6)=a(1,5);
a(2,7)=0;
a(3,5)=0;
a(3,6)=0;
a(3,7)=a(1,5);
a(4,5)=(1/2/rc+1/h);
a(4,6)=-i*n/2/rc;
a(4,7)=-i*k/2;
%Ac
a(1,9) =2*UR/RE*(-1/2/r/h+4/h^2);
a(1,10)=0;
a(1,11)=0;
a(2,9) =0;
a(2,10)=a(1,9);
a(2,11)=0;
a(3,9) =0;
a(3,10)=0;
a(3,11)=a(1,9);
a(4,9) =0;
a(4,10)=0;
a(4,11)=0;
%Ad
a(1,13)=-2*UR/RE/h^2;
a(1,14)=0;
a(1,15)=0;
a(2,13)=0;
a(2,14)=a(1,13);
a(2,15)=0;
a(3,13)=0;
a(3,14)=0;
a(3,15)=a(1,13);
a(4,13)=0;
a(4,14)=0;
a(4,15)=0;


%Loop for all the nodes in the domain
for j=2:N

    r=0.00+(j-1/2)*h;
    rc=r+h/2;

    if j>1
    %A3
    a(4*j-3,4*j-7)=2*UR/RE*(1/h^2-1/2/r/h);
    a(4*j-3,4*j-6)=0;
    a(4*j-3,4*j-5)=0;
    a(4*j-2,4*j-7)=0;
    a(4*j-2,4*j-6)=a(4*j-3,4*j-7);
    a(4*j-2,4*j-5)=0;
    a(4*j-1,4*j-7)=0;
    a(4*j-1,4*j-6)=0;
    a(4*j-1,4*j-5)=a(4*j-3,4*j-7);
    a(4*j-0,4*j-7)=0;
    a(4*j-0,4*j-6)=0;
    a(4*j-0,4*j-5)=0;

    %P2
    a(4*j-3,4*j-4)=1/2/r^2+1/r/h;
    a(4*j-2,4*j-4)=i*n/2/r^2;
    a(4*j-1,4*j-4)=i*k/2/r;
    a(4*j-0,4*j-4)=0;
    end

    %A1
    a(4*j-3,4*j-3)=-i*omega+i*k*interp1(ru,U(1,:),r,'linear')
⇒       -2*UR/RE*((1+n^2)/r^2+k^2+2/h^2);
    a(4*j-3,4*j-2)=2*Omega+i*n*2*UR/RE*2/r^2;
```

```
    a(4*j-3,4*j-1)=0;
    a(4*j-2,4*j-3)=-a(4*j-3,4*j-2);
    a(4*j-2,4*j-2)=a(4*j-3,4*j-3);
    a(4*j-2,4*j-1)=0;
    a(4*j-1,4*j-3)=-interp1(ru,U(2,:),r,'linear');
    a(4*j-1,4*j-2)=0;
    a(4*j-1,4*j-1)=a(4*j-3,4*j-3)+2*UR/RE/r^2;
    a(4*j-0,4*j-3)=1/2/rc-1/h;
    a(4*j-0,4*j-2)=-i*n/2/rc;
    a(4*j-0,4*j-1)=-i*k/2;

    %P1
    a(4*j-3,4*j+0)=1/2/r^2-1/r/h;
    a(4*j-2,4*j+0)=i*n/2/r^2;
    a(4*j-1,4*j+0)=i*k/2/r;
    a(4*j-0,4*j+0)=0;

    if j<N
    %A2
    a(4*j-3,4*j+1)=2*UR/RE*(1/h^2+1/2/h/r);
    a(4*j-3,4*j+2)=0;
    a(4*j-3,4*j+3)=0;
    a(4*j-2,4*j+1)=0;
    a(4*j-2,4*j+2)=a(4*j-3,4*j+1);
    a(4*j-2,4*j+3)=0;
    a(4*j-1,4*j+1)=0;
    a(4*j-1,4*j+2)=0;
    a(4*j-1,4*j+3)=a(4*j-3,4*j+1);
    a(4*j-0,4*j+1)=1/2/rc+1/h;
    a(4*j-0,4*j+2)=-i*n/2/rc;
    a(4*j-0,4*j+3)=-i*k/2;
    end
end;

%conditionnumb=condest(a)
x=a\b;

clear rr
clear rrp
clear vr
clear vt
clear vs
clear q

%Pressure and velocity influence function values found close to the wall
vr(N-2)=x(4*(N-2)-3);
vr(N-1)=x(4*(N-1)-3);
vr(N)=x(4*N-3);
rrp(N-1)=0.00+(N-1)*h;
rrp(N)=0.00+N*h;
q(N-2)=x(4*(N-2)-0);
q(N-1)=x(4*(N-1)-0);
q(N)=x(4*N-0);
%Evaluation of the pressure flux influence function on the wall
q(N+1)=(15*q(N)-10*q(N-1)+3*q(N-2))/8;
stressout=zeros(3,1);
%Pressure and velocity influence function values close to the wall
rw=1-delta;
piw=q(N+1)/rw;
vsw1=x(4*N-1);
vtw1=x(4*N-2);
vrw1=x(4*N-3);
vsw2=x(4*N-5);
vtw2=x(4*N-6);
vrw2=x(4*N-7);
%Velocity influence function derivatives close to the wall
dvtdr=(3*vtw-4*vtw1+vtw2)/2/h;
dvsdr=(3*vsw-4*vsw1+vsw2)/2/h;

%Fluid stresses per unit v-perturbation on the wall
stressout(1)=-piw+4*UR/RE*(i*n*vtw/rw+i*k*vsw-vrw/rw);
```

```
stressout(2)=2*UR/RE*(-vtw/rw+dvtdr-i*n/rw*vrw);
stressout(3)=2*UR/RE*(-i*k*vrw+dvsdr);
```

```
%%%%%%%%%%%%%%%%%%%%%%%%%%%%%%%%%%%%%%%%%%%%%%%%%%%%%%%%%%%%%%%%%%%%%%%%%%%%
% ORDER2PROFILEW.M : FUNCTION RETURNING THE FLUID FORCES PER UNIT OF w-PERTURBATION
%%%%%%%%%%%%%%%%%%%%%%%%%%%%%%%%%%%%%%%%%%%%%%%%%%%%%%%%%%%%%%%%%%%%%%%%%%%%
function stressout = order2profilew(n,Omega,omega,k,Lambda,UR,RE,N,delta)

h=(1-delta)/(N+1/2);            %Distance between two pressure points
clear a;                        %[a]{x}={b}
clear b;
clear x;
a=sparse(4*(N),4*N);
b=sparse(4*N,1);

%Compute the velocity profile and its derivative over the section
ru=0:1/(2*N-1):1;
U=profile(UR,RE,2*N-1,delta);   %Compute the velocity profile

%Boundary Conditions
r=0;
b(1)=0;

%Velocity influence functions at the wall
r=1-delta;
vrw=i*omega-i*k*interp1(ru,U(1,:),r,'linear');
vtw=0;
vsw=-interp1(ru,U(2,:),r,'linear');

%Boundary conditions
r=1-h-delta;
rc=r+h/2;
b(4*N-3)=-2*UR/RE*(1/h^2+1/2/r/h)*vrw;
b(4*N-2)=0;
b(4*N-1)=-2*UR/RE*(1/h^2+1/2/r/h)*vsw;
b(4*N-0)=-(1/2/rc+1/h)*vrw+i*k/2*vsw;

%Special first node next to the centre of the flow
r=h/2;
rc=h;
%Aa
a(1,1)=-i*omega+i*k*interp1(ru,U(1,:),r,'linear')-2*UR/RE*(3/2/r/h+(1+n^2)/r^2+k^2-2/h^2);
a(1,2)=2*Omega+i*n*2*UR/RE*2/r^2;
a(1,3)=0;
a(2,1)=-a(1,2);
a(2,2)=a(1,1);
a(2,3)=0;
a(3,1)=-interp1(ru,U(2,:),r,'linear');
a(3,2)=0;
a(3,3)=a(1,1)+2*UR/RE/r^2;
a(4,1)=1/2/rc-1/h;
a(4,2)=-i*n/2/rc;
a(4,3)=-i*k/2;
%P1
a(1,4)=1/2/r^2-1/r/h;
a(2,4)=i*n/2/r^2;
a(3,4)=i*k/2/r;
a(4,4)=0;
%Ab
a(1,5)=2*UR/RE*(2/r/h-5/h^2);
a(1,6)=0;
a(1,7)=0;
a(2,5)=0;
a(2,6)=a(1,5);
a(2,7)=0;
a(3,5)=0;
a(3,6)=0;
a(3,7)=a(1,5);
a(4,5)=(1/2/rc+1/h);
a(4,6)=-i*n/2/rc;
```

```
a(4,7)=-i*k/2;
%Ac
a(1,9) =2*UR/RE*(-1/2/r/h+4/h^2);
a(1,10)=0;
a(1,11)=0;
a(2,9) =0;
a(2,10)=a(1,9);
a(2,11)=0;
a(3,9) =0;
a(3,10)=0;
a(3,11)=a(1,9);
a(4,9) =0;
a(4,10)=0;
a(4,11)=0;
%Ad
a(1,13)=-2*UR/RE/h^2;
a(1,14)=0;
a(1,15)=0;
a(2,13)=0;
a(2,14)=a(1,13);
a(2,15)=0;
a(3,13)=0;
a(3,14)=0;
a(3,15)=a(1,13);
a(4,13)=0;
a(4,14)=0;
a(4,15)=0;


%Loop for all the nodes in the domain
for j=2:N

    r=0.00+(j-1/2)*h;
    rc=r+h/2;

    if j>1
    %A3
    a(4*j-3,4*j-7)=2*UR/RE*(1/h^2-1/2/r/h);
    a(4*j-3,4*j-6)=0;
    a(4*j-3,4*j-5)=0;
    a(4*j-2,4*j-7)=0;
    a(4*j-2,4*j-6)=a(4*j-3,4*j-7);
    a(4*j-2,4*j-5)=0;
    a(4*j-1,4*j-7)=0;
    a(4*j-1,4*j-6)=0;
    a(4*j-1,4*j-5)=a(4*j-3,4*j-7);
    a(4*j-0,4*j-7)=0;
    a(4*j-0,4*j-6)=0;
    a(4*j-0,4*j-5)=0;

    %P2
    a(4*j-3,4*j-4)=1/2/r^2+1/r/h;
    a(4*j-2,4*j-4)=i*n/2/r^2;
    a(4*j-1,4*j-4)=i*k/2/r;
    a(4*j-0,4*j-4)=0;
    end

    %A1
    a(4*j-3,4*j-3)=-i*omega+i*k*interp1(ru,U(1,:),r,'linear')
⇒       -2*UR/RE*((1+n^2)/r^2+k^2+2/h^2);
    a(4*j-3,4*j-2)=2*Omega+i*n*2*UR/RE*2/r^2;
    a(4*j-3,4*j-1)=0;
    a(4*j-2,4*j-3)=-a(4*j-3,4*j-2);
    a(4*j-2,4*j-2)=a(4*j-3,4*j-3);
    a(4*j-2,4*j-1)=0;
    a(4*j-1,4*j-3)=-interp1(ru,U(2,:),r,'linear');
    a(4*j-1,4*j-2)=0;
    a(4*j-1,4*j-1)=a(4*j-3,4*j-3)+2*UR/RE/r^2;
    a(4*j-0,4*j-3)=1/2/rc-1/h;
    a(4*j-0,4*j-2)=-i*n/2/rc;
    a(4*j-0,4*j-1)=-i*k/2;
```

```
    %P1
    a(4*j-3,4*j+0)=1/2/r^2-1/r/h;
    a(4*j-2,4*j+0)=i*n/2/r^2;
    a(4*j-1,4*j+0)=i*k/2/r;
    a(4*j-0,4*j+0)=0;

    if j<N
    %A2
    a(4*j-3,4*j+1)=2*UR/RE*(1/h^2+1/2/h/r);
    a(4*j-3,4*j+2)=0;
    a(4*j-3,4*j+3)=0;
    a(4*j-2,4*j+1)=0;
    a(4*j-2,4*j+2)=a(4*j-3,4*j+1);
    a(4*j-2,4*j+3)=0;
    a(4*j-1,4*j+1)=0;
    a(4*j-1,4*j+2)=0;
    a(4*j-1,4*j+3)=a(4*j-3,4*j+1);
    a(4*j-0,4*j+1)=1/2/rc+1/h;
    a(4*j-0,4*j+2)=-i*n/2/rc;
    a(4*j-0,4*j+3)=-i*k/2;
    end
end;

%conditionnumb=condest(a)
x=a\b;

clear rr
clear rrp
clear vr
clear vt
clear vs
clear q

%Pressure and velocity influence function values found close to the wall
vr(N-2)=x(4*(N-2)-3);
vr(N-1)=x(4*(N-1)-3);
vr(N)=x(4*N-3);
rrp(N-1)=0.00+(N-1)*h;
rrp(N)=0.00+N*h;
q(N-2)=x(4*(N-2)-0);
q(N-1)=x(4*(N-1)-0);
q(N)=x(4*N-0);
%Evaluation of the pressure flux influence function on the wall
q(N+1)=(15*q(N)-10*q(N-1)+3*q(N-2))/8;
stressout=zeros(3,1);
%Pressure and velocity influence function values close to the wall
rw=1-delta;
piw=q(N+1)/rw;
vsw1=x(4*N-1);
vtw1=x(4*N-2);
vrw1=x(4*N-3);
vsw2=x(4*N-5);
vtw2=x(4*N-6);
vrw2=x(4*N-7);
%Velocity influence function derivatives close to the wall
dvtdr=(3*vtw-4*vtw1+vtw2)/2/h;
dvsdr=(3*vsw-4*vsw1+vsw2)/2/h;

%Fluid stresses per unit w-perturbation on the wall
stressout(1)=-piw+4*UR/RE*(i*n*vtw/rw+i*k*vsw-vrw/rw)-Omega^2*rw;
stressout(2)=2*UR/RE*(-vtw/rw+dvtdr-i*n/rw*vrw);
stressout(3)=2*UR/RE*(-i*k*vrw+dvsdr+interp1(ru,U(2,:),1-delta,'linear'));
```

```
%%%%%%%%%%%%%%%%%%%%%%%%%%%%%%%%%%%%%%%%%%%%%%%%%%%%%%%%%%%%%%%%%%%%%%%%%%%%
% PROFILE.M : FUNCTION RETURNING MEAN VELOCITY PROFILE
%%%%%%%%%%%%%%%%%%%%%%%%%%%%%%%%%%%%%%%%%%%%%%%%%%%%%%%%%%%%%%%%%%%%%%%%%%%%
function U = profile(UR,RE,N,delta)  %UR and RE are the average values over the pipe
                                     %radius
```

```
r=0:1/N:1;

%eta=1; %For a laminar profile, use eta=1. Higher eta leads to higher polynomial profiles.
%for j=1:N+1
%    rr=r(j);
%    U(1,j)=UR*(1/2*(1-rr^(2*eta))/eta*(2*eta+1));
%    U(2,j)=UR*(-rr^(2*eta-1)*(2*eta+1));
%end

%return

%Viscous sublayer
fi=sqrt(0.02);
for jj=1:25
    fi=(-2*log10(delta/7.4+2.51/RE/fi))^(-1);
end
fcolebrook=fi^2;
dusublayer=-fcolebrook*UR*RE/16;
usublayer=(r-1)*dusublayer;

%Core region power law model
a2c=.8750000000;
URc=UR/a2c;
for j=1:N+1
    rr=r(j);
    upow(j)=URc*(1-rr)^(1/7);
end;

U=zeros(2,N+1);
for j=1:N+0
    U(1,j)=min(upow(j),usublayer(j));       %Mean velocity profile
    if U(1,j)==usublayer(j)
        U(2,j)=dusublayer;                  %r-derivative of the mean velocity profile
    else
        rj=r(j);
        U(2,j)=URc*(-1/7*1/((1-rj)^(6/7)));
    end
end

return
```

Bibliography

Bélanger, F. (1991) A Numerical Method for Confined Unsteady Flows Related to Fluid-Structure Interactions, Ph.D. Dissertation, McGill University, Montreal.

Burden, R.L., Faires, J.D. (2001) *Numerical Analysis,* Seventh Edition., Pacific Grove, California: Brooks/Cole.

Chandrasekhar, S. (1961) *Hydrodynamic and Hydromagnetic Stability* **§78**. Oxford: Clarendon Press.

Chaumond, N. (2003) Stability of Thin Elastic Tube Containing Viscous Rotating Flow, Internal Report, Dept. of Mechanical Engineering, McGill University, Montreal.

Chow, C.-Y. (1969) Swirling flow in tubes of non-uniform cross-sections. *Journal of Fluid Mechanics*, **38**, pp. 843-854.

Cortelezzi, L. (2002) Unpublished derivation for a rotating viscous flow.

Cortelezzi, L., Pong, A., Paidoussis, M. P. (2004) Flutter of Rotating Shells with a Co-rotating Axial Flow. *Journal of Applied Mechanics*, **71**, 143-145

Dowell, E. H. (1971) Generalized Aerodynamic Forces on a Flexible Plane Undergoing Transient Motion in a Shear Flow with an Application to Panel Flutter. AIAA Journal, **9**(5), 834-841.

El Chebair, A. (1988) Theoretical and Experimental Study of Internal and Annular Flow Induced Instabilities of Cylindrical Shells, Ph.D. Dissertation, Department of Mechanical Engineering, McGill University, Montreal.

El Chebair, A., Misra, A. K., Païdoussis, M. P. (1990) Theoretical Study of the Effect of Unsteady Viscous Forces on Inner- and Annular-Flow-Induced Instabilities of Cylindrical Shells. *Journal of Sound and Vibration*, **138**(3), 457-478.

Harlow, F.H., Welch, J.E. (1965) Numerical Calculation of Time-Dependnent Viscous Incompressible Flow of Fluid with Free Surface. *The Physics of Fluids*, **8**(12), 2182-2189.

Howard, L. N. & Gupta, A. S. (1962) On the Hydrodynamic and Hydromagnetic Stability of Swirling Flows. *Journal of Fluid Mechanics,* **14,** 463-476.

Kallinderis, Y. (1992) A Finite Volume Navier-Stokes Algorithm for Adaptative Grids. *International Journal for Numerical Methods in Fluids*, **15**, 193-217.

Karagiozis, K.N. (2006) Experiments and theory on the nonlinear dynamics and stability of clamped shells subjected to axial fluid flow or harmonic excitation. Ph.D. Thesis, Department of Mechanical Engineering, McGill University, Montreal.

Karagiozis, K. N., Amabili ,M., Paidoussis M. P., Misra A. K. (2005) Nonlinear vibrations of fluid-filled clamped circular cylindrical shells. *Journal of Fluids and Structures*, **21**(5-7) 579-595.

Kraus. H. (1967) *Thin Elastic Shells*, New York: John Wiley & Sons.

Kress, W., Nilsson, J. (2003) Boundary Conditions and Estimates for the Linearized Navier-Stokes Equations on Staggered Grids. *Computers and Fluids*, **32**, 1093-1112.

Lai, Y.-C. & Chow, C.-Y. (1973) Stability of a Rotating Thin Elastic Tube Containing a Fluid Flow, *Zeitschrift für Angewandte Mathematik und Mechanik*, **53**, 511-517.

Lai, Y.-C. (1972) *The Stability of a Thin Elastic Tube Containing Rotating Fluid Flow*, Ph. D. Thesis, Department of Aerospace Engineering Sciences, University of Colorado, Boulder.

Leissa, A. W. (1973) *Vibration of Shells*, NASA SP-288, NASA, Washington D.C.

Mateescu, D., Païdoussis, M.P., Bélanger F. (1994a) Unsteady Annular Viscous Flows between Oscillating Cylinders. Part I: Computational Solutions based on a Time-Integration Method. *Journal of Fluids and Structures*, **8**, 489-507.

Mateescu, D., Païdoussis, M.P., Bélanger F. (1994b) A Time-Integration Method Using Artificial Compressibility for Unsteady Viscous Flows. *Journal of Sound and Vibration,* **177**, 197-205.

Mateescu, D., Mekanik, A., Païdoussis, M.P. (1996) Analysis of 2-D and 3-D Unsteady Annular Flows with Oscillating Boundaries, based on a Time-Dependent Coordinate Transformation. *Journal of Fluids and Structures*, **10**, 57-77.

Maslowe, S. A. (1974) Instability of Rigidly Rotating Flows to Non-axisymmetric Disturbances. *Journal of Fluid Mechanics,* **64,** part2, 307-317.

Mekanik, A. (1994) General Solution for Unsteady Annular Flows between Concentric Cylinders and Annular Flow-Induced Instabilities, Ph.D. Thesis, McGill University.

Munson, B.R., Young, D.F., Okiishi, T.H. (2002) *Fundamentals of Fluid Mechanics,* Fourth Edition. New York: John Wiley & Sons.

Nguyen, V.B., Païdoussis, M.P., Misra, A.K. (1994) A CFD-Based Model for the Study

of the Stability of Cantilevered Coaxial Cylindrical Shells Conveying Viscoud Fluid. *Journal of Sound and Vibration*, **176**(1), 105-125.

Paidoussis and Denise (1972) Flutter of thin cylindrical shells conveying fluid. *Journal of Sound and Vibration,* **20**, 9-26.

Païdoussis, M.P. (2003) *Fluid-Structure Interactions: Slender Structures and Axial Flow, Volume 2.* London: Elsevier Academic Press.

Païdoussis, M.P., Chan, S.P., Misra, A.K. (1984) Dynamics and Stability of Coaxial Cylindrical Shells Containing Flowing Fluid. *Journal of Sound and Vibration*, **97**, 201-235.

Païdoussis, M.P., Misra, A.K., Chan, S.P. (1985) Dynamics and Stability of Coaxial Cylindrical Shells Conveying Viscous Fluid. *Journal of Applied Mechanics*, **52**, 389-396.

Pareschi A. and Montanelli P. (1980) Numerical Solution of the Navier-Stokes Equations for a Rotating Fluid Flow in a Cylindrical Pipe, *Meccanica*, **15**(3), 140-153.

Patankar, S.V. (1980) *Numerical Heat Transfer and Fluid Flow,* Chapter 6. Washington: Hemisphere Publishing Corporation,.

Pong, A. (2000) Dynamic Stability of Elastic Shells Containing Rotating or Swirling Flows, Honours Thesis, Department of Mechanical Engineering, McGill University, Montreal.

Rayleigh, Lord J.W. (1917) On the Dynamics of Revolving Fluids. *Proceedings of the Royal Society of London. Series A*, **93**(648), 148-154.

Sadeghi, V. M., Higgins, B. G. (1991) Stability of Sliding Couette-Poiseuille Flow in Annulus subject to Axisymmetric and Asymmetric Disturbances. *Physics of Fluids A-Fluid Dynamics*, **3**(9), 2092-2104.

Sadeghi, V. M. (1991) Linear Stability Analysis of Sliding Couette-Poiseuille Flow in a Concentric Annulus. Ph.D. Thesis, University of California, Davis.

Schlicting, D. (1979) *Boundary Layer Theory*, Seventh Edition, New York: McGraw Hill.

Shapiro, A.H. (1977) Physiologic and Medical Aspects of Flow in Collapsible Tubes. *Proceedings 6th Canadian Congress of Applied Mechanics*, Vancouver, B.C., Canada, pp. 883-906.

Soedel, W. (2004) *Vibrations of Shells and Plates,* Third Edition. New York: Marcel Dekker, Inc.

Soh, W.Y., Goodrich, J.W. (1988) Unsteady Solution of Incompressible Navier-Stokes Equations. *Journal of Computational Physics*, **79**, 113-134.

Srinivasan, A.V., Lauterbach, G.F. (1971) Traveling Waves in Rotating Cylindrical Shells. ASME Journal of Engineering for Industry, **92**, 1229-1232

Verzicco, R., Orlandi, P. (1996) A Finite-Difference Scheme for Three-Dimensional Imcompressible Flows in Cylindrical Coordinates. *Journal of Computational Physics,* **123**, 402-414.

Vinokur, M. (1982) On One-Dimensional Stretching Functions for Finite-Difference Calculations. *Journal of Computational Physics*, **50**, 215-234.

Yih, C.-S. (1965) *Dynamics of Nonhomogeneous Fluids.* New York: MacMillan.